AUSTRIAN
MARSHALL PLAN FOUNDATION

Noise Cancellation for Headphones

Marshall Plan Scholarship Report

Markus Guldenschuh

6/03/2013

Institute of Electronic Music and Acoustics,
University of Music and Performing Arts Graz,
Inffeldgasse 10/3
8010 Graz

Mechanical and Aerospace Engineering,
University of California, San Diego,
9500 Gilman Drive, La Jolla,
California 92093, USA

Table of Contents

1 Introduction

Portable communication devices and music players allow users to communicate and enjoy music wherever they want. However in many environments, ambient noise might be so loud that it masks the music or communication signal and/or forces the user to harmfully loud playback volumes. Closed headphones with ear-cups already show a good passive attenuation of high-frequency ambient noise, but there is hardly any attenuation of the low-frequency noise. Headphones with Active Noise Cancellation (ANC) fill this gap and reduce the low-frequency noise with 'anti-noise' that destructively interferes with the ambient noise.

In this report the strengths and drawbacks of different ANC methods are reviewed and new contributions to the field of ANC for headphones are presented. The methods that are used for ANC headphones can on the one hand be divided into feedforward and feedback methods and on the other hand into digital and analogue methods. Feedforward means that ambient noise is sensed outside of the headphone and is fed forward as inverted 'anti-noise' to the loudspeaker of the headphone. Feedback means that the noise which already penetrated the headphone is sensed inside the headphone. The sensed and inverted 'anti-noise' is thus fed back to the loudspeaker.

Both, feedback and feedforward structures can be implemented analogue or digital. Analogue technology has the advantage of being delayless and inexpensive. Digital technology on the other hand has the advantage of being able to adapt to different (acoustic) situations. In this report, new ways of reducing the time delay of digital systems and new efficient algorithms to adapt to different acoustic conditions are presented. In the beginning however, the problem of assessing ANC headphones will be addressed and a robust and reliable measurement procedure is presented.

2 Optimal Measurement Procedure

The performance of Active Noise Cancellation (ANC) headphones is measured by putting the headphone on a measurement device (e.g. a dummy head), playing back a measurement signal from outside, and comparing the residual noise at the measurement device with and without activated ANC. However, experience has shown that the measured results strongly depend on the measurement device. A same ANC-headphone can lead to good results on one measurement device and to poor results on another.

The goal is to define a measurement procedure that leads to realistic and reliable results. Realistic results in a sense that they would match the opinion of the users. Therefore, a listening test was conducted to evaluate the opinion and judgment of (experienced) users on different ANC-headphones. In parallel, the ANC of the very same headphones was measured with different measurement devices. A comparison of these measured results with the subjective evaluations leads to a conclusion about which measurement procedure best reflects the user judgment.

2.1 ANC Measurement with Different Measuring Devices

Five headphones are measured with four different measurement devices for the comparison with the subjective evaluation of the users.

The four used measurement devices are depicted in Figure 2.1.

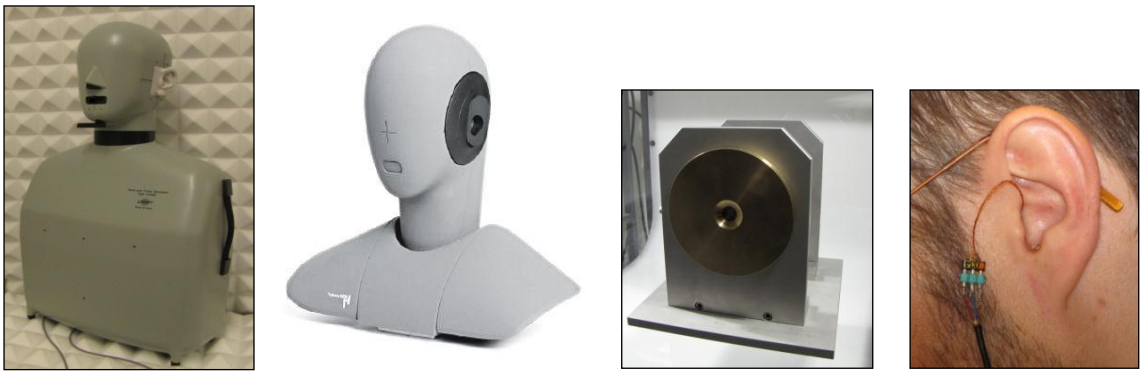

Figure 2.1: Measuring devices.

The measurements were done in a semi-anechoic chamber, where a loudspeaker, which played back the measurement noise, was placed approximately 1 m ahead of the measurement device with the ANC-headphone. The loudspeaker was placed in the horizontal plane of the headphones, and measurements were done for different azimuth-angles of incident signals. (From 0° to 350° in 10° steps.)

The median noise reduction of one sample headphone is shown in Figure 2.2. The amount of noise reduction slightly depends on the measurement directions and might vary +/- 5dB. More relevant than the dependency on the measurement direction is, that the five measurement devices deliver different results for one and the same headphone as can be seen in Figure 2.3, where the median values over all directions of incident sound are displayed.

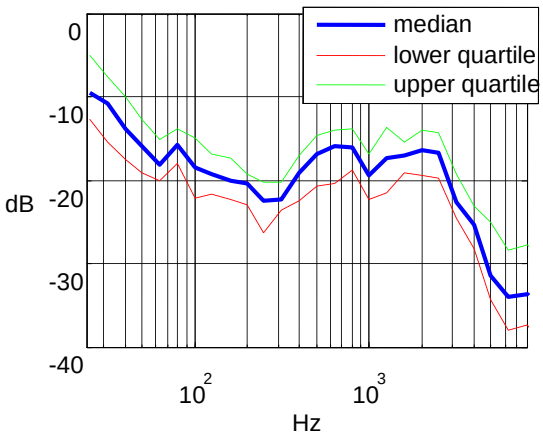

Figure 2.2: Median reduced noise level of an exemplary headphone. The amount of noise reduction slightly depends on the measurement direction. The upper and lower quartile of the measured noise reduction is marked with the dotted and dashed line.

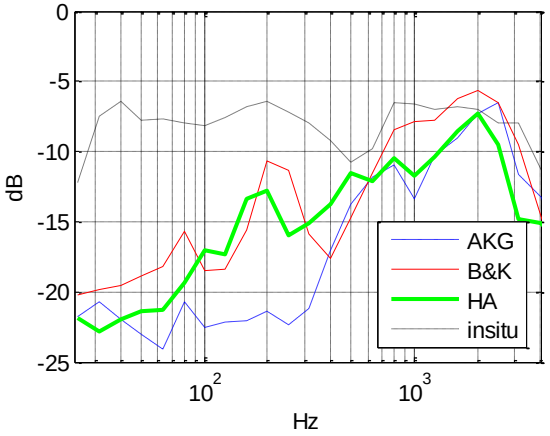

Figure 2.3: Median ANC performance of one headphone on four different measurement tools.

2.2 Subjective ANC Evaluation in a Listening Test

In a listening test, 26 persons were asked to give a subjective evaluation over the ANC performance of the five headphones presented above. The listening test comprises three parts, each of which is described below.

2.2.1 Listening Test Part I

For the first part of the listening test, residual ANC noises were pre-recorded. The five ANC-headphones were put on a dummy head while noise was played back by a 5.1 surround system. The surround system created an uncorrelated diffuse sound-field. This way, recordings of residual ANC noises were done under exactly the same conditions for each of the five headphones. Three different kinds of noise have been recorded:

- Aircraft noise (broadband noise)
- Train noise (impulse noise)
- Speech noise (small-band noise)

The chosen noises on the one hand all represent typical situations where ANC would be used; on the other hand they differ in their sound characteristics.

In the listening test, the subjects then judged the ANC performance of the headphones based on these recordings. The advantage of the pre-recorded residual noises is that the subjects could fast and easily switch from one headphone to the other, which facilitates the comparison. The subjects compared the five headphones for each of the three different noises via the recordings. The results of the subjective evaluation are shown in Figure 2.4.

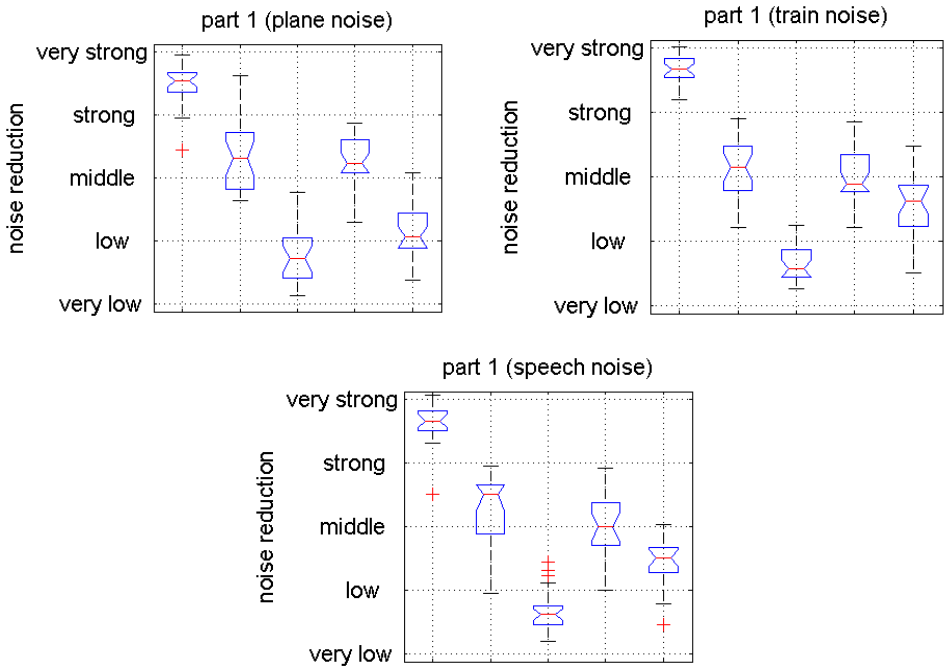

Figure 2.4: The boxplot displays the variability among the perceived noise reduction for 5 different headphones. The red bar indicates the median value; the blue box frames the 1st and the 3rd quartile. The ranking of the headphones is independent of the noise source.

2.2.2 Listening Test Part II

The first part of the listening test was not only important to see the influence of the noise pattern to the ANC evaluation; it was also a training of the subjects for the second part. In the second part, the very same sound-field that was generated for the recordings in part one was produced again for only one of the three noises. In this sound-field, the subjects evaluated the real ANC-headphones. The ANC-headphones were placed on the subjects' head from behind such that they could not see or touch the headphone.

Figure 2.5: Listening test, part II. A test person judges an ANC headphone. The headphones are put onto the test person's head by a tutor, such that the test person cannot recognize the brand of the headphone.

The results from the 2nd part differ slightly from those in the 1st part, as can be seen in Figure 2.6. This figure shows the median value above all answers disrespect the kind of noise that has been played back. This is justified as a multifactorial ANOVA shows that the noise source does not have a significant influence onto the results. All differences in the headphone ranking are statistically significant, except for one pair. However, this pair is not significantly equal either.

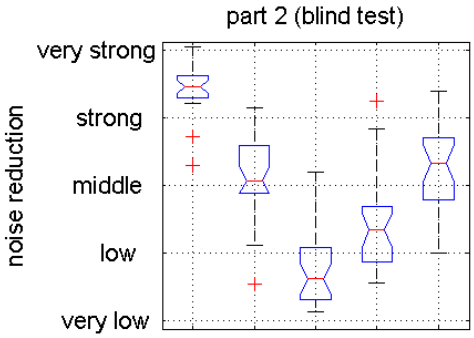

Figure 2.6: The second part of the listening test shows different results from the first ones. Headphone Nr 4 and 5 changed places. All differences in the ranking are significant except for the headphones Nr.2 and Nr. 5.

2.2.3 Listening Test Part III

In the third part of the listening test, the ANC headphones were presented visibly to the subjects. The subjects than evaluated the headphones in four categories (see also Figure 2.7):

- Noise reduction
- Wearing comfort
- Design
- Sound quality
- Price estimate

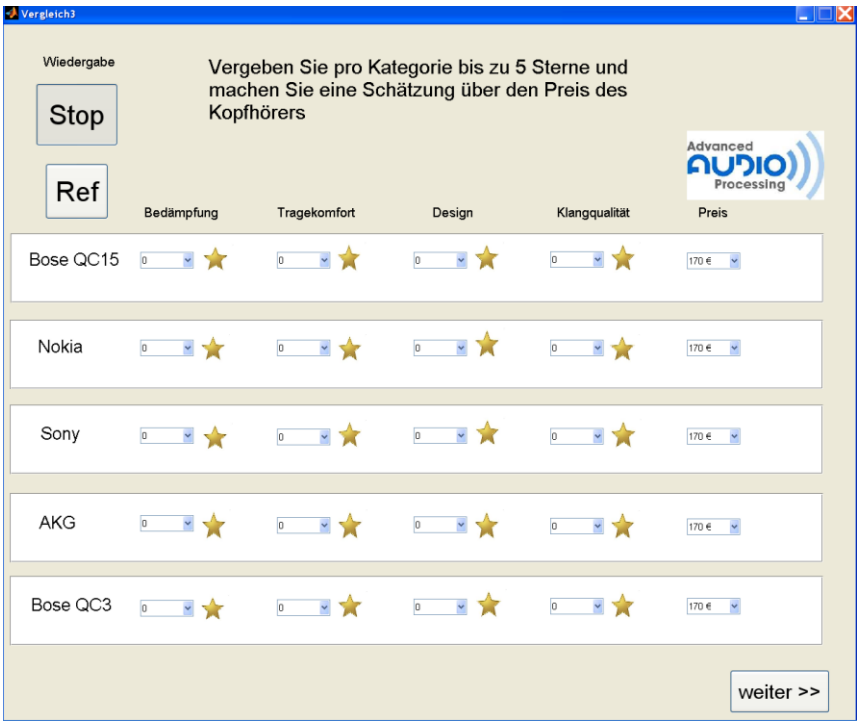

Figure 2.7: In the last part of the listening test, the subjects could see the 5 ANC headphones and judged noise reduction, comfort, design, sound quality by awarding a different amount of stars. Additionally, an estimate about the price could be given.

The results in the *noise reduction* category once again show the same ranking as the blind evaluation in part 2. Also, the ranking in terms of comfort is the same, as can be seen in Figure 2.8. The only category where headphone Nr. 1 is not ranked in the first place is sound quality. The price estimation finally reflects the overall judgment.

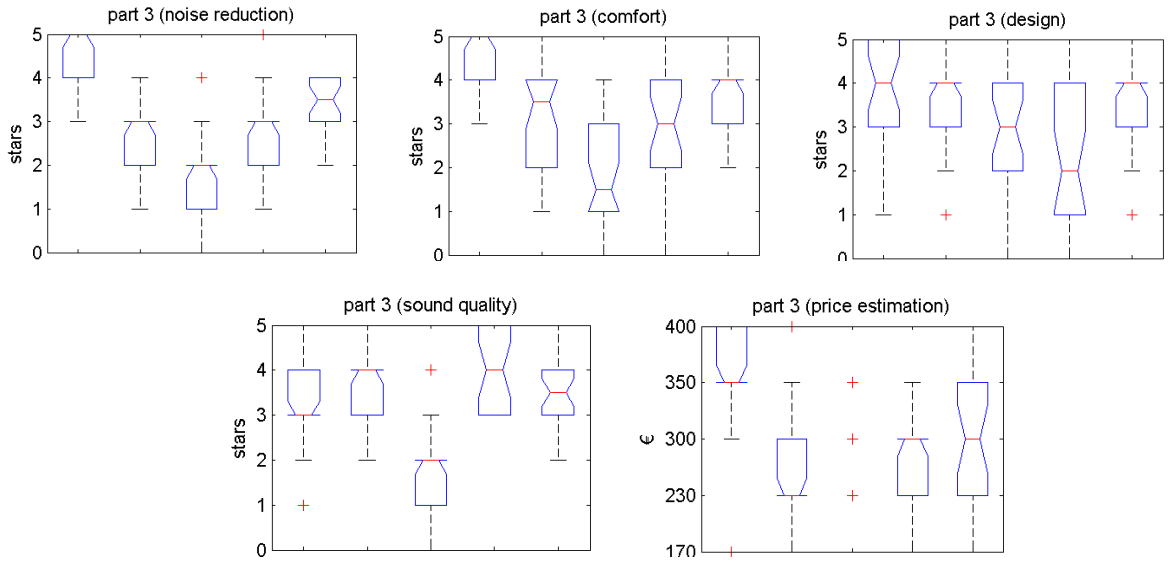

Figure 2.8: Subjective judgment in five categories. The category noise reduction shows the same results as the blind 2nd part of the listening test.

2.3 Regression between Measurements and Subjective Evaluation

Figure 2.9, once again, shows the differences between part 1 and 2 of the listening test. Headphone Nr. 4 and 5 changed places. Apparently, the headphone Nr. 5 does not match very well on the Brüel & Kjaer HATS. Therefore the recordings that were made with this coupler reached less ANC. On the other hand, headphone Nr. 4 seemed to fit better on the HATS than on real person's ears. This finding once again urges to examine the correlation of the coupler results with subjective evaluations.

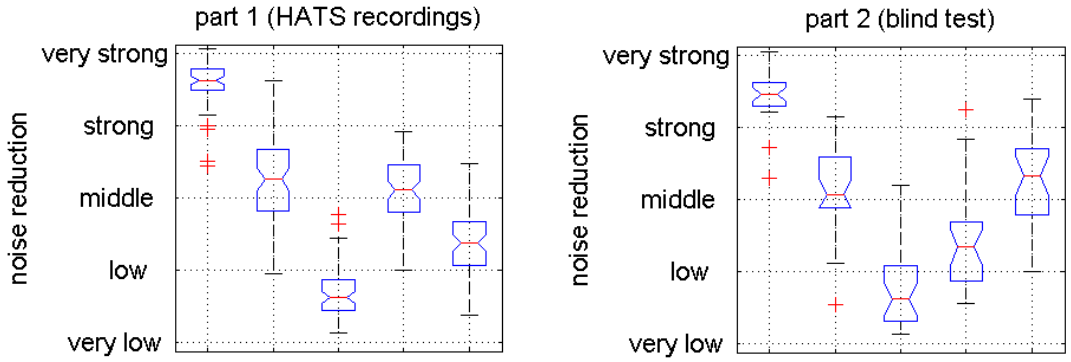

Figure 2.9: The ratings of the 5 headphones (over all three noises) differ from part one to part two of the listening test. The results of part 2 are used for the regression.

In order to get more differentiated regressions, the measurement data from different angles of incident sound are divided into six groups including measurements from

- -40° to 40° (frontal direction)
- 50° to 130° (left lateral direction)
- 140° to 220° (dorsal direction)
- -50° to -130° (right lateral direction)
- from all directions
- from surround positions (0°, +/- 30°, +/-110°)

Additionally they are post processed in five different ways:

- Broad band (BB): Logarithm of the signal power from 20 Hz - 20 kHz
- Low band (LB): Logarithm of the signal power from 20 - 100 Hz
- Mid band 1 (MB1): Logarithm of the signal power from 100 - 700 Hz
- Mid band 2 (MB2): Logarithm of the signal power from 700 - 3000 Hz
- Sone: loudness over the broadband signal

With all four measurement tools, this leads to a total of 120 predictors that are used in a stepwise regression to represent the subjective evaluations.

2.3.1 Stepwise forward Regression

A stepwise forward regression starts with one predictor that best explains the variability of the target (the subjective evaluations) [1]. In every following step another predictor is included or removed from the model, always with the goal to increase the coefficient of determination (R^2), which relates the residual sum of squares (prediction error variance, SS_{err}) with the total sum of squares of the target (sample variance, SS_{tot})

$$R^2 = 1 - \frac{SS_{err}}{SS_{tot}}. \tag{1.1}$$

The result of the stepwise forward regression can be seen in Table 1.1. Three predictors are used for the regression:

- Logarithm of the signal power from 20 Hz - 20 kHz, measured with artificial ear Nr. 2 with the measurement signals coming from all directions.
- Logarithm of the signal power from 100 - 700 Hz, measured again with artificial ear Nr. 2.
- Logarithm of the signal power from 20 Hz - 100 Hz, measured artificial ear Nr. 3 with the measurement signals coming from surround positions.

Table 1.1: Results of the stepwise forward regression. Out of 120 predictors, three are chosen for the regression. The maximal Cook's distance has the extreme large value of 25 451.

Artificial ear	direction	post-processing	*b*	R^2	max *D*
			-9.123	0.79	25 451
2	all	log(P(20-20 000Hz))	1.273		
2	all	log(P(100-700Hz))	-2.778		
3	surround	log(P(20-100Hz))	-0.846		

The coefficients of the predictors have different signs, which means that one measurement result is subtracted from the other to yield a prediction of the perceived noise reduction. As all measurements should have the same tendency (less sound pressure with better ANC), it is questionable if this regression is not over fitting the data. A robustness

measure of regressions is the Cook's Distance *D*. It compares the regression results, when observation points (evaluation-data for one headphone) are missing. *D* should not be greater than 1, however, for the above regression it is over 25 000 in the worst case. Also stepwise regressions with predictors of only one headphone are not more reliable. Therefore a simple regression with only one predictor is proposed.

3 Analogue ANC

3.1 Analogue Feedback ANC

Most commercial ANC-headphones use an analogue feedback (also called closed loop) from a microphone inside the ear cup to the loudspeaker [2,3,4], as depicted in Figure 3.1. The advantages of the closed loop approach are that it does not require much hardware and that the ANC is independent of the incident sound direction. The drawback is that a closed loop can run unstable if the filter H in the feedback loop is not designed very conservatively.

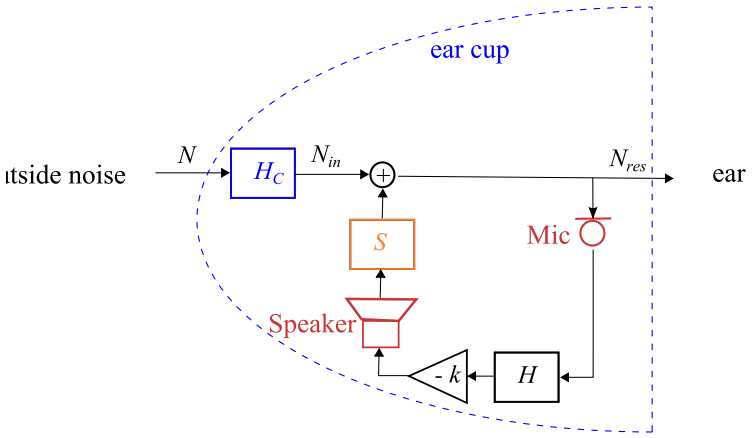

Figure 3.1: Block diagram of an ear cup with analogue feedback ANC. The microphone signal inside the ear cup is fed back to the loudspeaker via the filter *H* and inverted with the gain *k*. Block *S* denotes the transfer path from the speaker to the microphone (also called secondary path). The passive noise reduction due to the ear cup is represented by the block H_c.

3.1.1 Stable Feedback Design

The transfer function of the closed loop in Fig. 3.1 reads as

$$\frac{N_{res}}{N} = \frac{H_c}{1 + kHS} \tag{2.1}$$

and the goal is to reduce N_{res}. This can be done by increasing the denominator, hence the gain factor k. The noise is reduced because the feedback signal is added with opposite phase ($-k$) to the entered noise N_{in}. However, if the phase of the feedback loop turns another 180°, the signals at the summation point superpose constructively and the feedback loop runs into a resonance catastrophe. The filter H is inserted to attenuate the frequency, where the phase of the open loop has turned to 180°. Thus, H is designed with respect to the frequency response of the open loop to keep the closed loop stable [5,6].

Figure 3.2 shows the open loop frequency response of an exemplary headphone without any filter H and for k= -1. Three different wearing situations from very leaky to tight are considered. The wearing situation changes the acoustic impedance of the headphone and has especially influence on the low frequencies of the secondary path.

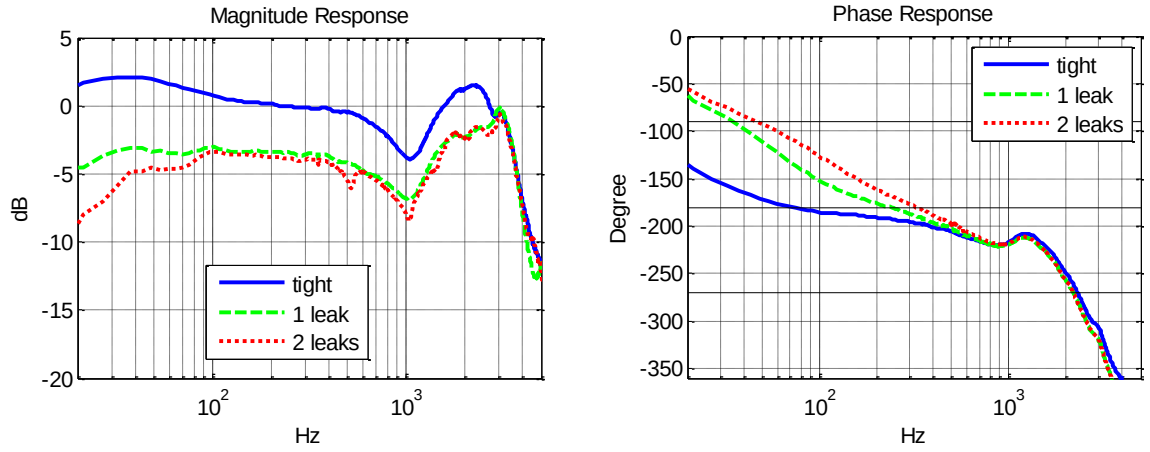

Figure 3.2: Magnitude and phase response of the secondary path *S* for three differently leaky wearing conditions. Two things can be observed: 1. The leakier the headphone, the stronger is the amplitude roll off at low frequencies. 2. The phase response of the tight headphone stays in a +/-45° range around 180° until 1300 Hz. A phase shift of another 180° is reached at 3500 Hz. At this frequency the magnitude is at -2 dB. Hence there is no room to increase the gain factor *k*.

The phase of the inverted secondary path turns to -360° (and is in phase again) at 3500 Hz. At this frequency, the magnitude response should lie clearly below 0 dB. As the magnitude at this frequency is at -2 dB only, the gain factor *k* cannot be increased anymore; hence hardly any ANC is possible. Inserting a low pass filter *H*, helps to boost the low frequencies, while attenuating the high ones. A shelving filter even works better, because it has a flatter phase response. It allows a gain factor of 15 dB for low frequencies and still attenuates the critical frequencies for 10 dB, as it can be seen in Figure 3.3.

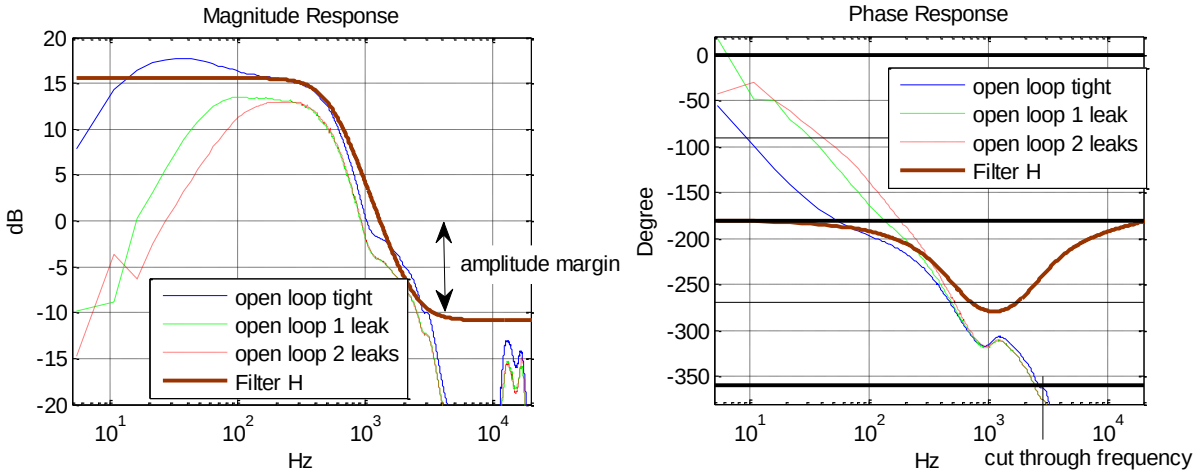

Figure 3.3: Magnitude and phase response of the stabilization Filter *H* and its consequences on the open loop response for different wearing conditions. The phase of the open loop does now reach the -360° already at 2500 Hz because of the phase drop of the shelving filter. However, the magnitude is attenuated 10 dB at this frequency, while the lower frequencies are amplified to approximately 15 dB, depending on the tightness of the wearing condition.

With the proposed feedback loop, an ANC of 15 dB up to 400 Hz can be expected for tight headphones, as it is shown in the ANC simulation of Figure 3.4.

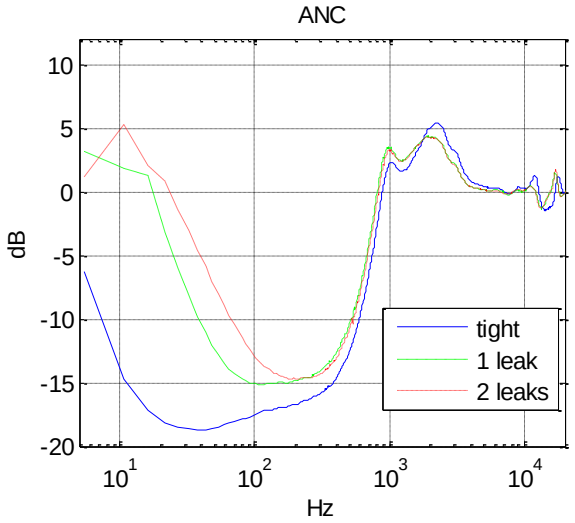

Figure 3.4: Simulation of the ANC performance with the proposed filter *H* in the feedback loop for different wearing situations. For a tight headphone an attenuation of 15 dB in a bandwidth up to 400 Hz is expected. The overshoot at very low frequencies and above 1000 Hz is very small. Hence, a stable feedback loop is expected.

In order to increase the bandwidth of ANC, the phase of the open loop response would need to have a flatter slope. This could be reached by a linearization of the loudspeakers, as described in the following section.

3.1.2 Loudspeaker linearization

The magnitude as well as the phase response of a loudspeaker can be flattened, if the loudspeaker is damped. Damping can be increased by reducing the total resistance of the loudspeaker, e.g. by making the source resistance of the amplifier negative [7]. This can be achieved via a feedback of the loudspeaker current, as depicted in Figure 3.5.

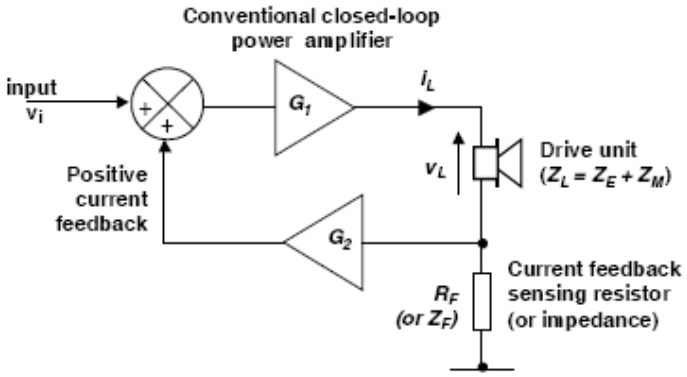

Figure 3.5: Loudspeaker linearization with current feedback according to Turner & Wilson [7].

The undamped transfer function of a loudspeaker can be simulated with the Thiele-Small-parameters. The Thiele-Small-parameters of an exemplary headphone are listed in Table 2.1.

Table 2.1: Thiele-Small-Parameters of the prototype headphone.

Thiele-Small-Parameter	Abbreviation	value	unit
Total electrical resistance	R_T	25.1	Ohm (Ω)
Force factor	Bl	1.836	Tm
Voice coil inductance	L_E	0.2	mH
Mass	M	0.0773	g
Coefficient of friction	K_F	0.0158	Ns/m
Spring stiffness	K_S	176.51	N/m

The loudspeaker transfer function from voltage U(s) to the voice coil velocity V(s), where s is the Laplace transform operator, reads as

$$\frac{V}{U} = \frac{sBl}{(R_T + sL_E)(s^2M + sK_F + K_S) + s(Bl)^2}. \tag{2.2}$$

The transfer function of the loudspeaker with and without the current feedback of Figure 3.5 is compared in Figure 3.6. The components are chosen to be:

- G_1 = 1,
- G_2 = -8 and
- R_F = 3 Ω.

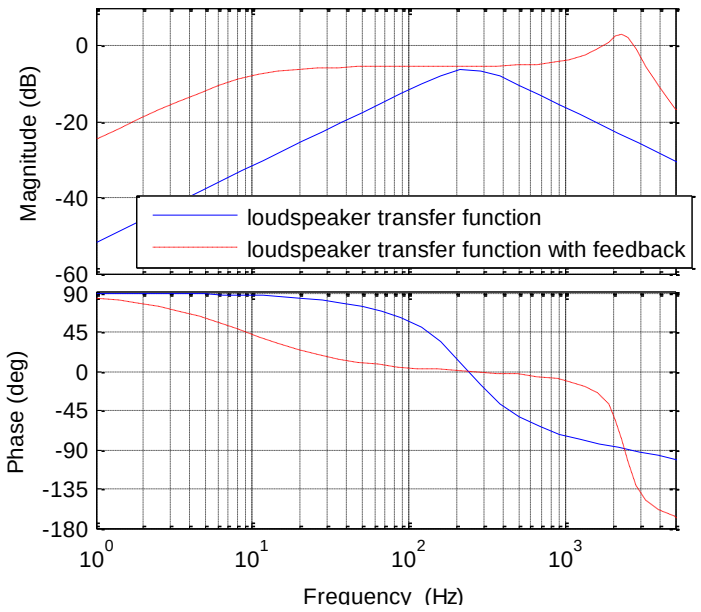

Figure 3.6: Comparison of the loudspeaker transfer function with and without current feedback. With current feedback, the magnitude as well as the phase response is flattened. The reduced resistance R_T increases the influence of the voice coil inductance onto the transfer function. This can be seen in the peak at 2200 Hz.

The current feedback flattens the magnitude and phase response, but it increases the influence of the voice coil inductance onto the impedance of the loudspeaker. This inductance now causes a resonance at 2200 Hz. In order to attenuate this resonance, another low pass filter would be needed in the ANC feedback loop. This low pass however would again cause a stronger phase roll off. Hence the positive effect of the loudspeaker linearization is undone. It is therefore easier and more efficient to design the feedback ANC-headphone without loudspeaker linearization.

3.2 Analogue Feedforward ANC

Analogue feedforward (open loop) ANC only needs a microphone outside the ear cup [19,20]. It has a fixed analogue filter that simulates the transfer function form outside the ear cup to inside. However this transfer functions varies with the direction of incident sound. Open loop ANC headphones therefore either work very well for one dedicated direction of incident sound, or they work on average for all possible directions of incident sound.

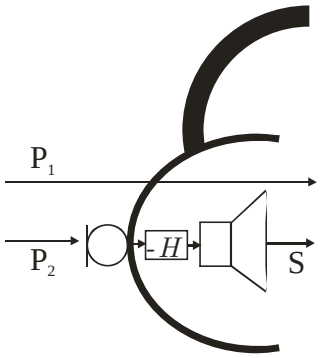

Figure 3.7: Open Loop headphones have only one fixed filter *H* that should simulate all possible transfer functions from outside to inside.

3.2.1 Ideal Open Loop Filter

It shall be investigated which measurement direction is most representative for all other directions of incident sound. The ratio K=P1/P2 was measured for eight angles of elevation (from 0° to 90°) and twelve angles of azimuth (0° to 330°).

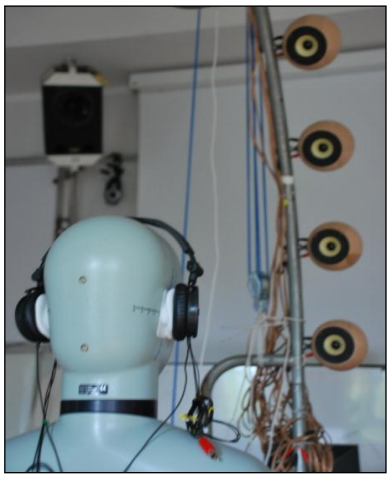

Figure 3.8: Setup to measure the open loop transfer functions for 8 angles of elevation and 12 angles of azimuth.

An exemplary set of transfer functions K is shown in Figure 3.9. They all show low-pass characteristics because of the headphone's passive attenuation of high frequencies.

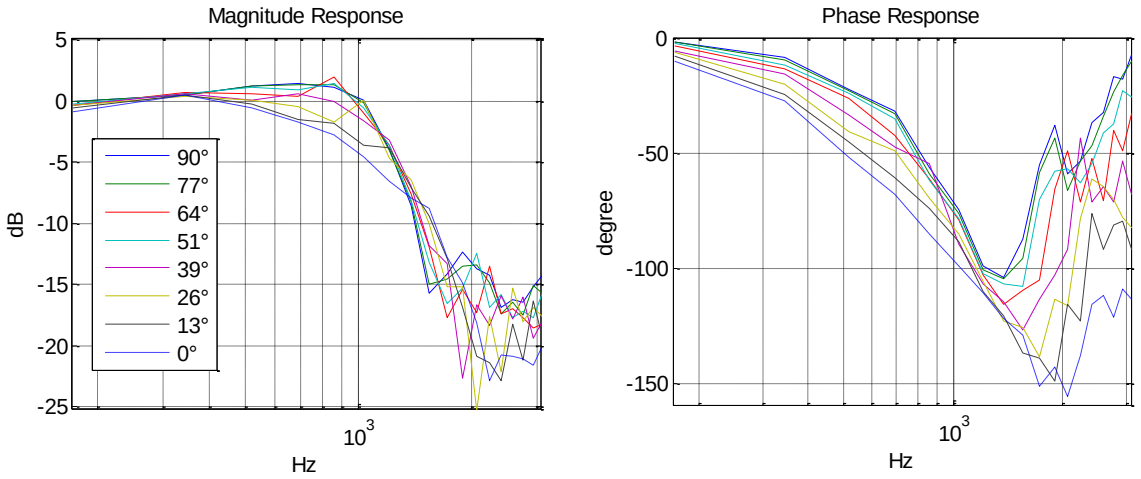

Figure 3.9: Magnitude and phase response of the ratio $K=P_1/P_2$ for 8 angles of elevation and 0° azimuth (frontal direction). Especially the phase response varies remarkably above 1200 Hz.

With the measurement data, ANC is simulated with the difference K - H, where H is the chosen open-loop filter. In order to figure out which direction of incident sound is most representative for all the other directions, we plug in different K_j for H, whereas the resulting frequency response is reduced to a Phon value. Thus

R_{ij}=phon{$K_i(\omega) - K_j(\omega)$},

where R is the ANC residual in Phon and i and j vary from 1 to 85 (corresponding to the 85 measured directions of incident sound). The resulting matrix R is symmetric and the sum over all columns (or rows respectively) is a measure on how well the transfer function

of the corresponding direction cancels all other transfer function. The comparison shows that the frontal transfer function for 39° elevation reaches the best median ANC over all directions of incident sound. Table 3-1 lists the three transfer functions with the best median ANC. All three transfer functions come from elevated angles, whereas +39° elevation is predominant. The first two transfer functions have a frontal direction and the third one comes dorsal, whereas frontal and dorsal transfer functions are very similar due to the head-(phone) symmetry. It can thus be concluded that frontal transfer functions from approx. 40° of elevation are the best representation of the overall transfer functions.

Table 3-1: Directions of the transfer functions with the strongest median noise-reduction. The frontal transfer function from 39° elevation reaches the best median noise reduction of 9.4 Phon (evaluated in a bandwidth of 2500 Hz).

Elevation	Azimuth	Noise Reduction
39°	0°	14.3 Phon
39°	-30°	13.8 Phon
51°	-150°	13.5 Phon

Figure 3.10 compares the ANC of the ideal transfer functions with transfer functions from either lateral or horizontal directions. The difference in the median ANC is at least 6 Phon.

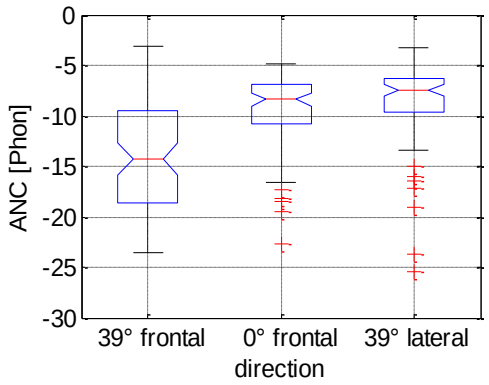

Figure 3.10: Noise reduction level of three different transfer functions over all directions of incident sound in Phon. The worst ANC is reached with lateral transfer functions. Also transfer functions from the horizontal plane (0° elevation) do not reach the best ANC.

If several open loop filters are combined, more directions of incident noise can be optimally fought. The combination of the different open loop filters can be adaptive via adjustable filter gains.

A Principal Component Analysis (PCA) is used to find those eigenvectors which best explain the variability in the measured transfer functions. The PCA in the bandwidth of 2500 Hz shows that four (mathematically derived) transfer functions account for almost 99% of the variability in the measured transfer functions (See Figure 3.11). These four transfer functions are modeled as IIR filters. As the modeled filters differ from the original PCA-transfer-functions, one cannot expect the same results in the explanation of the variability. Therefore, four diverging measured transfer functions are additionally modeled as IIR filters. The frequency response of the eight modeled filters is shown in Figure 3.12. The difference between a modeled filter and a measured transfer function can be seen in Figure 3.13.

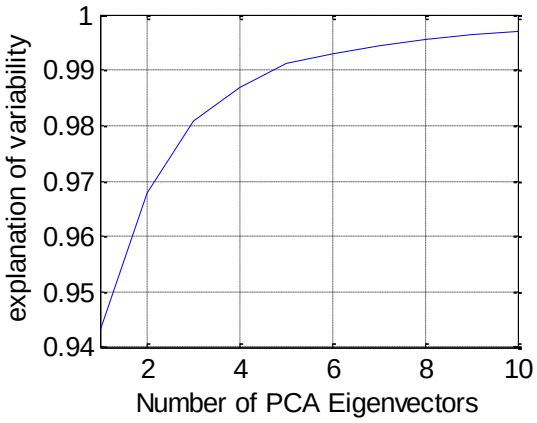

Figure 3.11: The explanation of the measured transfer function variability in dependence on the number of used PCA eigenvectors. With four eigenvectors already more than 98% are explained.

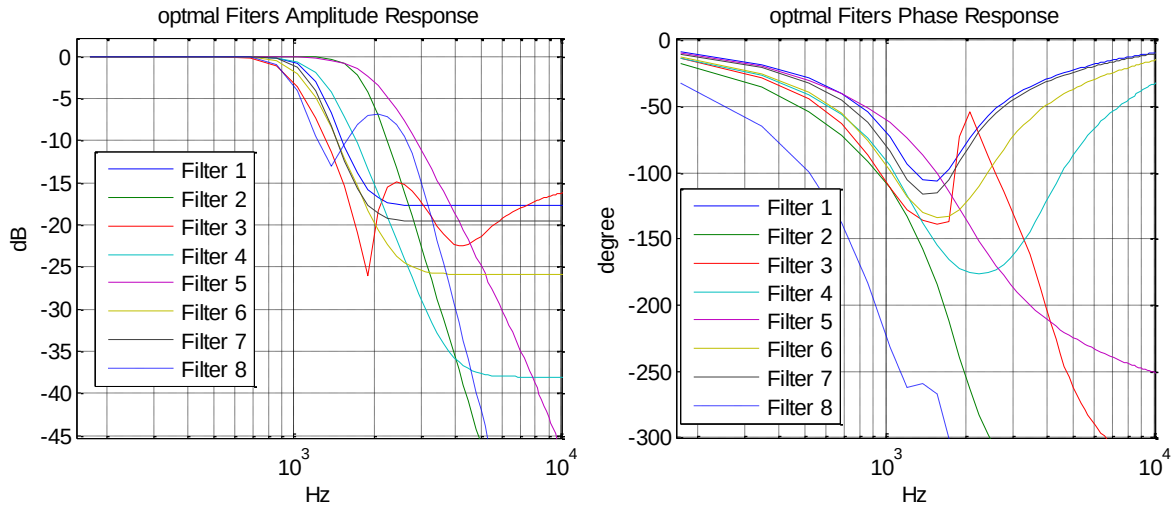

Figure 3.12: Magnitude and phase response of the 8 modeled IIR filters.

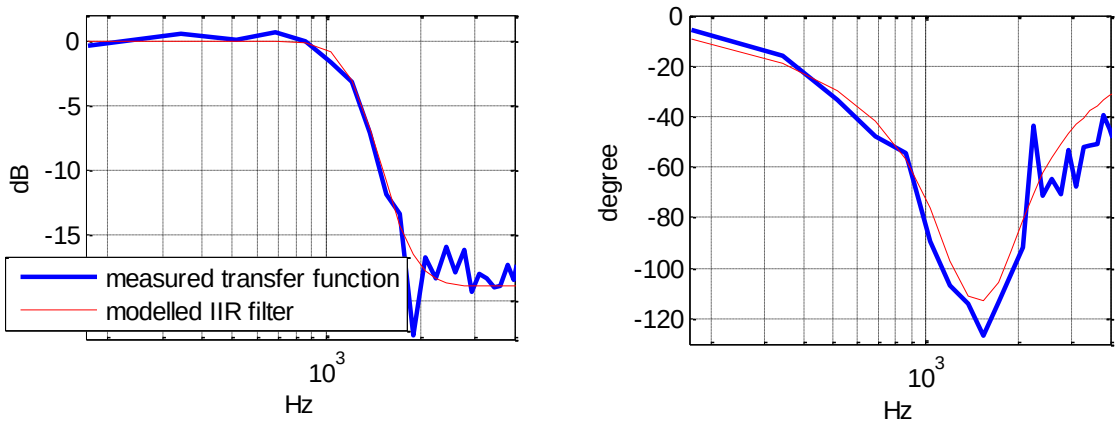

Figure 3.13: Difference of a measured transfer function and the modeled IIR filter in the frequency response.

A weighted combination of the eight modeled filters shall now explain the variability of all transfer functions over all measured directions. A stepwise forward regression is used to determine in which order the filters are added into the model. This way, it can be compared how much improvement is reached by adding another filter. This comparison is shown in Figure 3.14. Every additional filter brings a statistically significant improvement to the ANC, except for the second filter. The median ANC over frequency is shown in Figure 3.15. It can be seen that an increased amount of filters brings up to 5 dB more broadband ANC.

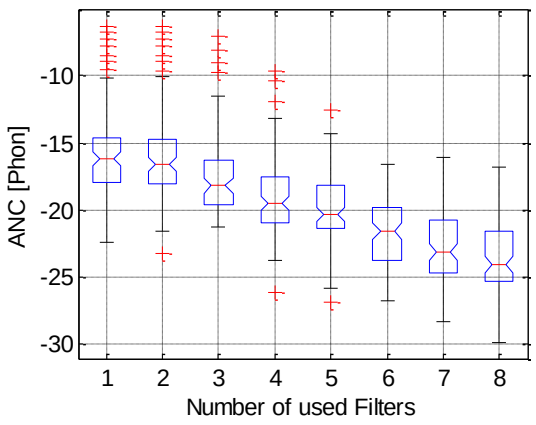

Figure 3.14: ANC over all directions of incident sound dependent on the number of used filters in Phon (evaluated up to 2500 Hz). With one filter, a median noise reduction of 16.2 Phon is reached. With 8 filters, 24 Phon are reached.

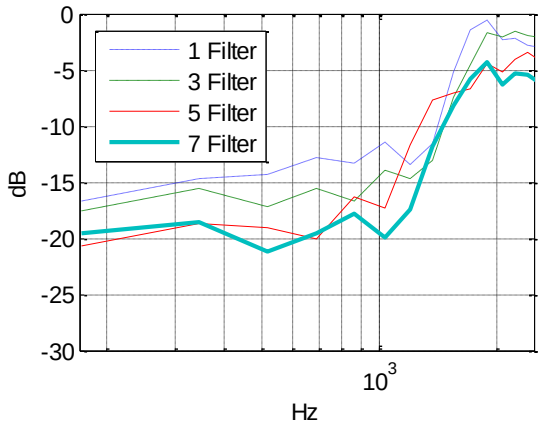

Figure 3.15: Median ANC frequency response over all directions of incident sound dependent on the number of combined filters.

Adaptively weighted analogue filters allow the adaptation to different sound-fields and do not have the latency problem of digital ANC headphones. In order to design the parallel analogue filters, transfer functions K(jω)from the outside-to the inside microphone were measured. Fig. 3.10 shows their amplitude and phase variance.

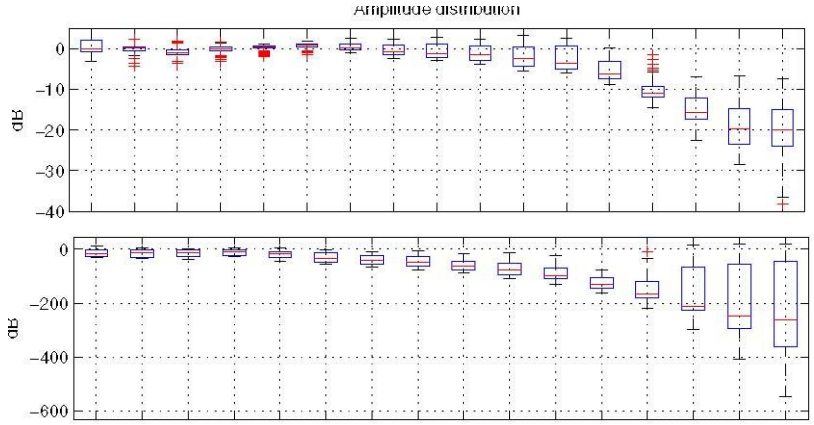

Figure 3.10 Amplitude and phase distribution of the measured transfer functions

The dominant transfer functions were extracted via a Principal Component Analysis (PCA) and then modeled as a third order IIR filter H(jω). With a matrix of all measured transfer functions K and a matrix of modeled IIR Filters H the matrix of least squares weights for the filters read as

$$W = (H^T H)^{-1} H^T K.$$

The residual error follows to

$E = K - HW$

The frequency dependent residual error is calculated for 1 to 8 modeled Filter $H(j\omega)$ and expressed as a single Phon value. The contribution of each additional Filter to the ANC performance is shown in Fig. 3.11.. It can be seen that only the second additional filter brings a statistically significant ANC improvement. The amplitude and phase response of the first two filters is shown in Fig. 3.12. The ANC performance in the LMS approach is shown in Fig. 3.13.

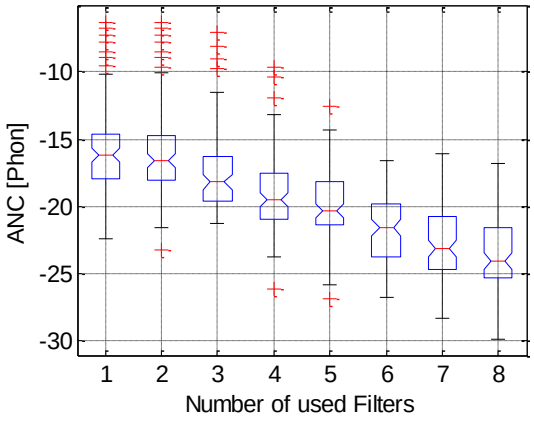

Figure 3.11: Contribution of additional parallel filters to the ANC performance.

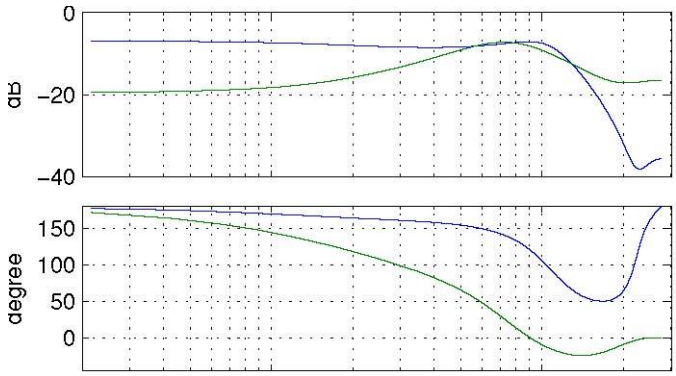

Figure 3.12: The two filters which are modeled from the first two PCA transfer functions.

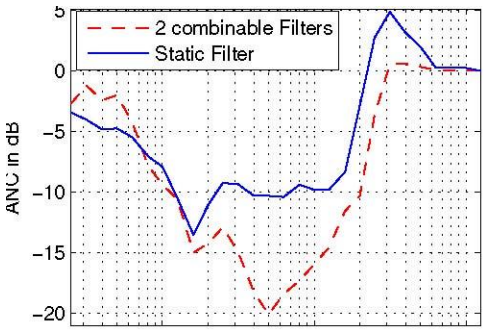

Figure 3.13: Analogue Feedforward ANC with one static Filter of 6th order and two adaptively combinable Filters of 3rd order.

4 Adaptive ANC

Digital ANC has the advantage that it can be adapted to different conditions, like the fitting of the headphone or the directions of the incident noise. However, it suffers from the latency that is caused by the AD- and DA-conversion. Therefore, with common audio converters, ANC is more or less limited to periodic signals.

4.1 Adaptive Feedforward ANC

An adaptive filter needs two inputs. Besides the reference signal (e.g. the noise outside the headphone), it also needs an error signal that gives feedback about the performance of the filter. In an ANC headphone, this error signal is sensed with a microphone inside the ear cup, where the noise should be reduced. (See Figure 4.1.)

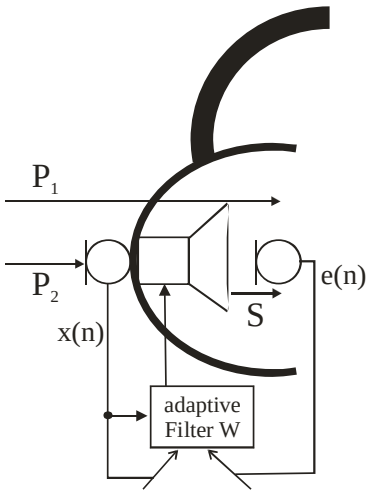

Figure 4.1: The adaptive-feedforward ANC-headphone needs two microphones. One for a reference noise signal and another one that tracks the residual error of the ANC inside the ear cup.

The filter coefficients are adapted with the reference input and the error signal, as indicated in Figure 4.1. There are several algorithms for the coefficient update, among which the Normalized Least Mean Squares (NLMS) algorithm is the most popular one. It is easy to implement, does not require much resources and is more stable than most of the other adaptive algorithms [8]. The coefficient update equation reads as

$$\vec{w}(n+1) = \vec{w}(n) + \mu e(n) \frac{\vec{x}(n)}{\vec{x}'(n)\vec{x}(n)}, \tag{2.4}$$

where $\vec{w}$ is the vector of filter coefficients, n is the time index, $\vec{x}$ is a vector of noise input-samples and μ is the learning rate that lies in the interval [0, 2]. As can be seen in this equation, the error signal e and the input signal x need to arrive at the same time basis n. Figure 4.2 shows, that the input x is delayed by one AD conversion. The error e is delayed by the same ADC, but additionally by a DAC, the secondary path S and another ADC. Thus, the same additionally delay has to be introduced to x for the coefficient update in the LMS algorithms. Therefore an estimate of the secondary path $\hat{S}$ has to be implemented. This modified structure is called filtered x LMS (fxLMS).

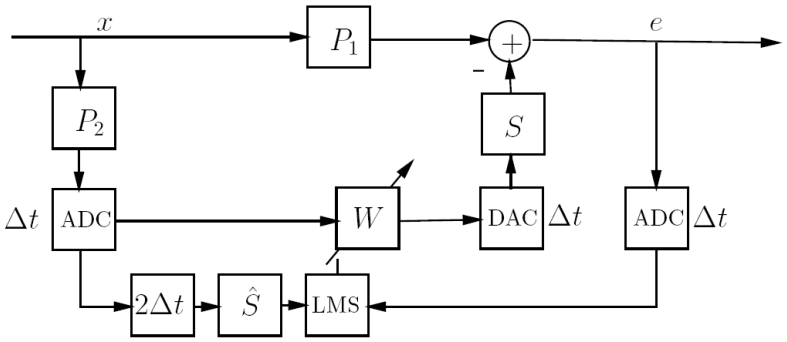

Figure 4.2: Block diagram of ANC with the filtered x LMS algorithm. The outside microphone measures the noise *x*, that comes along the direct transfer path P_2. The inside microphone measures the superposition of *x* that entered the headphone via P_1 and the anti-noise signal played back by the loudspeaker (over the secondary path *S*). The input signal *x* has to be delayed with two times the conversion time and an estimate of the secondary path $\hat{S}$ before it comes to the coefficient update in the LMS block.

4.1.1 Latency Influence on ANC

On the one hand side, there is a gain of sound travel-time from the outside microphone to the error microphone in the ear cup. It is the group delay of the ratio P_1/P_2. Because of the enclosure, this group delay is rather independent of the direction of incident sound. As depicted in Figure 4.3, it is almost the same for frontal sound as for lateral (where the largest group delay is expected). However, this gain of time decreases, if the headphone is leaky. Figure 4.4 shows that it can even become negative, which means that the noise arrives at the error microphone before it arrives the outside microphone.

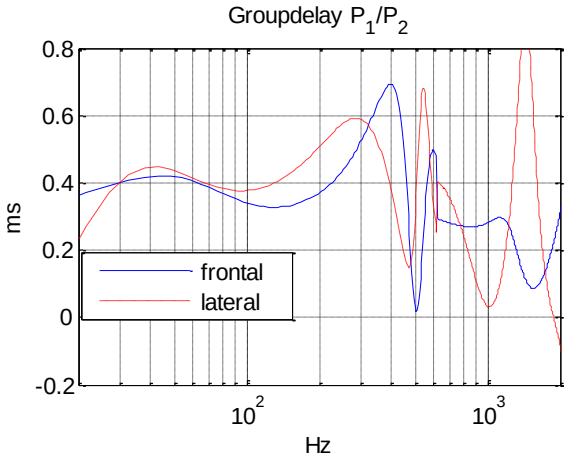

Figure 4.3 The group delay of P_1/P_2 represents the gain of sound travel-time from the outside microphone to the error microphone. Due to the tightness of the enclosure, it does not depend on the direction of the incident sound.

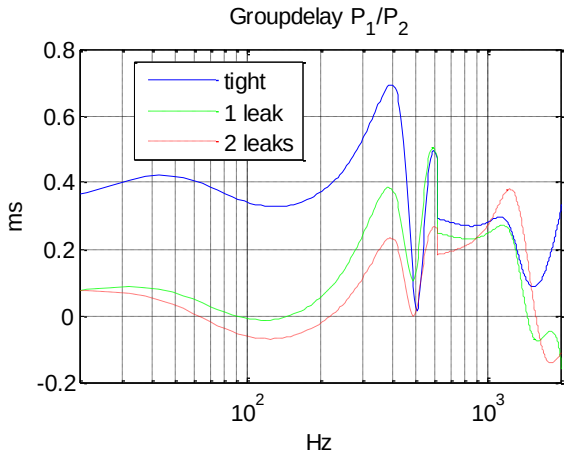

Figure 4.4 Group delay of P_1/P_2 for frontal sound and differently tight headphones. The gain of time is lost, if the enclosure is leaky.

On the other hand side, there is the delay of signal x and e due to the AD- and DA conversion and the group delay of the secondary path S, which is above 0.5 ms for frequencies below 100 Hz. (See Figure 4.5.) So the gain of time of about 0.4 ms faces a loss of time, which is usually much larger. Thus, the adaptive filter has a causality problem. In this case, the fxLMS algorithm acts as a predictor. The ANC then depends on the predictability of the noise.

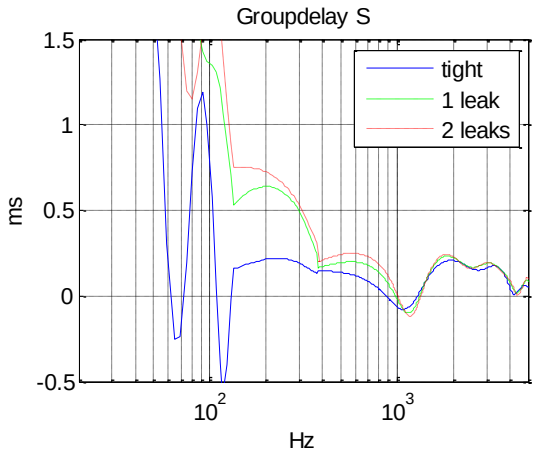

Figure 4.5: Group delay of the secondary path for differently tight headphones. The group delay is mostly around 0.2 ms. For frequencies below 100 Hz, it increases rapidly, especially for leaky headphones.

Figure 4.6 compares ANC simulations for different latencies. The simulations are done with recorded airplane noise with real measurement data for *S, P_1* and *P_2*. The direction of incident sound (P_1/P_2) changes from 0° to 90° azimuth in the middle of the simulations, which lasts one second in total. The simulations show that effective ANC can only be reached with latencies below 250 µs. (See also [10:13].) Optimal ANC is reached with about 60 µs latency.

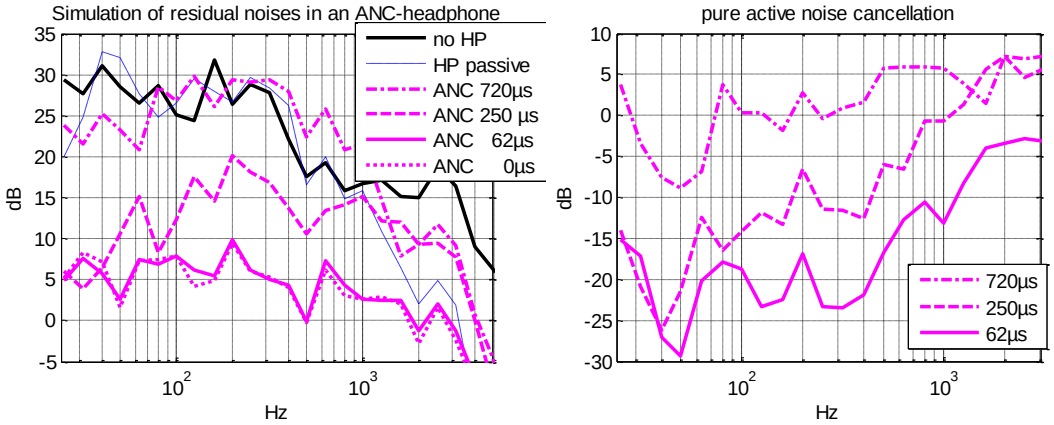

Figure 4.6: The simulation on the left compares the SPL of airplane noise at the ears without headphones (no HP), with a passive headphone, and with ANC of different latencies. The right figure shows the influence of pure active noise cancellation.

4.1.2 Tightness Influence on ANC

Figure 4.4 and Figure 4.5 showed that the gain of time from the outside microphone to the inside microphone and the group delay of the secondary path depend on the tightness of the headphone. A leaky headphone has two times negative influence on ANC. On the one side, it decreases the gain of sound travel-time, on the other hand it also decreases the group delay of the secondary path and hence the reaction time of the system. Figure 4.7 compares the ANC performance of differently tight headphones with a latency of 60µs. Again measured S, P_1 and P_2 are used for the simulation. The increased leakage deteriorates the performance drastically.

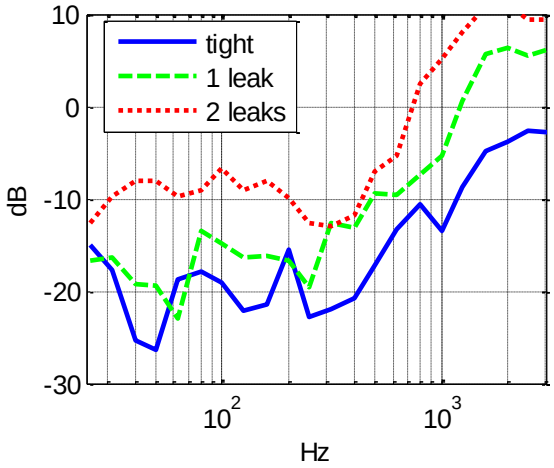

Figure 4.7: ANC simulation for differently tight headphones at a latency of 60µs. The leakage deteriorates the performance drastically.

4.2 Adaptive Feedback ANC

4.2.1 Feedback fxLMS

There also exists a feedback strategy for adaptive noise cancellation [14], like depicted in Figure 4.8. In this strategy only the error microphone inside the ear cup is needed. Adaptive feedback ANC works under the assumption that we know the anti-noise signal that is played back by the headphone. Hence the noise can be regenerated from the error signal as

$$\hat{x}_{in} = e + \hat{y}, \tag{2.5}$$

where $\hat{y}$ is an estimate of the loudspeaker signal. The advantage of the feedback strategy on the one hand is, that it takes the entered noise as reference input instead of the noise outside the headphone and that this entered noise is already low pass filtered, which makes some processing steps, like anti-aliasing filtering easier. On the other hand, it completely loses the gain of time that the outer microphone had with respect to the inner one.

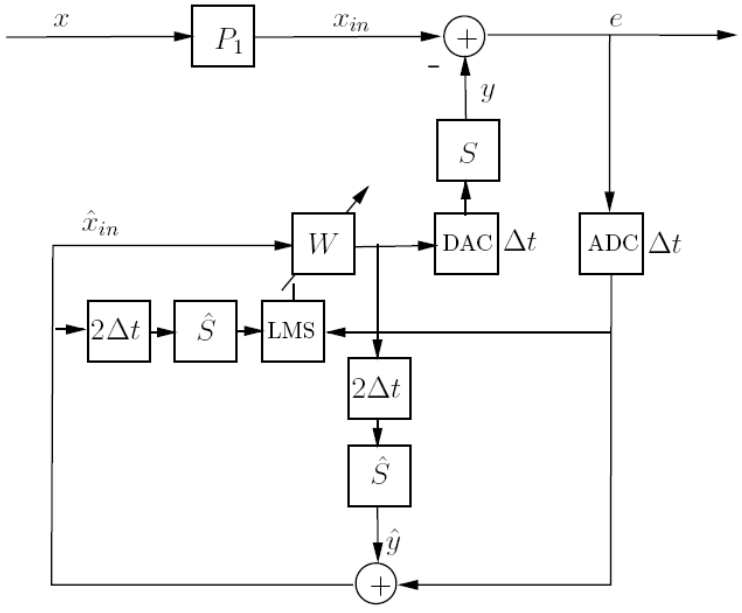

Figure 4.8: Adaptive Feedback ANC. The reference input signal $\hat{x}_{in}$ is generated from the error signal *e*. Hence, only one microphone inside the ear cup is needed.

Figure 4.9 compares the feedback with the feedforward ANC. Because of the low pass filtered input, the feedback method generates less error at higher frequencies. However the general performance of the feedforward structure is - calculated according to [15] - almost 3 Phon better.

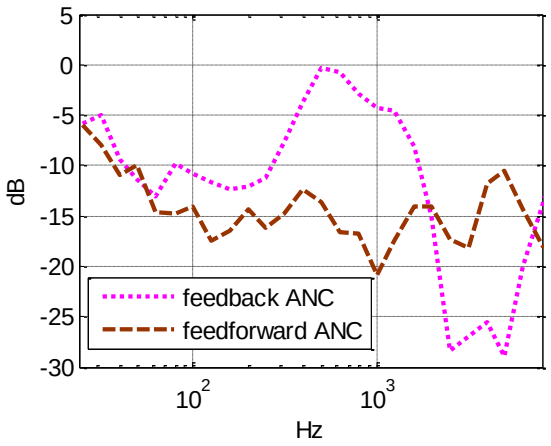

Figure 4.9: This simulation of combined active and passive noise attenuation compares the feedback- and the feedforward ANC-algorithm. Latency was set to 250µs. Although the feedforward method generates a larger prediction error around 3000 Hz, it over all still performs better than the feedback method.

4.2.2 Feedback ANC with Kalman Filters

The feedback structure does not generate as large prediction errors as the feedforward structure at high frequencies. Still the feedforward structure of the fxLMS reaches a better ANC. In literature [16], a Kalman filter is proposed as predictor. However, the Kalman filter does not predict better, it only is more robust against measurement noise. In Figure 4.10, the influence of the Kalman filter is compared for sensor noise that is 40 and 20 dB under the noise inside the headphone. If the sensor noise is large (-20 dB) the Kalman filter stabilizes the adaptive filter and prevents it from producing large errors at high frequencies.

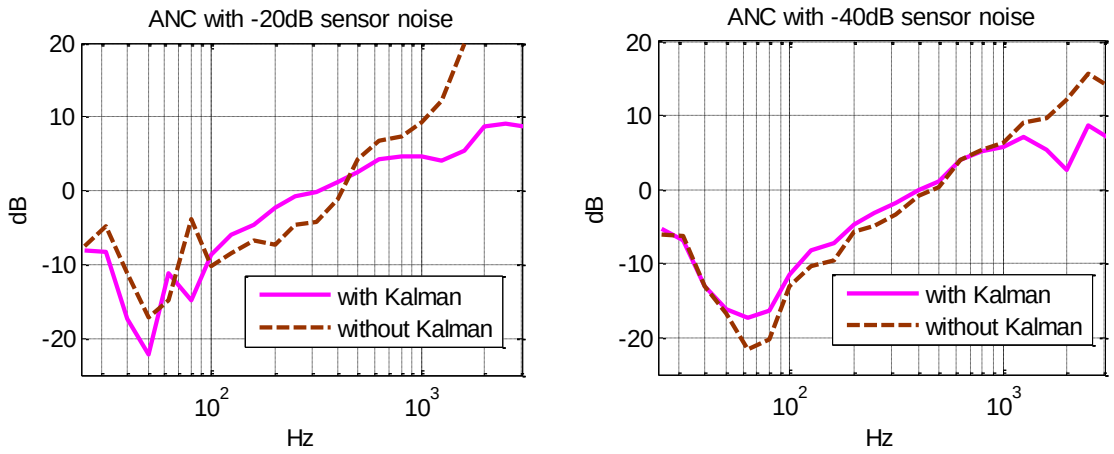

Figure 4.10: ANC simulations with and without Kalman filter and a latency of 250µs. For the left figure, the sensor noise is 40 dB below the actual noise in the headphone. The Kalman filter has hardly any effect here. For the right figure, the sensor noise is only 20 dB under the actual noise. In this case, the Kalman filter prevents the adaptive filter to generate large errors at high frequencies.

4.2.3 Feedback Active Noise Control with sparse update of the prediction filter

The latency of conventional audio converters severely limits the ANC performance. In these cases, the adaptive filter has to predict the noise to compensate for the delay. In the feedback ANC approach, the prediction is based on noise that actually entered the headphone. This has two advantages. Firstly, ANC is independent from the direction of incident noise and also works in diffuse sound-fields [17, 18]. And secondly, the upper frequencies of the entered noise are damped by the ear cup. This low-pass characteristic is advantageous when it comes to signal prediction [19].

In literature, prediction is mostly done by different kinds of the least mean squares (LMS) algorithm [20, 21] or by iterated one-step-ahead predictions [16]. Both algorithms are based on sequential updates of the prediction filter. In this section, it is shown how a direct multi-sample prediction leads to improved ANC results while the computational burden can still be kept low. In particular, the fact that noise signal statistics mostly change little is exploited to reduce the amount of updates. In the case of broadband noises, the signal characteristic is determined by the passive damping of the ear cups. Hence, the prediction filter can be designed a priori and no real-time computation is needed at all.

Headphones with feedback ANC, as depicted in Figure 4.11, only require one microphone inside each ear cup. This microphone measures the residual error signal *e(t)* which is the superposition of the entered noise *x(t)* and the played-back anti-noise *y(t)*. With omitted time dependency, *e = x + y*.

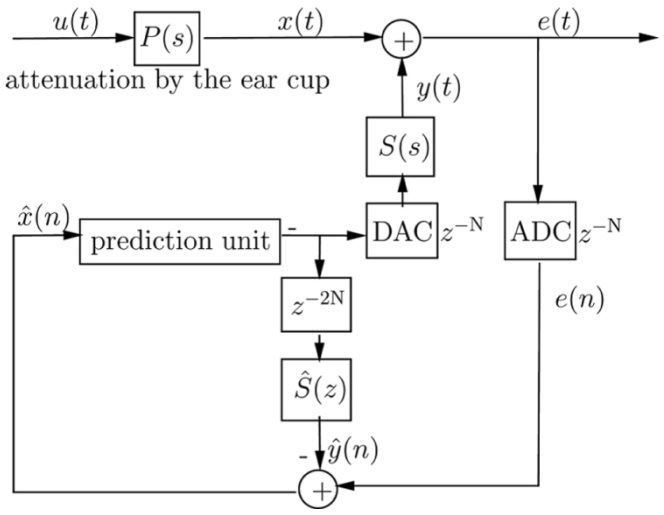

Figure 4.11: Digital feedback ANC: An estimate of the noise inside the ear cup $\hat{x}(n)$ is used as input for the prediction unit. The inverted output is played back to cancel the entered noise *x(t)*.

Since *y* should equal *x* with an inverted phase, an estimate of *x* is required. This estimate $\hat{x}$ can be obtained by subtracting the played-back anti-noise from the sensed residual error, $\hat{x} = e - \hat{y}$. The actual anti-noise *y* is digitally unavailable. This is because the digital noise cancellation signal is digital to analogue converted and modified by the loudspeaker transfer-function *S(s)*, also called secondary path. Thus, an estimate ˆy is generated by means of a secondary-path measure $\hat{S}(z)$.

The resulting noise estimate $\hat{x}$ is delayed by the digital to analogue converter (ADC) and the final anti-noise *y* will be delayed once again by a DAC and the group delay of *S(s)*. To compensate for these delays, the prediction unit tries to predict future samples. If ADC and DAC each have a latency of N samples, at least 2N samples have to be predicted.

Assuming that a correct estimate of x is given, $\hat{x}(n)$ equals $x(n - N)$. With this, the prediction unit builds a weighted sum of the available past samples to predict the future noise sample

$$x(n+N) = \sum_{i=0}^{L-1} w_i x(n-N-i) \tag{2.6}$$

with L being the prediction order and w_i the coefficients of a linear prediction filter. The residual error e follows as

$$e(n) = x(n) - \boldsymbol{w}^{\mathrm{T}}\mathbf{S}\boldsymbol{x}(n - \mathrm{D}), \tag{2.7}$$

where w is the vector of filter coefficients, S is a convolution matrix of the secondary-path impulse response and $\boldsymbol{x}$ is a signal vector starting from D = 2N samples in the past. The minimum of the expected squared error leads to the well-known Wiener-Hopf equation [8] and to the solution of the optimal prediction filter

$$\boldsymbol{w}_{opt} = (\boldsymbol{S}\boldsymbol{R}_x\boldsymbol{S}^{\mathrm{T}})^{-1}\boldsymbol{r}, \tag{2.8}$$

where $\boldsymbol{R}_x$ is the autocorrelation matrix of the latest available noise samples

$$\boldsymbol{R}_x = \begin{bmatrix} r_0 & r_1 & \cdots & r_{L-1} \\ r_1 & r_0 & \cdots & r_{L-2} \\ \vdots & \vdots & \ddots & \vdots \\ r_{L-1} & r_{L-2} & \cdots & r_0 \end{bmatrix}$$

and $\boldsymbol{r}$ is a vector of autocorrelation elements starting from lag D

$$\boldsymbol{r} = \begin{bmatrix} r_D \\ r_{D+1} \\ \vdots \\ r_{D+L-1} \end{bmatrix}.$$

The matrix inversion in eq. (2.8) can be avoided with the Levinson-Durbin algorithm [22], but only if D = 1. The resulting one-step-ahead predictor can still be used for a delay of 2N samples when the linear prediction of eq. (2.6) is iterated 2N times. However, since the prediction filter is stable, the recursive one-step-ahead prediction converges to zero. Thus, the filter outputs have to be amplified to get a reasonable multi-sample prediction.

To avoid this problem, gradient search algorithms are often used for prediction problems with more than one sample delay. Gradient search algorithms like the normalized LMS use the noise estimate and the error signal to recursively calculate the prediction filter

$$\boldsymbol{w}(n+1) = \boldsymbol{w}(n) + \mu \frac{e(n)\hat{\boldsymbol{x}}}{\hat{\boldsymbol{x}}^T \hat{\boldsymbol{x}}} \tag{2.9}$$

where μ is the step size parameter which determines the speed of convergence. In the LMS algorithm, the convergence speed has to be held rather low to keep the recursion stable.

Instead of a recursive procedure, we suggest to directly invert the autocorrelation matrix of eq.(2.8). The computational burden can still be kept low, if the prediction filter is updated only sparsely. This is practicable as long as the noise field is stationary; and in ANC applications, as e.g. in airplanes, noises are often long time stationary. Furthermore, noises with prominent spectral peaks are easily predicted with only a few coefficients. Thus, the matrix to be inverted can be kept small.

The most important benefit of the feedback ANC approach however is that a part of the noise characteristic is always known. The upper frequencies of the outside noise u (as in Figure 4.11) will always be damped by the physical barrier *P(s)* of the ear cup. This passive attenuation can be written down as a convolution operation

$$\boldsymbol{x} = \mathbf{P}\boldsymbol{u},$$

where **P** is a convolution matrix of a low-pass impulse response that simulates the passive attenuation. With this, the autocorrelation matrix $\boldsymbol{R}_x$ follows to

$$\boldsymbol{R}_x = \mathbf{P}\boldsymbol{R}_u\mathbf{P}^{\mathrm{T}}. \tag{2.10}$$

When u has a flat spectrum, its autocorrelation matrix Ru reduces to an identity matrix and Rx solely depends on P. The calculation of the optimal prediction filter (eq.(3)) then simplifies to

$$\boldsymbol{w}_{\mathrm{opt}} = (\mathbf{S}\mathbf{P}\mathbf{P}^{\mathrm{T}}\mathbf{S}^{\mathrm{T}})^{-1}\mathbf{p}, \tag{2.11}$$

where **p** is column number D of the low-pass autocorrelation matrix $\mathbf{P}\mathbf{P}^{\mathrm{T}}$. This equation allows for an a priori filter design where no real-time calculation of the filter coefficients is

needed because all required data ($S(\omega)$ and $P(\omega)$) can be measured and designed in advance. The prediction filter that follows from this a priori calculation can be used as a default filter in the ANC headphone.

The following simulations are based on measurement data from an exemplary headphone. Its passive damping and the low-pass filter that is used to derive the default prediction filter are displayed in Figure 4.12. The pass-band of the low-pass filter is chosen to be narrower than the one of the ear-cup damping. On the one hand, this increases the prediction error for the upper frequencies, but on the other hand it leads to better prediction in the low frequency band.

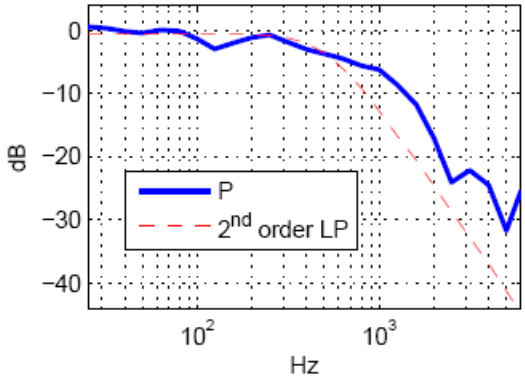

Figure 4.12: Transfer function $P(\omega)$ of the passive attenuation by the ear cup and the second order low-pass that is used for the default prediction filter.

In order to reduce computational load, the DSP might be sampled down to 24kHz. Lower sampling frequencies are not advisable because they would reduce the spectral information of the passive attenuation. Common audio codecs have a talk through latency of about 170µs at 192 kHz. At 24kHz this corresponds to a total delay of approximately 4 samples.

In the first simulation, the default prediction filter is used for airplane noise and its ANC performance is compared with adaptive methods like LMS and one-step linear prediction. Figure 4.13 shows the spectrum of the airplane noise and the spectra of the residual noises after ANC.

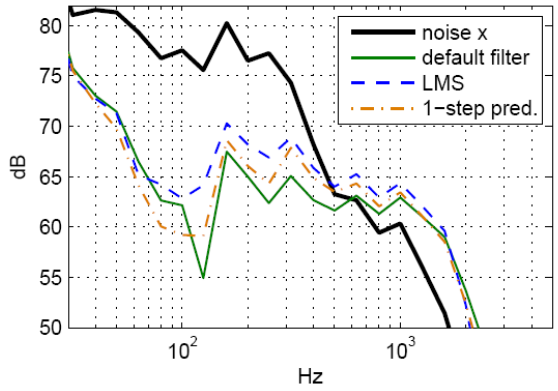

Figure 4.13: Spectrum of the airplane noise x that entered the headphone and the residual noises after ANC with the proposed default filter, an LMS filter and after iterated 1-step ahead prediction. The default filter performs best between 100 and 1000 Hz. The deteriorated ANC below 80 Hz comes due to the long group delay of the loudspeaker in the low frequency band.

Above 2000 Hz, the LMS algorithm and the iterated one-step-ahead prediction produce a lower error than the proposed default prediction filter, but the ANC performance of the proposed filter between 100 and 1000 Hz is superior to the other two methods. As the passive noise attenuation above 1000 Hz is already very pronounced, the ANC of the default predictor is preferable.

In the second simulation (Figure 4.14), the noise of an accelerating engine is used for the ANC comparison. The default prediction filter still leads to a slightly better performance, although the engine-noise is narrowband. An update of the default filter by an autocorrelation of $\hat{x}$ did not lead to further ANC improvement.

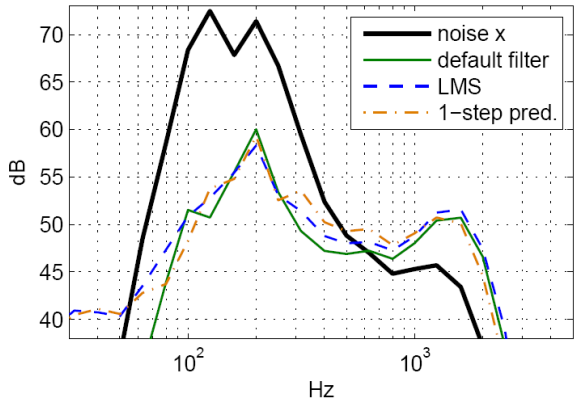

Figure 4.14: Engine noise x that entered the headphone and the residual noises after ANC with the three compared methods. Again, the default filter performs slightly better, although it is designed a priori and does not change during runtime.

For the third simulation, another narrowband noise is used. This time, pink noise was filtered with a forth order Butterworth bandpass filter with cut-off frequencies at 100 and 270 Hz. The spectra of the noise and the residual noises after ANC are shown in Figure 4.15.

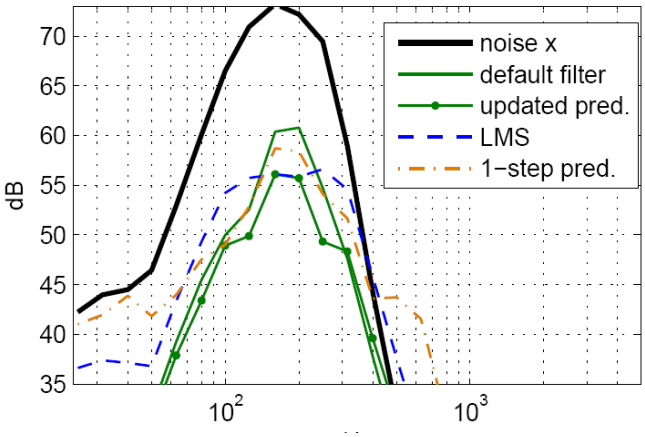

Figure 4.15: Narrowband noise *x* ant the residual noises after ANC with the compared methods. Here, the default prediction filter needs to be updated with a noise autocorrelation. The resulting updated 4th order prediction filter yields the best ANC again.

In this case the one-step-ahead predictor and especially the LMS yield better results than the default filter. An update of the filter is required to improve the ANC. The first 150 available noise samples are taken to perform an autocorrelation. From this autocorrelation, only four samples (beginning form time lag 0) are taken for the autocorrelation matrix $\boldsymbol{R}_x$ and four further samples, starting from lag 2D = 4, are taken for **r**. Thus an inversion of a 4x4 matrix is required to calculate the prediction filter coefficients. This updated 4th order prediction filter again performs better than the iterated one step-ahead prediction and the LMS prediction.

In this section, we showed that a main part of the noise characteristic is determined by the passive attenuation due to the ear cups. With this information, we design an a-priori prediction filter that does not need any real-time adaptation. Simulations show that this filter reaches better results than adaptive prediction methods like the LMS or an iterated one-step-ahead linear prediction, for a broad-band noise like airplane noise and also for a narrowband noise, like from an accelerating engine. The proposed prediction filter might also be used in hybrid ANC systems like proposed in where it is expected to lead to improved ANC results too.

4.2.4 Comparison of different extrapolation methods

Four different predictive methods are compared for the feedback ANC structure of Fig. 2.18.

1. Normalized fxLMS
2. Default prediction filter based on the transfer function of the passive damping by the ear cup
3. Slepian Extrapolation
4. Iterated 1-step-ahead prediction

The design of the default prediction filter as well as the LMS and LPC prediction are explained in the previous section. Slepian extrapolation is based on the property that the Fourier transform of any Prolate sequence ψm of order m and length(N +1) is a scaled version of the Prolate function itself.

$$\mu\Psi_m[n] = \sum_{k=-N/2}^{N/2} \psi_m[k] e^{-jn2k/N}$$

Hence, if the Prolate function is known in the Fourier domain from -1 to 1, it is entirely known in the time domain. Any time-and frequency concentrated signal x[n] can be expressed as a weighted sum of orthonormal Slepian functions. The weights are derived as

$$g_m = \frac{1}{\lambda_m} \sum_n x[n]\psi_m[n],$$

where λ_m are the eigenvalues of the Slepian functions. With these weights, the signal x[n] can be extrapolated to

$$x[n+\delta] = \sum_m g_m \psi_m[n+\delta].$$

Fig. 2 shows the results of the 4 extrapolation methods for a broadband airplane noise. The default prediction filter performs best, although it is not adapted during run-time.

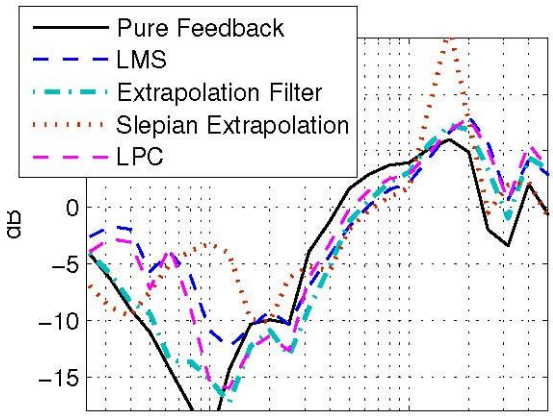

Figure 4.16: ANC of different extrapolation methods. The default prediction filter performs best, although it is not adapted during run-time.

5 Hybrid ANC

The implementation of a low latency adaptive ANC headphone would be very promising, but there is no ready to use hardware solution available on the market. Another strategy is a hybrid ANC-headphone, where an analogue feedback cancels low broadband noise and a digital adaptive path cancels periodic noises as this is also possible at large latencies [23,24]. The analogue feedback (as in Section 3.1.1) is combined with the adaptive feedforward structure in Figure 5.1.

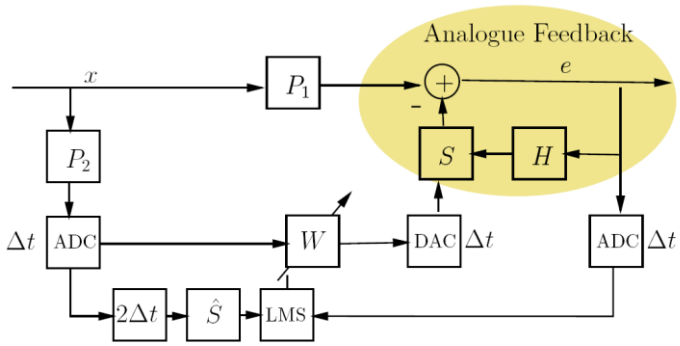

Figure 5.12: Hybrid ANC solution. It consists of an analogue feedback and an adaptive feedforward path.

A circuit for such a hybrid solution has been assembled. It comprises an analogue shelving filter and auxiliary in- and outputs for the digital path. For the following measurements, the digital processing was done with the software program “pure data” using a rme fireface as audio interface and a Brüel & Kjaer dummy head as measurement device.

For the measurements with the hybrid ANC solution, white noise was combined with three sinusoidal tones at 440, 1500 and 2500 Hz. The white noise was filtered with a 4th order lowpass at a cut off frequency of 2000 Hz. Figure 5. shows the results of the measurement. The hybrid solution is very efficient in cancelling this combination of noises.

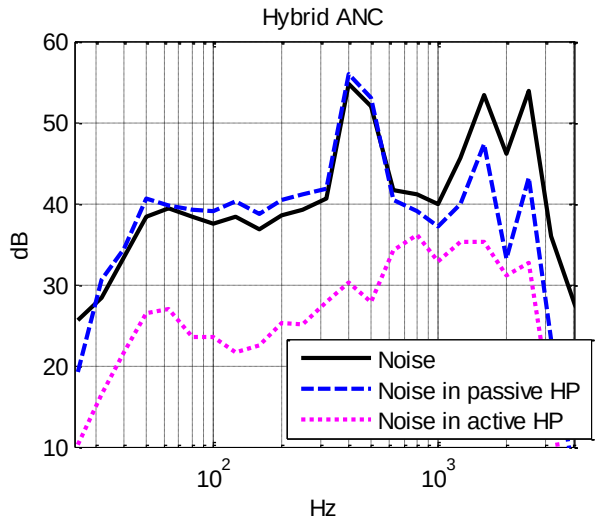

Figure 5.43: ANC measurement with the hybrid solution. The analogue feedback cancels the broadband noise below 1000 Hz and the adaptive path cancels sinusoidal components at arbitrary frequencies.

6 Secondary Path Identification

6.1 Identification of Secondary Path Irregularities via the Adaptive ANC-Filter in Feedback Applications

Headphones with Active Noise Control (ANC) cancel ambient noise by playing back destructively interfering 'anti-noise'. It can be distinguished between feedforward ANC-headphones that pick up the ambient noise outside the headphone and feedback ANC-headphones that sense the residual noise inside the headphone, which is especially advantageous in diffuse sound fields. Figure 6.1 shows a typical realization of a digital feedback ANC-headphone. It uses a model $\widehat{G}(j\omega)$ of the secondary path (i.e. the transfer function from the loudspeaker to the microphone inside the ear cup) to estimate the entered noise x(t). This internal model controller (IMC) is preferably used in digital feedback ANC because the noise cancelling filter W(jω) can be designed as a feedforward controller and therefore also as adaptive filter. This is beneficial when facing noises with changing spectral characteristics.

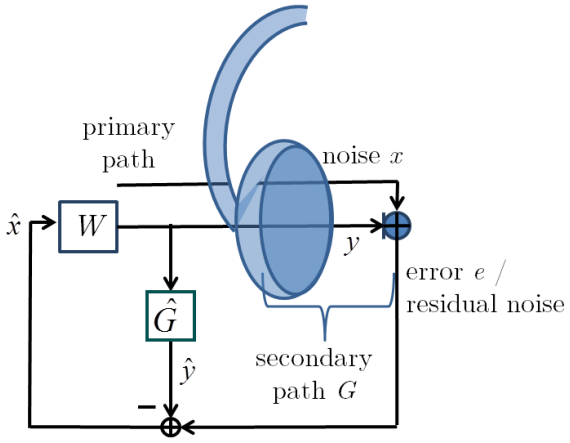

Figure 6.1 Feedback ANC with an internal model controller (IMC): The internal model $\widehat{G}(j\omega)$ of the secondary path is used to derive an estimate $\hat{x}[n]$ of the noise.

However the performance and stability of this feedback ANC-system depends on the accuracy of the model $\widehat{G}(j\omega)$. An initial nominal model can easily be determined off-line by injecting an appropriate broadband signal (e.g. a swept cosine) into the headphone and measuring the system response with the microphone inside the ear cup. The secondary path G(jω) however changes considerably once the headphone is lifted or pulled away completely. The deviation of G(jω) from the nominal $\widehat{G}(j\omega)$ can then drive the system

unstable. In [20], they show that an additional analogue feedback-controller can reduce the deviation from the nominal model, but the analogue controller design is non-trivial and stability cannot be assured in general. Consequently, the controller has either to incorporate an uncertainty about the secondary-path model or an on-line secondary-path estimation that tracks changes in G(jω) has to be implemented. While the first suffers from a loss of performance under optimal conditions, the latter only works for slow and minor changes in G(jω) and is more suitable for feedforward ANC headphones where a reference microphone outside the ear cup is available. Also, these methods inject additional noise into the headphone to identify the secondary path; an approach that is counterproductive for a noise-cancelling application.

We introduce a simple and efficient method to identify changes in the secondary path without the need of an extra reference microphone and without the need of injecting additional noise. In particular, we show that lifting and pulling away the headphone mainly affects the low frequencies of G(jω) and that the adaptive filter W(jω) which tries to invert G(jω) can be used to detect those low frequency changes. Once this irregularity in G(jω) is detected, the adaptive filter changes to a robust stable default-setting before it starts a least mean square (LMS) adaption again. This way, we yield optimal ANC performance as long as the headphone is worn properly, and we still can avoid instabilities even during sudden changes in G(jω).

The sensitivity function S(jω) (i.e. the transfer function from the input noise x to the residual error e) of the feedback system in Fig. 1 reads as (from now on with omitted dependency on jω)

$$S = \frac{1}{1 - G\dfrac{W}{1 + \widehat{G}W}} = \frac{1 + W\widehat{G}}{1 + W(\widehat{G} - G)}. \qquad (6.1)$$

In the case of $G = \widehat{G}$, the denominator of the sensitivity function S vanishes and the filter W should become $W = -\widehat{G}^{-1}$ in order to minimize |S|. However, the inverse of $\widehat{G}$ in general will not exist since $\widehat{G}$ willnot have minimum phase. Thus the filter W can only try to compensate for the phase delay and the dynamics of $\widehat{G}$ e.g. in an H_2 or H_∞ optimal sense. The accuracy of the compensation depends on the bandwidth in which $\widehat{G}$ shall be compensated. It is easier to compensate for the phase delay and the magnitude at a single frequency than in a broad bandwidth. Thus, the optimal filter W depends on the current spectral characteristic of the input noise x. It is therefore advantageous to implement an adaptive

filter W that yields the compensation in the band where it is currently needed. Note that the adaptive filter tries to do a system identification of the inverse secondary-path. This fact will be used later to detect changes in the secondary path.

The adaptive filter is most commonly adapted with the Least-Mean-Square (LMS) algorithm for it has a low computational complexity. In applications with dynamically varying excitation and a non-negligible delay in the secondary path, the Normalized Filtered-x LMS (NFxLMS) is used to yield stable convergence.

The LMS (and so the NFxLMS) is a gradient based adaptive algorithm that eventually converges to the Minimum Mean Square Error (MMSE). Figure 6.2 shows the FIR filter W of the MMSE solution for white input noise that was filtered with a second-order low-pass at a cut-off frequency of 500Hz. The second-order filter simulates the passive attenuation of the headphone and the filter W has $L = 32$ taps at 44.1 kHz sampling frequency. Since there is no high-frequency excitation, the filter W has a lot of freedom in the upper frequency band. This results in a boost of the high frequencies which is not applicable in real life condition, where e.g. sensor noise or estimation errors of $\hat{x}$ would be stronglyamplified.

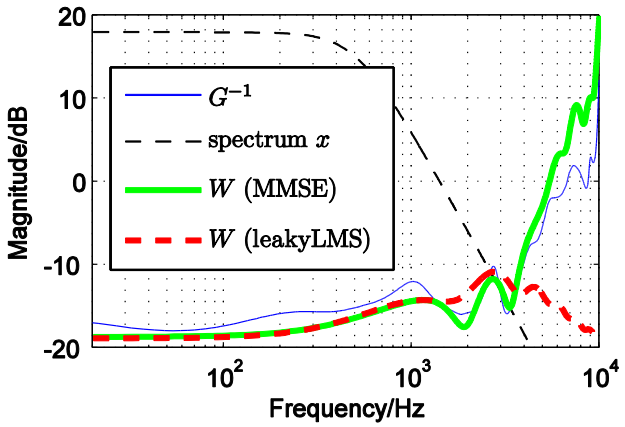

Figure 6.2 The filter W tries to match the inverse of G. Without constraints, it has the freedom to heavily boost the high frequencies since there is no noise excitation in this band. The leaky LMS (with $\gamma = 0.005$) minimizes the filter's energy which leads to a desirable roll-off at high frequencies.

It is therefore necessary to penalize the energy of W. The cost function shall not only include the squared error but also the weighted norm of the filter's tap-weight vector w. This extended cost function $J(w) = e^2 + \gamma(w^T w)$ results in the leaky LMS algorithm. Its normalized filtered-x version has the following coefficient update:

$$w(n+1) = (1 - \mu\gamma)w(n) + \mu\frac{e(n)\hat{G}\hat{x}}{\hat{x}^T\hat{x}}, \qquad (6.2)$$

where n is the discrete time index, μ is a stepsize parameter, $\hat{G}$ is the convolution matrix of the secondary-path model and $\hat{x}(n)$ is a vector of the latest L estimated noise input-samples as in Fig. 2.24.

Figure 6.2 also compares the solution of the converged leaky NFxLMS to the MMSE solution. The leaky NFxLMS matches the inverse of G less accurately but it prevents the filter from excessively amplifying the high frequencies. It still yields ANCup to 15 dB as can be seen in Figure 6.3. The leaky LMS version is also more robust against mismatches of the secondary-path model $\hat{G}$, which is very important as will be shown in the following section.

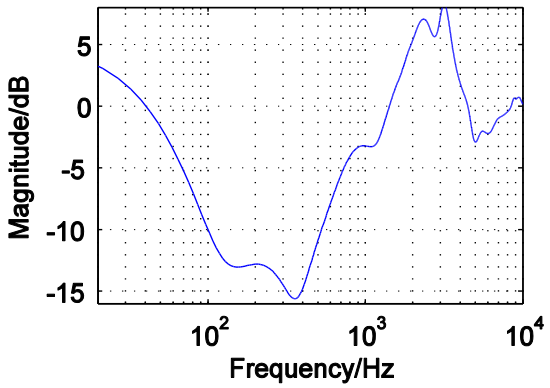

Figure 6.3 Sensitivity function of the leaky NFxLMS for $G = \hat{G}$. Negative dB values denote noise cancellation, positive values denote noise enhancement.

6.1.1 Stability of the Adaptive Feedback Loop

In the given adaptive feedback-ANC-system, two stability issues arise:

1 Stability of the NFxLMS adaptation.

The stability of the recursive adaptation depends mainly on the phase error between G and $\widehat{G}$ which has to stay below 90° for the usual NFxLMS algorithm. However, the leakage factor γ prevents the adaptive filter from diverging also for larger mismatches. A larger γ leads to a more robust stability on the one side, but increases the MMSE on the other side.

2. Stability of the feedback loop.

The stability of the feedback loop depends on the poles of the sensitivity function S in eq. (6.1) that all have to lie within the unit circle. It thus depends on $\widehat{G} - G = U$ the additive uncertainty of the secondary-path model, and on the adaptive filter W.

In both cases, the stability depends on the deviation of G from $\widehat{G}$. We therefore will have a closer look on the variations of the secondary path in the following and treat the two stability issues in more detail in the following paragraphs.

The biggest change in G and thus the greatest uncertainty and the greatest phase error is expected when the headphone is pulled away from the ears. We therefore measured the secondary-path response on a dummy head for four different leakage situations.

- A tight sitting headphone.
- A situation where a leak of 105 mm3 is introduced between the ear and the headphone.
- A situation where two such leaks are introduced between the ear and the headphone.
- A completely loose headphone.

Figure 6.4 shows the bode plots of the measurements. It can be seen that an increased leakage leads to an increased drop-off at low frequencies.

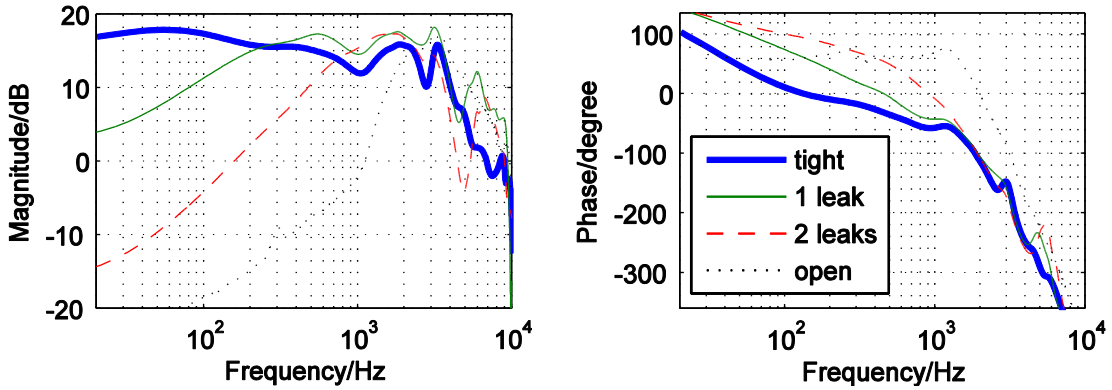

Figure 6.4 Frequency response of the secondary-path for a tight, leaky and completely loose headphone. The increased leakage leads above all to a magnitude drop-off at low frequencies.

The tight wearing situation is the regular use-case; consequently the secondary-path measure under tight condition will be the nominal model $\widehat{G}$. This however implies that there is a high uncertainty on this model if the headphone is lifted as shown in Figure 6.5.

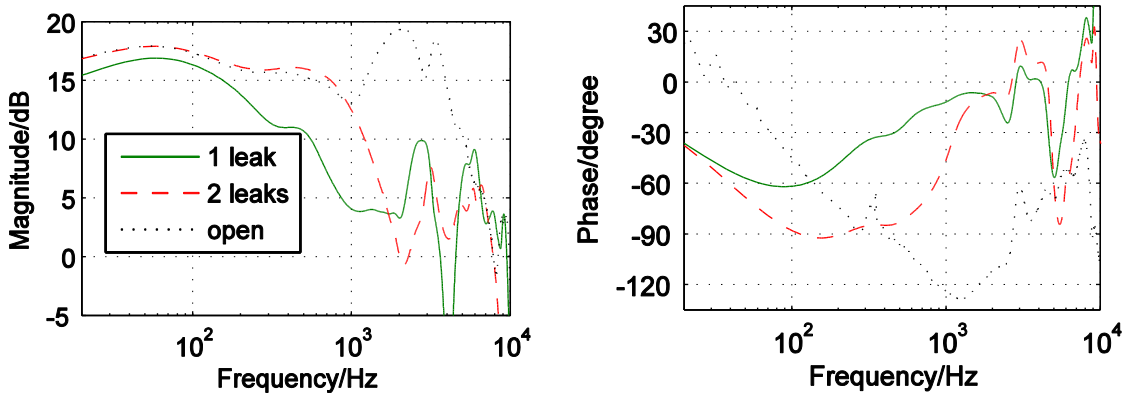

(a) Additive Uncertainty **(b) Phase Error**

Figure 6.5 Magnitude of the additive uncertainty and the phase error of differently leak headphones for the nominal model $\widehat{G}$ of a tight sitting headphone.

Figure 6.5 b shows that the largest phase-error occurs at 1300 Hz if the headphone is completely loose. A narrowband excitation at this frequency is therefore the first choice to test if the leaky NFxLMS stays stable. The second and third test scenario are broadband excitations for the open headphone and for the headphone with two inserted leaks. The broadband excitation is again white noise that is filtered with a second order low-pass (which simulates the passive attenuation of the ear cups.) We test the leaky NFxLMS in open loop condition in order to decouple the convergence of the filter from the possible feedback

instability. The stepsize is set to $\mu = 0.001$ and the leakage factor to $\gamma = 0.005$. Figure 6.6 shows that the adaption stays stable in all three scenarios. In the broadband cases, the filter even yields a small noise reduction. In the narrowband case, the filter causes an amplification of the input noise of 1.4 dB which on the one hand proofs that the NFxLMS does not converge to the optimal solution anymore, but on the other hand the simulation also shows that the filter coefficients stay bounded because of the leakage factor γ.

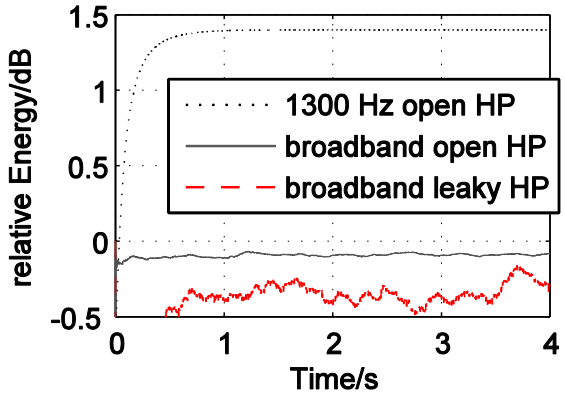

Figure 6.6 The energy of the residual error e in relation to the excitation energy for 3 worst case scenarios: A narrowband excitation at 1300 Hz and $\widehat{G}$ of the open headphone (HP), and a broadband excitation for the open headphone and for the headphone with 2 inserted leaks. The excitation at 1300 Hz causes an error which is 1.4 dB over the excitation level, but the adaption stays stable in all three cases.

As stated earlier, the feedback loop is stable if all poles of S lie within the unit circle. This is the case, if (and only if) the product WU does not encircle the point -1 in the Nyquist plot. It cannot encircle -1 if the absolute value $|WU| < 1$. This would be a sufficient (yet not necessary) condition for stability, but taking a look at the converged filter W from Figure 6.2 and the additive uncertainties U of Figure 6.5 it is already clear that this condition does not hold. Figure 6.7 combines said W and U to show that their magnitudes violate or closely violate this condition in almost the entire frequency range.

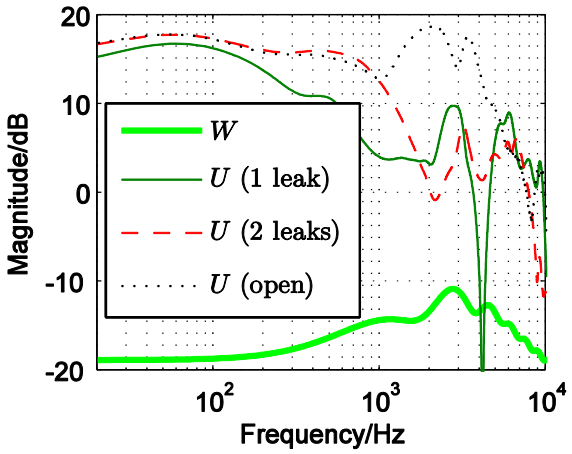

Figure 6.7 Magnitude of the converged filter W and the additive uncertainties U. Stability of the feedback loop is assured if $WU < 1$, thus if the added dB values are below 0. This is clearly not the case e.g. around 2000 Hz and only marginally fulfilledat the low frequencies.

It is hence necessary to examine the stability condition in more detail. The uncertainty U could be derived through measurements and is static, but the filter W, which also accounts for the stability, is adaptive and depends on two conditions: the input signal x and the actual secondary path G. We therefore examine the stability with computer simulations for various input noises:

- Sinusoidal excitation at 50 Hz and in 100 Hz steps from 100 Hz to 1400 Hz.
- Narrowband excitation with white noise passed through a 2nd order peak filter with a quality factor of Q = 8 and centre frequencies as above.
- Broad band excitation with white noise.
- Broad band excitation with pink noise.

Each of the excitation signals is filtered with the mentioned 2nd order filter of passive attenuation and run through the leaky NFxLMS simulation with

- an initial worst-case G and for
- a sudden change from G = $\widehat{G}$ to the worst case G.

The worst case G depends on the frequency and is the one with the highest uncertainty as in Fig. 5. For the broadband excitation both, G with 2 leaks and G of the open headphone, are used. The NFxLMS is run with simulated white sensor noise of -60dB relative to the excitation level and with the same μ and γ as in the previous section.

All simulations show instabilities or ringing except for excitations between 400 Hz and 800 Hz. The poles of WU which cause the instabilities can be grouped in three frequency bands:

1. Poles around 100 Hz. These poles appear whenever the input noise x includes excitation around 100 Hz, be it narrow- or broadband.
2. Poles around 1000 Hz. These poles appear only for narrowband excitations below 100 Hz. It is thus not the excitation x but the sensor noise that causes the instability.
3. Poles above 1200 Hz. These poles appear for any excitation signal with frequency content above 1200 Hz.

Figure 6.8 shows exemplary sensitivity-functions for each of the three cases and Figure 6.9 compares the derived filters W with the maximum additive uncertainty U.

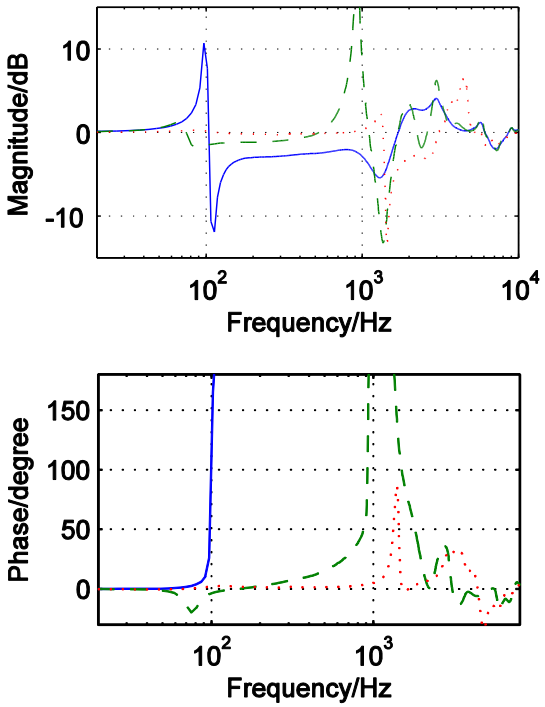

Figure 6.8 Sensitivity function of the unstable feedback loop due to poles outside the unit circles. These pole locations are indicated by peaks in the magnitude response that come with a positive phase shift.

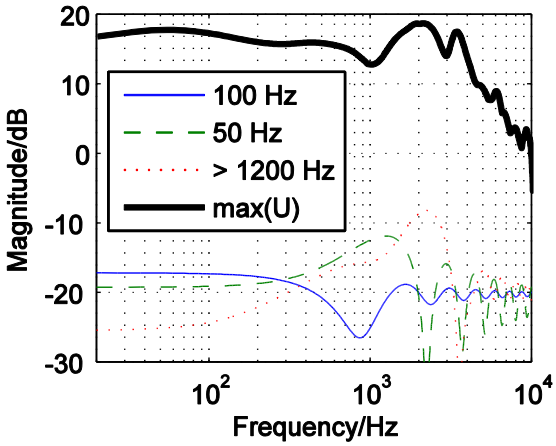

Figure 6.9 Exemplary filters W for the three cases of instabilities and the maximum value of U. $WU < 1$ is violated below 200 Hz for excitations including 100 Hz, around 1000 Hz in the case of a narrowband 50 Hz excitation and around 2000 Hz for the high frequency excitation.

Instabilities due to case 3 can be avoided by restricting ANC to frequencies below 1200 Hz. The error e can be filtered by a first-order low-pass filter H which then also has to be considered in the secondary-path model as in Figure 6.10. The new model G' will then be GH. The additional filter H increases the group delay of the system and will consequently degrade the ANC performance a little bit. Apart from that, H hardly restricts the ANC bandwidth compared to Fig. 2.26 because above 1200 Hz the phase change is too fast for broadband ANC anyway. In addition, the ear cups already yield more than 15 dB passive attenuation above 1200 Hz.

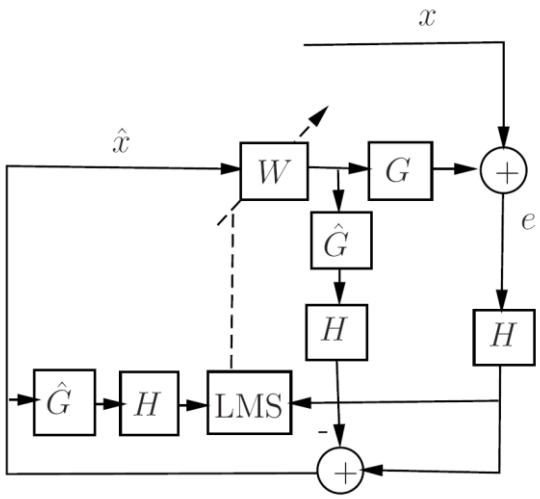

Figure 6.10 Block diagram of the adaptive feedback system with a low-pass filter that prevent instabilities due to high frequency uncertainties.

Cases 1 and 2 however, are a severe problem since they affect frequency bands where ANC is most desirable. In the following section we show how the adaptive filter W can be used to detect the changes in G and keep the feedback loop stable.

As stated above, W does a system identification of a causal version of G-1 if $\widehat{G} = G$ In the case of large mismatches between $\widehat{G}$ and G, this is not generally true because the convergence of W to the optimum Wiener solution is not assured anymore.

Still, Figure 6.11 shows that the filter W changes clearly when the secondary path changes from tight to loose. The figure compares the adaption result of all the simulations whose excitation noise x includes low-frequency content up to 300 Hz. In the loose cases, the low frequencies of G drop off and (as a counter reaction) the filter W amplifies the low frequencies. An analysis of variances (ANOVA) shows that this low-frequency gain differs significantly (with a p-value<0.001) between the tight and the loose cases.

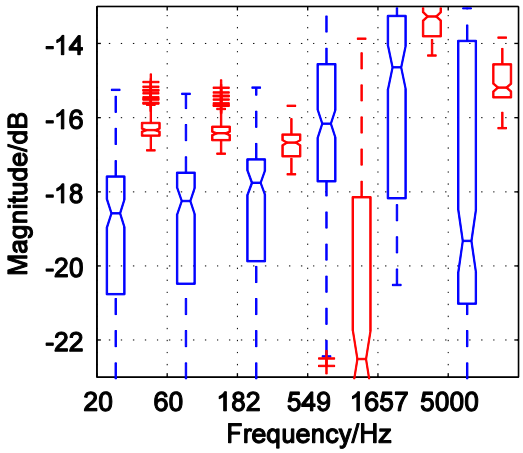

Figure 6.11 Amplitude distribution of W under stable condition (on the left of each frequency grid) and under instable conditions when the headphone is strongly leaky or loose (on the right of each frequency grid). The boxes include the magnitude of 50% of the derived filters and the whiskers show the distribution limits except for the outliners which are marked as crosses. The bars in the middle of the boxes denote the median value and the notches indicate the confidence interval. The low frequency behavior between the two cases differs significantly.

Figure 6.12 compares the filter gains with the additive uncertainty U and shows that the amplification of the low frequencies violates |WU|<1 which leads to the observed instabilities.

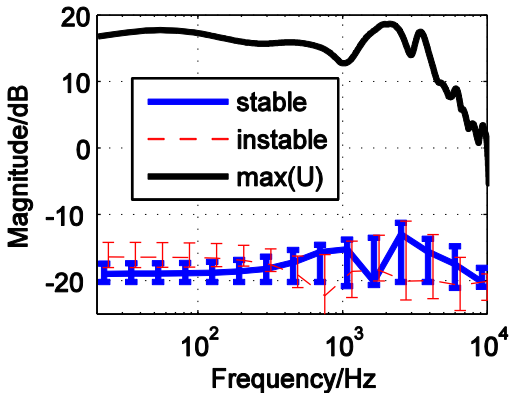

Figure 6.12 As long as the sum of the dB values of W and U are below 0 (i.e. |WU|<1 in linear notation) the feedback loop cannot become unstable. This condition holds as long as the headphone sits regularly tight, but is violated if the headphone is very leaky or loose because the filter W tries to compensate the low-frequency amplitude drop-off in G.

These instabilities can be avoided if the low-frequency gain of W is constrained. The low-frequency gain of W is very constant up to 300 Hz since a 73 ms long filter does not allow for a lot of variations in the low-frequency response. Therefore it is sufficient to constrain the direct-current (DC) gain of the filter. This is especially beneficial because the constraint can be formulated in the time domain as $\sum_i w_i < \beta$, where wi are the filter coefficients and β is the threshold of the constraint which in our case is set to 0.14 (equivalent to -17dB). Figure 6.12 also shows that the adaptive filter exceeds this threshold in a tight and stable condition too in some cases. Therefore ANC should not be turned off completely when the threshold is exceeded. Instead, the filter W should change to a stable default filter that works for the tight as well as for the leaky case.

From Figure 6.9 it is clear that the default filter W should have a magnitude response of -20 dB in almost the entire frequency range to assure |WU|<1. A trivial choice for the default filter is thus an impulse that is scaled to -20 dB. In order to prevent time invariances during the filter process, W should not change abruptly, but converge to the scaled impulse smoothly. In particular, the current filter coefficients w shall converge within 40 samples (at 44.1 kHz) to the scaled impulse.

The whole adaptive feedback-ANC algorithm can be summarized as follows:

1. Filter the error e with a 1st order low-pass H with a cut-off frequency at 1200 Hz.
2. Update the coefficients of w via the leaky NFxLMS algorithm as in eq. (2.13).
3. Check if $\sum_i w_i < \beta$. If yes:
    - Calculate the gradient which leads to the stable default filter.
    - For the next 40 gradually change w to the scaled impulse.
    - After the 40 samples continue the usual algorithm beginning with step 1.

Apart from possible short breaks of 40 samples, the NFxLMS is constantly running also if the headphone is lifted or loose for a longer time. In that case, the filter starts growing again and it eventually exceeds the threshold β too again. It thus will constantly grow and scale back to the stable impulse.

We tested the algorithm again for the same excitation signal as above. In the loose case, the DC gain of W eventually always exceeds -17dB, and it exceeds β always early enough to prevent instabilities and ringing. A more thorough test of the algorithm follows in the following.

6.1.2 Experimental Results

To evaluate the algorithm, we asked two persons to put on the headphone in differently leaky or lifted positions. For all positions we measured the secondary path with a sine sweep of one second. It gives us 16 different measurements in total that can be seen in Figure 6.13.

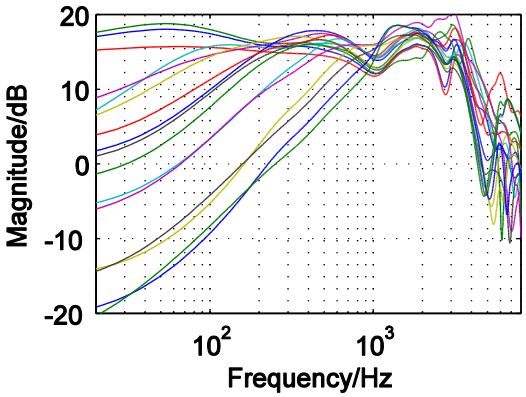

Figure 6.13 Magnitude response of the secondary paths measured on two persons with differently leaky headphones.

In the evaluation of the algorithm, the measured secondary-paths are randomly replaced by each other every 0.5 seconds. As secondary-path model, we still use G which we derived from the tight measurement on the dummy head. The excitation signal again is white noise which was filtered by a second-order low-pass.

First, we show that the headphone starts to ring and become unstable without our detection algorithm. Then for the same sequence of secondary-path changes, we demonstrate that the detection algorithm keeps the feedback loop stable. Figure 6.14 compares the residual errors of the trial without and with detection algorithm.

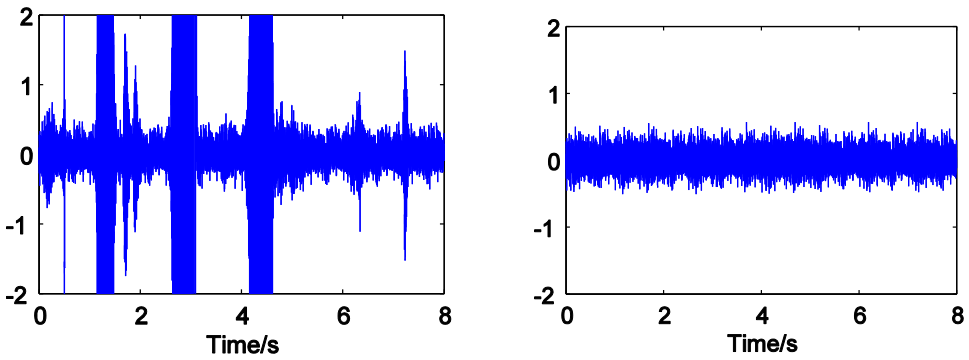

(a) without detection **(b) with detection**

Figure 6.14 The DC-detection algorithm clearly keeps the feedback loop stable.

The sensitivity function of the stable trial is shown in Figure 6.15. The algorithm prevents the error from increasing more than 3 dB below 100 Hz. It therefore avoids ringing and instabilities. The loss of performance compared to Fig. 2.26 comes due to the additional group delay of H, but the system still yields ANC of 10 dB.

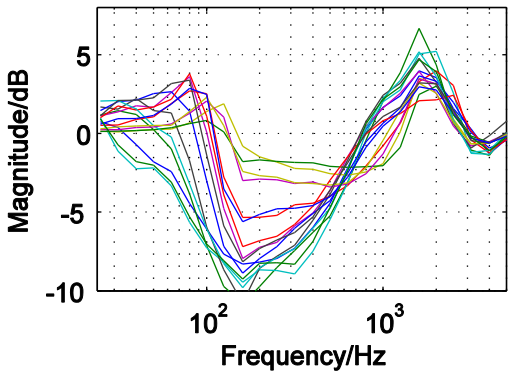

Figure 6.15 Sensitivity function of the trial with the proposed detection algorithm. In the tight cases, the system still yields 10 dB of noise reduction. At the same time it does not let peak the error more than 3 dB below 100 Hz.

We further tested the algorithm with narrowband excitations around 50 Hz and 100 Hz. Again, the excitation signal is white noise filtered with a 2nd order peak filter with a quality factor of Q=8. Without detection algorithm, the ANC system becomes unstable as can be seen in Figure 6.16.

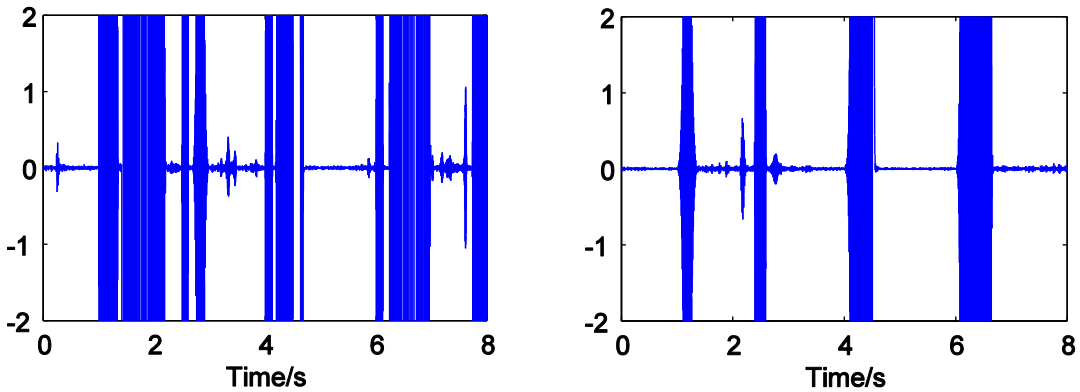

(a) 50 Hz excitation **(b) 100 Hz excitation**

Figure 6.16 Without DC-detection, the residual error starts ringing and the system becomes unstable for both excitation signals.

Figure 6.17 and Figure 6.18 show the sensitivity function and the residual noises when our DC-detection algorithm is used. Again in both cases, the stability of the system can be preserved and at the same time optimal ANC is possible in the cases of a tight sitting headphone.

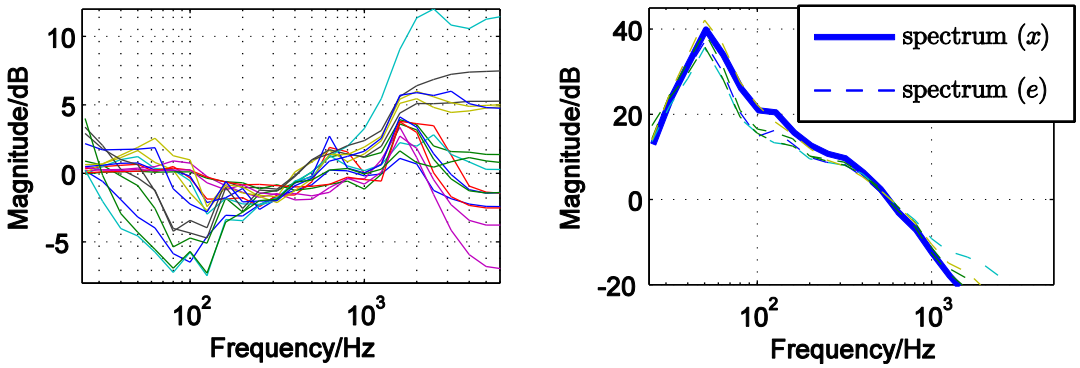

(a) Sensitivity function **(b) Excitation and error spectra**

Figure 6.17 Narrowband excitation around 50 Hz. The detection algorithm prevents strong peaks in the sensitivity function. The amplification above 2000 Hz that can be seen on the left hand side can be neglected because there is hardly any excitation in that frequency range as can be seen on the right hand side.

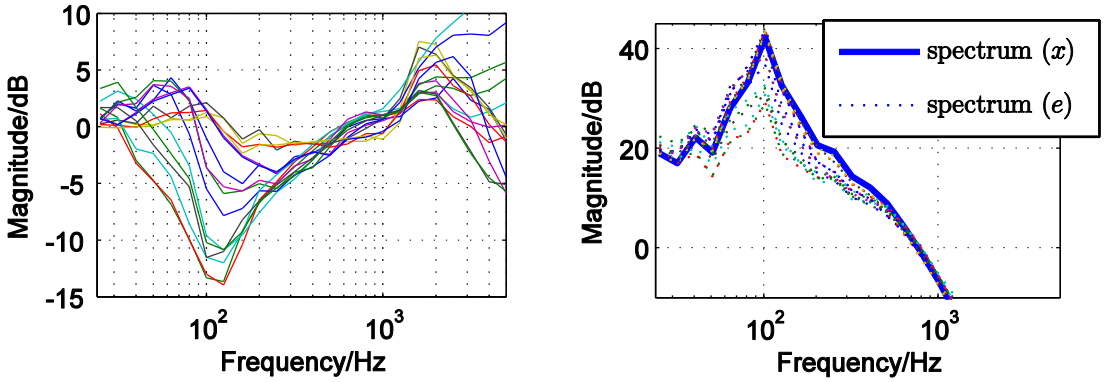

(a) Sensitivity function **(b) Excitation and error spectra**

Figure 6.18 Narrowband excitation around 100 Hz. The detection algorithm prevents peaks in the sensitivity function and yields more than 10 dB noise reduction if the headphone sits regularly tight. Again, the noise enhancement above 3000 Hz is acceptable because there is no excitation in that frequency band.

6.2 Secondary Path Identification with an Infrasonic Measurement Signal for Feedback ANC

Now, we introduce another method to identify such violent changes in G without the need of injecting additional white noise. We propose an 18 Hz excitation as measurement signal. It is an infrasound frequency that cannot be heard by humans but it is sufficient to detect irregularities in the secondary path soon enough to prevent instabilities.

In order to investigate the influence of changes in the secondary path, we measured the secondary path of a prototype headphone in a tight, a lifted, and in a loose situation, as in the previous chapter. The tight situation was measured on a measurement mannequin, and two leaks of 105 mm^2 each were inserted between the headphone and the artificial ear of the mannequin for the lifted situation. Figure 6.19 shows the magnitude responses of the measured secondary paths. The most prominent difference between the three cases is the magnitude drop-off at low frequencies. In the tight wearing condition, the headphone can be considered as a pressure chamber with the consequence that all low-frequent radiation energy stays within the headphone. Once the headphone is lifted, the low-frequency sound pressure diminishes since the omnidirectional low-frequent sound radiation leaks outside. This is not so much the case for the high-frequent radiation because it is much more directed to the ear and to the error microphone inside the headphone, respectively.

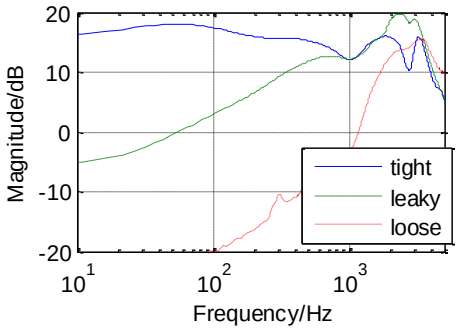

Figure 6.19 Magnitude responses of the secondary path measured under a tight, a leaky and a loose condition.

The stability of the feedback loop depends on the poles of the transfer function $S(j\omega) = \frac{E(j\omega)}{X(j\omega)}$ where E(jω) is the frequency dependent residual error and X(jω) the frequency dependent input noise. Once again with omitted frequency-dependency

$$S = \frac{1}{1 - G\frac{W}{1+\hat{G}W}} = \frac{1+W\hat{G}}{1+W(\hat{G}-G)}.$$

The stability thus depends on the filter W and on additive uncertainty of the model U = $\hat{G}$ -G. The model $\hat{G}$ is the secondary-path under tight measurement conditions. Thus under proper wearing conditions there will be no notable uncertainty and the denominator of eq. (1) will approximately be 1. However once the headphone is lifted, the uncertainty grows and the poles of WU might fall outside the unit circle.

The filter W can either be designed as a static ANC filter or as an adaptive FIR filter. Figure 6.20 shows a filter realization for broadband noise-excitation that was derived with the leaky Filtered-x-Least-Mean-Square (FxLMS) algorithm under tight wearing situation.

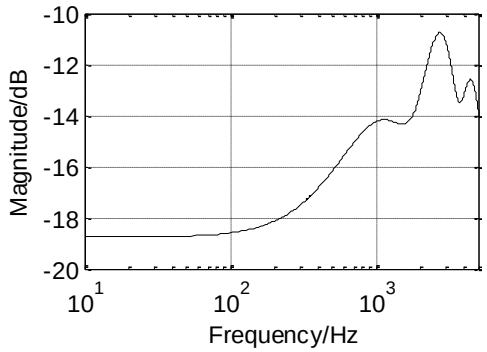

Figure 6.20 Magnitude Response of a 0.73 ms long adaptive FIR-filter W that converged with the leaky FxLMS algorithm for white input noise.

For a suddenly lifted headphone, we consider the converged filter W form Figure 6.20 and the leaky or lifted secondary path from Figure 6.19. The system is stable if and only if the Nyquist plot of WU does not encircle the point -1. Figure 6.21shows that this condition is violated for both deviations of the secondary path, for the leaky and for the completely loose case. This means that the feedback ANC system would drive unstable, if the headphone is abruptly lifted.

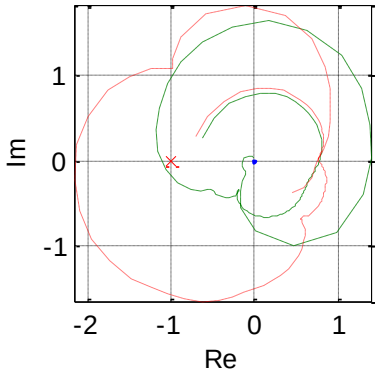

Figure 6.21 The Nyquist plot of the product WU encircles the point -1 in both cases, the leaky and the completely loose headphone. This means that the feedback loop is unstable.

The previously demonstrated changes in the secondary path have to be detected early enough to prevent instabilities. As already mentioned, the most prominent difference between the tight and the lifted headphone is the amplitude drop-off at low frequencies. Identifying the low-frequency response of the secondary path would thus be enough to detect that the headphone is being lifted. Instead of injecting white noise to identify the whole frequency response of G, it is thus sufficient to inject an 18 Hz sinusoid only which has the big advantage that it cannot be heard by humans.

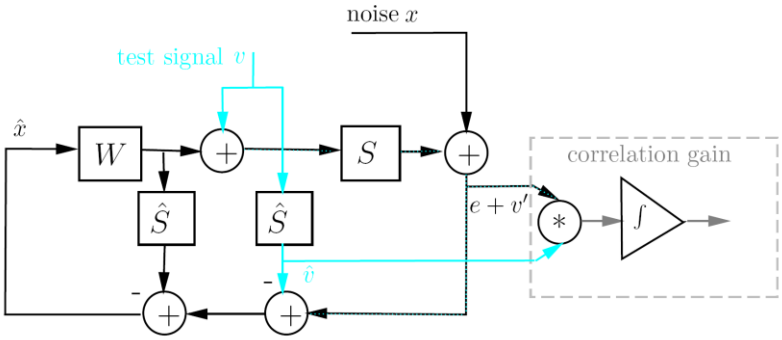

Figure 6.22 Block diagram of the feedback ANC system with a test signal to detect changes in the secondary path.

The error microphone inside the headphone does then not only sense the penetrated noise x, but also the 18 Hz test-signal v' that was passed through the secondary path as depicted in Figure 6.22. The mix e+v' is correlated with the filtered test-signal $\hat{v}$. The original test-signal v is filtered with $\widehat{G}$ such that v' and $\hat{v}$ have the same group delay. This maximizes the correlation gain under tight conditions. If the headphone is lifted, the secondary path G suppresses the 18 Hz sinusoid and the correlation gain decreases. The

correlation gain is attained by a leaky integration over the sample-wise multiplication of $(e+v')*\hat{v}$. Since v' is corrupted by the residual noise e, the test-signal has to be played back with +6dB relative to the low frequency sound pressure of e to get an acceptable signal to noise ratio. Figure 6.23 compares the correlation gain between the tight and the lifted headphone. Within 0.3 the two cases can clearly be distinguished. The filtered test-signal $\hat{v}$ is then also subtracted from the microphone signal to avoid a closed loop and to prevent the filter W from adapting to the test signal.

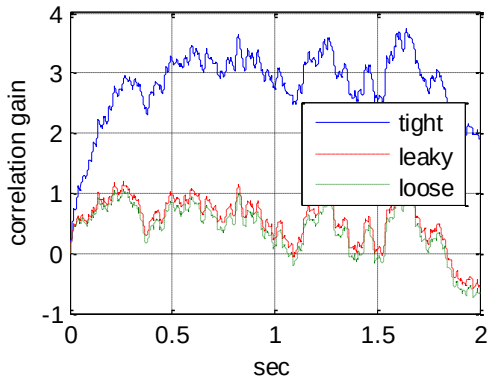

Figure 6.23 Correlation gain for the tight, the leaky and the loose headphone. The lifted headphone can be clearly distinguished from the regularly tight wearing situation.

From Figure 6.23, it can be seen that a correlation gain of 1.5 can be taken as threshold to distinguish between the tight and the lifted headphone. If the correlation gain falls below the threshold, the filter coefficients $\boldsymbol{w}$ have to be scaled down to keep the feedback loop stable and to avoid ringing. The filter can be scaled as $\boldsymbol{w}[n+1]=\gamma\boldsymbol{w}[n]$ (with n as time index and γ < 1) in order to prevent time invariances that would occur when the filter would be changed abruptly.

Simulations show that the detection algorithm with the suggested threshold and the filter scaling with γ = 0.99 is sensitive and fast enough to keep the feedback loop stable. The simulations are run with a leaky FxLMS and with white noise that is filtered with a second order low-pass at 500 Hz cut-off frequency. This filter simulates the passive attenuation of the headphone. The simulations run 1 second and after 0.5 seconds the secondary path is changed from the tight to the leaky or loose version respectively. First, the simulation is run without detection algorithm. Figure 6.24 shows that the feedback loop starts ringing when G is changed.

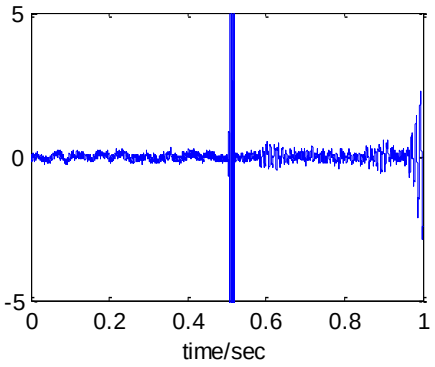

Figure 6.24 Residual error e for the simulation without detection algorithm when the secondary path changes form tight to lifted after 0.5 seconds.

With detection algorithm, the feedback loop stay stable as can be seen in Figure 6.25. Figure 6.26 shows the spectral magnitude of the input noise x and the output which is heard by the user. In the regular tight use case the ANC headphone reduces noise up to 10 dB. If the headphone is lifted, the filter W converges to zeros and no active noise cancellation is yielded. Denote that the 18 Hz peak of the test-signal can only be seen in the tight case. In the lifted case, the headphone does not radiate that much low-frequency energy towards the error microphone.

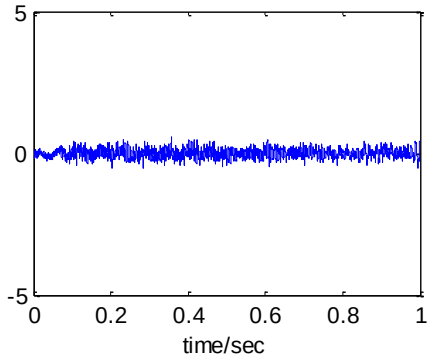

Figure 6.25 With detection algorithm, the feedback loop stays stable and no ringing occurs in the residual error.

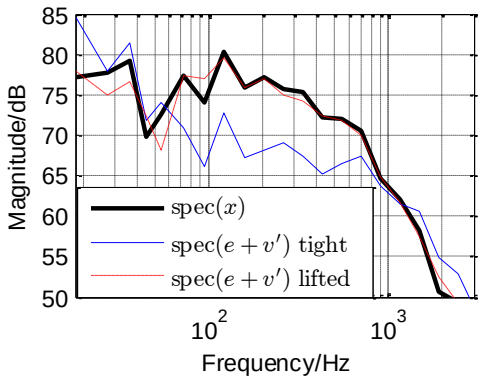

Figure 6.26 Spectral magnitude of the input noise x and the microphone signal (e+v'). The latter is also the signal that is heard by the user. The microphone signal is shown for the regularly tight and the lifted use case.

6.3 Secondary Path Models for Feedforward ANC

Active-Noise-Control (ANC) systems sense disturbance-noise in a reference point and filter it (invert its phase mainly) to get an 'anti-noise'. The anti-noise is played back over a secondary path and interferes destructively with the primary noise in a target point. Digital adaptive noise-control-systems also sense the residual error in the target point which allows adapting the noise-cancelling filter automatically to e.g. the optimum Wiener solution [25]. The Least-Mean-Square (LMS) algorithm is very efficient and widely used for adapting the filter coefficients [8]. However in headphone applications (as in most others), the secondary path introduces a non-negligible phase delay. As a consequence, the reference signal and the error signal are out of phase which impedes the correct filter update. The solution is to filter the reference signal with a model of the secondary path too which is then called the filtered-x-LMS (FxLMS) [26, 27].

Analyses of the FxLMS [28, 29, 30] show that the algorithm is robust against errors in the secondary-path model as long as the phase error stays below 90°. However, the secondary path of a tight sitting headphone differs from a lifted headphone by more than 90° as will be shown in the following. Thus, the FxLMS would diverge, if the headphone is lifted.

There are four main approaches to overcome the problem of changing secondary paths in FxLMS applications, but they all have severe drawbacks and/or limitations.

- An additional analogue feedback controller can reduce the phase deviation [24]. However, it increases the hardware complexity and its design is non-trivial.
- Online secondary-path estimation as in [31, 32, 33, 34, 35, 20, 36, 37] aims to track changes in the secondary-path. However these methods fail in large and sudden changes, and/or they inject white noise into the headphone which is counter-productive for a noise-cancelling application.
- Constraints or penalties on the norm of the adaptive-filter prevent the filter from diverging completely [38, 39, 40, 41, 42]. However, they do not avoid wrong filter updates.
- Keeping the norm of the secondary-path model smaller than the actual secondary path increases the robustness of the FxLMS [43]. However, manipulating the norm only does not prevent divergence if the phase error exceeds 90.

We present three solutions that are simple to implement, that do not require white noise injection and that yield robust noise-control with a correct update by the FxLMS algorithm. All solutions base on secondary-path measurements under different conditions reaching from a very tight to a completely loose headphone. First, we design a secondary-path model whose phase does not differ more than 70° from all measured secondary-paths. Secondly, we improve the convergence by implementing the two extreme cases of the secondary-paths measurements in parallel and weighting their contribution to the FxLMS dependent on the relation between the error and the reference input. Thirdly, we improve the robust performance by using an infrasonic test signal that detects when the headphone is being lifted. The results are compared with the system of [24, Zhang], because it combines two of the previously mentioned approaches, and finally, experiments proof the robustness of the proposed method.

6.3.1 FxLMS with Online Secondary Path Modelling

In this section, we review feedforward ANC with the FxLMS and the common way of online secondary-path estimation. We take the system proposed by [38, Zhang] as reference for it greatly eliminates the effects of the injected white noise, and it is the only one that takes sudden big changes in the secondary-path into account.

Fig. 6.27 shows the block diagram of the method of [38, Zhang]. The adaptive filters (W, H and $\hat{S}$) each minimize the squared error between their output and the output of the original plant that they should imitate. The LMS updates the adaptive filters with the negative gradient of this squared-error. For the adaptive filter W e.g., the vector of filter coefficients w is updated as

$$w(n+1) = w - \frac{de_w^2}{dw}.$$

With $\frac{de_w^2}{dw} \approx -e_w x'$ [8], the normalized LMS (which updates all adaptive filters in [38, Zhang]) reads as

$$w(n+1) = w(n) + \mu \frac{e(n)x'}{x'^T x'},$$

where μ is a stepsize parameter that controls the speed of convergence and x' is a vector of the latest N input samples (as in Fig. 6.27).

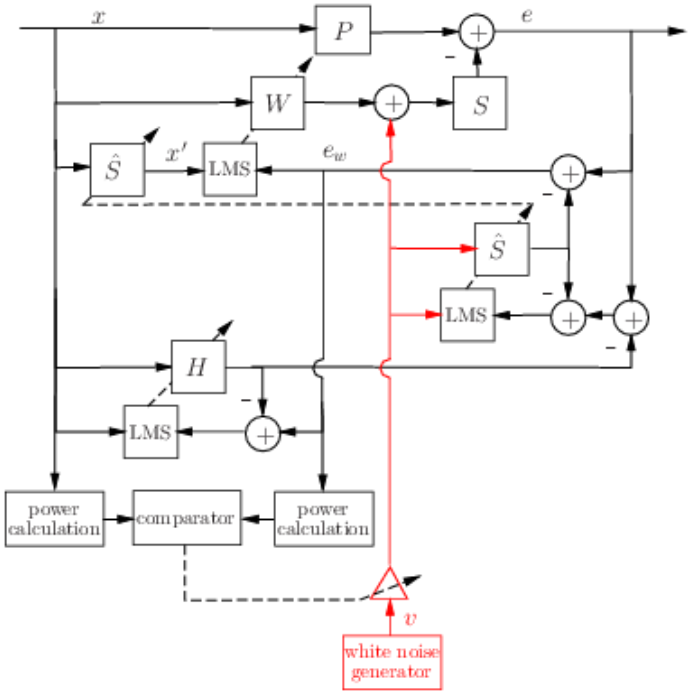

Figure 6.27 Block diagram of Zhang's method.

In the case of the adaptive noise-control-filter W, the LMS input x′ is not directly the same as the reference input to the plant P. The LMS input is the reference x that has been filtered by Ŝ, a model of the secondary path. Due to this filtered reference signal, this approach is called the filtered-x LMS.

The filter Ŝ introduces the same phase delay to the reference input as the real secondary-path S to the anti-noise signal. This shall make sure that the error sample e_w is correlated with the reference sample that actually caused this error. Only this time-aligned correlation is a correct gradient for the LMS update.

If Ŝ deviates from S, the correlation between the filtered reference x′ and the error e_w deviates from the real gradient too. For small deviations, the gradient is slightly wrong, but the LMS will still converge. For large deviation, (i.e. for phase differences > 90°), the gradient points into a completely wrong direction and the LMS diverges.

Therefore, white noise v is injected into the headphone to identify the secondary-path via the adaptive filter Ŝ. If Ŝ converges to the real secondary-path S, the effect of the white noise onto the adaptive noise-control filter W is eliminated. This however does not mean that v is eliminated from the residual error e, too. The injected white noise will still be heard by the user unless it lies below the masking level of the residual disturbance.

A third adaptive filter H is implemented to eliminate the effects of the incoming noise x onto the secondary-path identification. A comparison between the control-error power and the input-noise power is used to schedule the level of the injected white noise. In addition, the norms of the adaptive filters are constrained with a simple if-request to avoid divergence in case of a fast changing secondary-path S.

Instead of a white noise injection with two additional adaptive filters, norm computations, and norm constraints, we propose to measure the variation of the secondary-path off-line. The measured variety of secondary-paths will allow determining robust models $\hat{S}$ that prevent divergence of the FxLMS in all situations.

6.3.2 Secondary Path Measures

As stated above, small mismatches of the secondary-path model $\hat{S}$ do not matter much in the FxLMS [9]. However, fast and violent changes, e.g. when the headphones are suddenly lifted, can drive the adaptive filter unstable. We therefore measured the secondary path of a prototype headphone as already explained before on a dummy head under four very different conditions:

1. The headphone sits tightly on the artificial ear.
2. A leak of 105 mm3 is introduced between the artificial ear and the headphone.[1]
3. Two such leaks are introduced between the artificial ear and the headphone.
4. The headphone is completely loose.

Figure 6.28 once again shows the bode plots of the measurements. It can be seen that an increased leakage leads to an increased magnitude drop-off at low frequencies and to a positive phase shift.

[1] The leak is electrically equivalent to approx. 0.8 MΩ and 2.6 kH at 100 Hz.

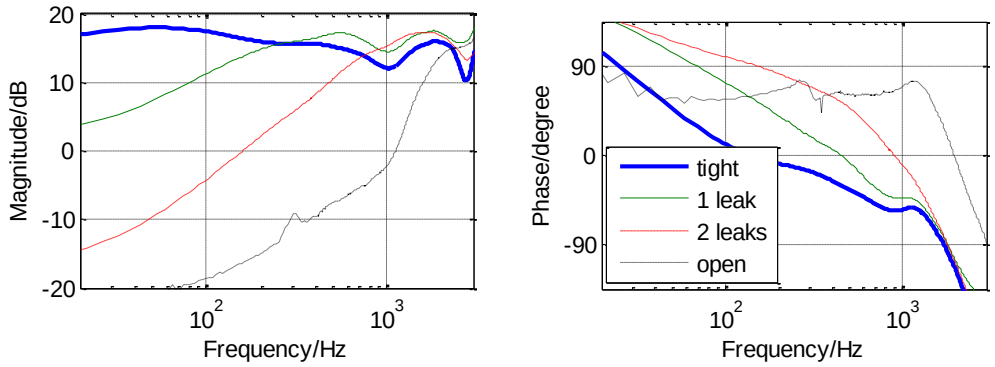

Figure 6.28 Frequency response of the secondary-path for a tight, leaky and completely loose headphone. The increased leakage leads above all to a magnitude drop-off at low frequencies.

The secondary path under tight conditions is assumed to be the regular use case. The phase error from the tight secondary path to the leaky and loose secondary-paths is shown in Figure 6.29. The phase error exceeds 90° for the secondary path with two leaks and the completely loose secondary path. As a consequence the FxLMS would diverge when the headphone is suddenly lifted (and the secondary path would change from tight to very leaky or completely loose.)

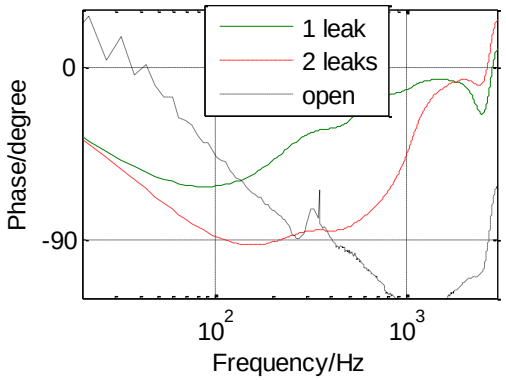

Figure 6.29 Phase error between the tight and the leaky/open secondary paths. For the secondary path with two inserted leaks, the error slightly exceeds 90° around 150 Hz. For the completely open secondary path, this phase-error tolerance is violated above 400 Hz.

Online secondary-path estimations without restriction on the filter-update are too slow to react on such fast changes. In the following, we present three solutions to prevent divergence of the FxLMS without restricting the filter-update.

6.3.3 Robust Secondary Path Models

6.3.3.1 Secondary Path Design from Phase Information

The easiest way to prevent divergence of the FxLMS is to omit the online estimation and to implement a secondary-path model whose phase differs less than 90° from all measured scenarios. This is possible, since the maximum difference between the phases of the measured secondary-paths is always smaller than 180° as can be seen from Figure 6.28 and Figure 6.29.

However, it is still favorable if $\hat{S}$ resembles the tight secondary-path for this is the regular use case of the ANC-headphone. Therefore, we choose a phase response $\phi_{\hat{S}}(\omega)$ that minimizes the error norm to the phase response of the tight secondary-path $\phi_{S_{\text{tight}}}(\omega)$ and keeps a phase difference of less than 70° to all measured secondary paths. This can be derived by constrained convex-optimization as

$$\min \left| \phi_{\hat{S}} - \phi_{S_{\text{tight}}} \right|_2$$

subject to

$$\phi_{\hat{S}}(k) - \phi_{S_{\max}}(k) < 70^\circ$$
$$\phi_{\hat{S}}(k) - \phi_{S_{\min}}(k) < 70^\circ,$$

where $\phi_{S_{\max}}$ and $\phi_{S_{\min}}$ are the maximum and minimum value of all measured phase responses per frequency bin k.

From the phase response $\phi_{\hat{S}}(k)$, a causal FIR sequence $\hat{s}(n)$ is derived over a fixed-point iteration as in [44]. In this approach, an initial $\hat{s}(n)$ is computed over an inverse Discrete Fourier Transform (DFT) from $\left|\hat{S}_0(k)\right| e^{j\phi_{\hat{S}}(k)}$ where $\left|\hat{S}_0(k)\right|$ is an initial guess of the magnitude of $\hat{S}$, e.g. the magnitude of the tight secondary-path measure. In an iterative process, the second half of the time domain sequence $\hat{s}(n)$ is forced to zeros to insure its causality. Then, the magnitude of the DFT of $\hat{s}(n)$ is taken as new initial guess for $\left|\hat{S}_0(k)\right|$.

The magnitude and phase of the converged $\hat{S}$ is shown in Figure 6.30, and the phase error from $\phi_{\hat{S}}$ to the 4 measured secondary-paths is depicted in Figure 6.31. As forced in the constrained convex optimization, the phase error stays below 70° in the whole bandwidth.

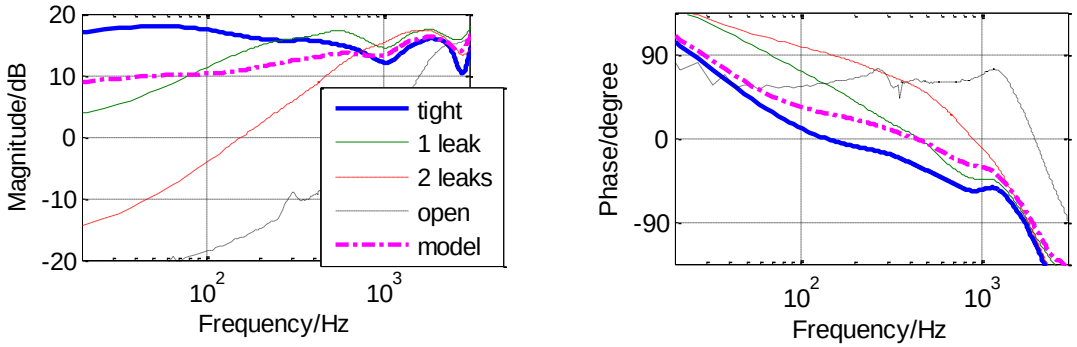

Figure 6.30 Frequency response of the measured secondary-paths and the chosen secondary-path model $\hat{S}$.

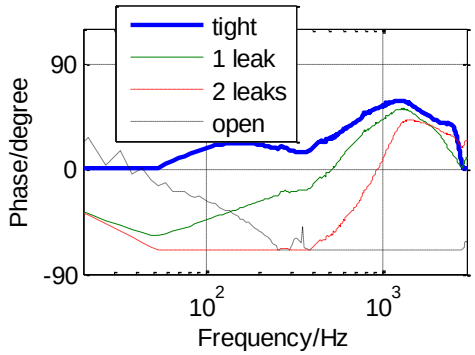

Figure 6.31 Phase error between $\hat{S}$ and the measured secondary-paths. The phase error to all measured scenarios stays below 70.

$\hat{S}$ is close to the tight secondary-path, but it deviates by 45° at 1000 Hz and by approximately 7 dB between 30 and 1000 Hz. Thus in the beginning of the FxLMS adaption (when the headphone sits regularly tight), the correlation between x' and e will not be as strong as when the secondary path is perfectly modeled. As consequence, there is less gain on the coefficient update and the FxLMS will converge slower. A comparison of the convergence-speeds will follow later on.

6.3.3.2 Two Secondary Path Models with Noise-Cancelling Analysis

To improve the speed of convergence, two secondary-path models can be implemented in parallel. $\hat{S}_1$ for the regular tight use-case and $\hat{S}_2$ for the lifted headphone. The latter is derived over a fixed-point iteration (as [44]) of the mean phase between the secondary-path measure with 2 inserted leaks and the one with the completely open headphones. Its frequency response is shown in Figure 6.32.

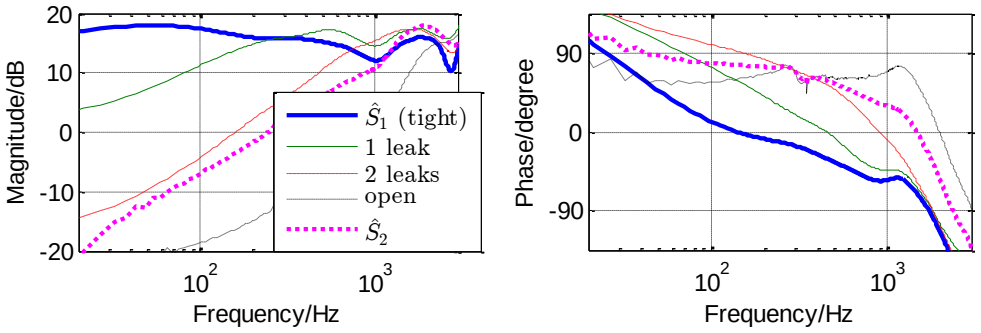

Figure 6.32 Frequency response of the measured secondary-paths and the chosen secondary-path models $\hat{S}_1$ and $\hat{S}_2$.

Dependent on the use-case, the contribution of each secondary-path model $\hat{S}_i$ to the FxLMS is weighted with an adaptive gain g_i as in Figure 6.33. The use-case itself can be identified by comparing the residual-error power with the input power.

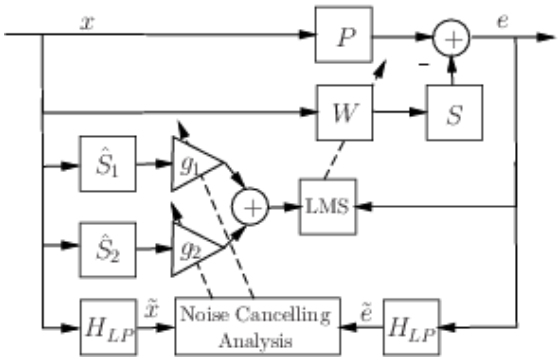

Figure 6.33 Parallel Implementation of two secondary-path models. $\hat{S}_1$ is for the regular tight use case and $\hat{S}_2$ is for the lifted headphone. Dependent on the use-case, the adaptive weights g_1 and g_2 control the contribution of each secondary-path model. The use-case itself can be identified by analyzing the noise-cancelling performance. The parallel arrangement of the filters only illustrates the idea; on a DSP it will be more beneficial to implement a single time-varying filter $\hat{S}(n) = g_1(n)\hat{S}_1 + g_2(n)\hat{S}_2$.

If the headphones sit regularly tight, the ear-cups build a pressure chamber which is important to reproduce enough low frequency sound pressure. If the headphones are lifted, the low-frequency sound leaks outside and the reproduction of the low-frequency anti-noise fails (compare Figure 6.28). As a consequence, the noise-cancelling performance is severely degraded, even if a perfect secondary-path model is available.

Figure 6.34 shows the relation between the residual error e and the input noise x in third-octave bands. The FxLMS is simulated with the 4 measured secondary-paths and the passive attenuation P of the prototype headphones is approximated by a second-order lowpass with a cut-off frequency of 500 Hz. $\hat{S}$ is chosen to always perfectly model the current secondary-path. Nevertheless, the passive attenuation is the only noise reduction that can be noticed if the headphones are lifted. Thus, the relation between the input power and the residual-error power below 500 Hz is a good indication whether the headphones sits regularly tight or not.

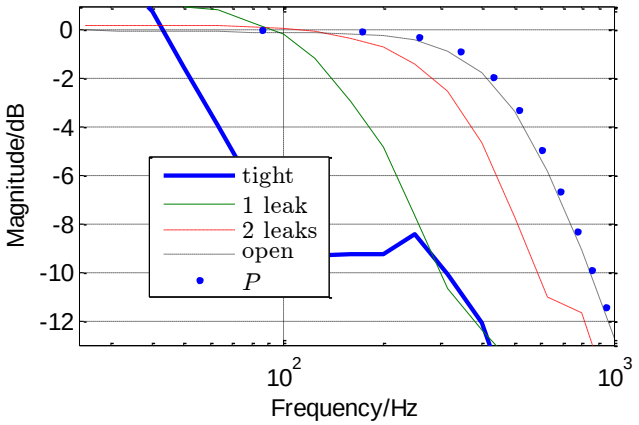

Figure 6.34 Relation between the residual error e and the input noise x in 3rd octave bands. In the tight case, good ANC is possible between 50 and 1000 Hz. In the very leaky and completely open case however, the only noise reduction that can be noted comes due to the passive attenuation P. As a comparison, the pure passive attenuation P is indicated as dots.

The input noise x and the residual error e are both filtered with a second-order low-pass with a cut-off frequency at 500 Hz. The power of the input noise P_x is calculated over a leaky integral as

$$P_x(n) = \alpha P_x(n-1) + \tilde{x}^2(n), \quad (3)$$

where α is the leakage factor and $\tilde{x}$ is the filtered input. The error-power P_e is calculated equivalently and α is chosen to be 0.999 in both cases. If the relation $\frac{P_e}{P_x}$ is small, noise has been effectively be cancelled which means that the headphones sit regularly tight. Consequently more weight has to be given to $\hat{S}_1$, the model of the tight secondary-path. If $\frac{P_e}{P_x}$ is close to 1, hardly any noise has been cancelled which means that the headphones are lifted and more weight has to be given to $\hat{S}_2$, the model of the loose secondary-path.

On the one hand, noise cancellation is already very pronounced if $\frac{P_e}{P_x}$ is below -10 dB (which corresponds to the linear factor 0.1). In this case, we want weight g_1 to be close to 1 and g_2 close to 0. On the other hand, we expect at least -5 dB (factor 0.3)if the headphone sits regularly tight. Above that level, we want g_2 to be close to 1 and g_1 close to 0. Hence we calculate the weights g_1 and g_2 as

$$\begin{aligned} g_1(n) &= 1 - g_2(n) \\ g_2(n) &= \frac{\frac{P_e}{P_x}(n) - 0.1}{0.3 + 0.1} \end{aligned}$$

but we restrict the weights to the interval [0,1]. If the weights should lie outside this interval they are rounded to 0 or 1 respectively.

Denote that the relation between P_e and P_x can also be used to detect divergence of the FxLMS when $P_e > P_x$; and note also that a single time-varying filter

$$\hat{S}(n) = g_1(n)\hat{S}_1 + g_2(n)\hat{S}_2 \quad (4)$$

can be implemented instead of the two parallel filter which saves computational power.

The filter W is initialized with a low-pass FIR. Therefore, an appropriate anti-noise is generated from the beginning of the usage. Consequently, also the relation between P_e and P_x is valid from the beginning of the usage. However, this noise cancelling analysis is only valid if there is a low-frequency noise excitation below 500 Hz. This is mostly the case when ANC-headphones are used, e.g. in airplanes, in traffic-noise and also in speech-noise, but might be situations where a user is exposed to high frequency disturbances only. In the following, we present an identification of the secondary-path for ambient noise with little low-frequency excitation.

6.3.3.3 *Two Secondary Path Models and Infrasonic Secondary-Path Identification*

In literature, a complete identification of the secondary-path is done with the injection of white noise. However, from Figure 6.28 it is clear that it suffices to identify the low-frequency response to be able to distinguish between the regular tight and the lifted use-case. In fact, it suffices to identify the magnitude at a single low frequency only. We propose to measure the secondary-path with a 18 Hz sinusoid for it is an infra-sound that cannot be heard by humans.

The 18 Hz test-tone is injected into the headphone as in Figure 6.35. Then the error signal e (which consists of the residual noise and the injected test-tone) is correlated with a delayed version of the original test-tone. The delay corresponds to the group delay of the tight secondary-path at 18 Hz such that the two signals are in phase if $S = S_{tight}$. Thus, the correlation gain reaches its maximum when the headphones are worn regularly tight.

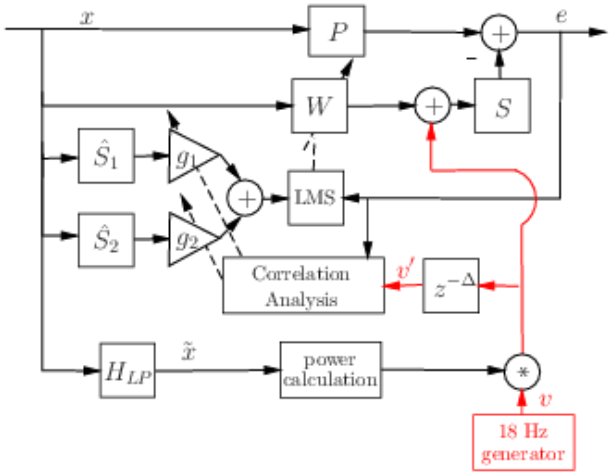

Figure 6.35 A 18 Hz tone detects whether the headphones are regularly tight or lifted and loose.

The correlation gain ξ is calculated over a leaky integral as

$$\xi(n) = \beta\xi(n-1) + e(n)v'(n)$$

where v′ is the delayed version of the test-tone and β is the leakage factor which is set to 0.99996. The signal-to-noise-ratio (SNR) of the correlation suffers from the residual ambient noise. The SNR can either be increased by the integration time or by the level of v within the error e. We have to set the level of v 10 dB above the level of the input noise because the test-tone already has a long periodicity and the application requires a fast detection of changes in the secondary path. Therefore the input noise x is filtered with a second order low pass at 50 Hz and the power of the filtered input x̃ (calculated as above) schedules the level of v to approximately +10 dB. Although this playback-level is rather

high, it does not disturb the listener and it does not deteriorate the FxLMS as will be shown in the following.

The correlation-gains for the four measured secondary-paths are shown in Figure 6.36. They are normalized such that the maximum correlation gain is around 1. This maximum occurs for the tight sitting headphone. In the leaky cases, ξ varies around 0. The filter weights are therefore defined as

$$\begin{aligned} g_1(n) &= \xi_{[0,1]}(n) \\ g_2(n) &= 1 - g_1(n) \end{aligned}$$

where $\xi_{[0,1]}$ is the normalized correlation gain with the negative values set to 0.

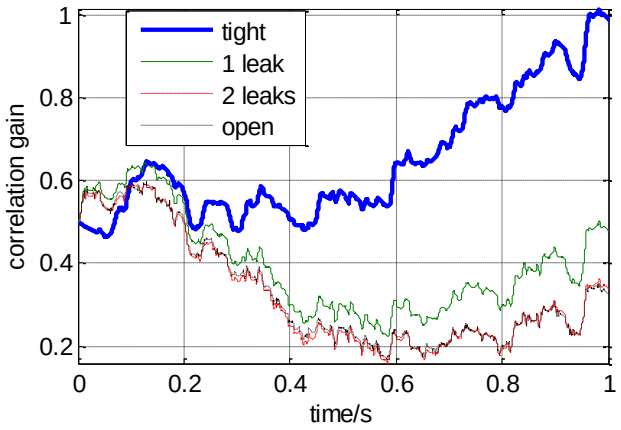

Figure 6.36 Correlation gain over time for the 4 measured secondary-paths. If the headphones sit tight, the 18 Hz tone is played back loud enough and yields a large correlation gain. In the other cases, especially for the very leaky and the open headphones, the 18 Hz tone is hardly played back. This is why the correlation gain varies randomly around 0. The tight and the leaky cases can be distinguished after about 0.2 seconds.

6.3.3.4 Two Secondary Path Models with a Combined Detection Approach

Approaches 6.3.3.2 and 6.3.3.3 both rely on a pair of secondary-paths models that are derived from laboratory-measurements. The model $\hat{S}_1$ is designated for the regular tight use-case and $\hat{S}_2$ for the lifted headphones. On the one hand, approach 6.3.3.2 identifies the current use-case over the relation between the input-power and the residual-power. However, this relation is only a meaningful measure if there is enough low frequency content in the ambient noise. On the other hand, approach 6.3.3.3 injects an infrasonic test-tone into the headphones and detects the current use-case via a single correlation. However, its drawback is a poor correlation-SNR if there is a lot of very low-frequency content in the ambient noise. Since one approach benefits from a strong low-frequency excitation and the

other from a low, it is obvious to combine both approaches to yield an optimal use-case detection for all kind of disturbance noises.

Both approaches measure the low-frequency power of the input noise anyway. We define a threshold of this power as $\theta = 60$ dBA. If the input-power is above 60 dBA, there is enough low-frequency excitation to do the noise-cancelling analysis of approach B. If the low-frequency input-power is below 60 dBA, the 18 Hz test-tone can be played back with up to +20dB which yields a very good correlation-SNR and consequently a very fast detection of changes in the secondary-path as can be seen in Figure 6.37.

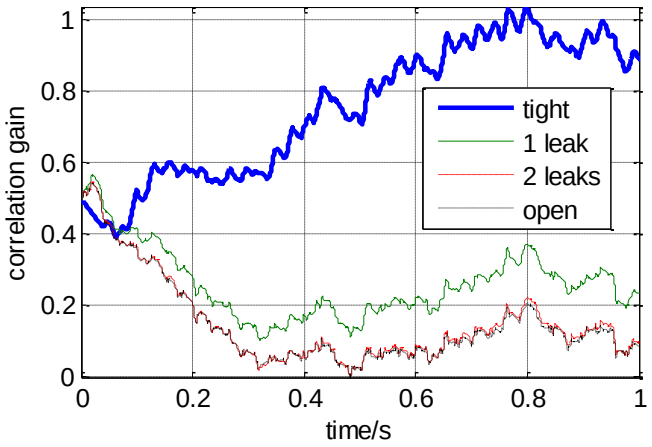

Figure 6.37 Correlation gain over time for the 4 measured secondary-paths with +20 dB SNR. The regular use-case can be distinguished earlier and more clearly as with the -10 dB SNR from Fig. 10.

The increased play-back level requires a new value for the leakage factor β. In general, the normalized correlation gain $\tilde{\xi}$ can be formulated as

$$\tilde{\xi}(n) = \beta\tilde{\xi}(n-1) + e(n)v'(n)\frac{SNR}{P_x}$$

with the linear signal-to-noise-ratio SNR and with

$$\beta = 1 - \frac{SNR}{10^{-5}}.$$

In the following section, we compare the performance of the 3 approaches whereas the latter approaches are used depending on the low-frequency excitation as proposed here in the combined approach.

6.3.4 Results

To evaluate the proposed approaches, we simulate the FxLMS with $\mu = 0.003$ for 5 seconds. We are interested in the FxLMS behavior when the phase of the secondary path changes more than 90°. Therefore, we change the secondary-path every second according to the following sequence: $S_{tight} \rightarrow S_{2leaks} \rightarrow S_{tight} \rightarrow S_{open} \rightarrow S_{tight}$. The comparison is done for

- white noise input,
- for a high-pass filtered white noise and
- for a narrow-band noise input. For the narrow-band input, we filter white noise with a second-order peak filter around 800 Hz.

As passive attenuation P, we choose a second-order low pass filter again. In case of the white noise input, there is a strong low frequency excitation. Therefore, the noise-cancelling analysis is taken for the combined approach. The normalized squared residual-error is shown in Figure 6.38. It is normalized by the power of the noise which entered the headphone.

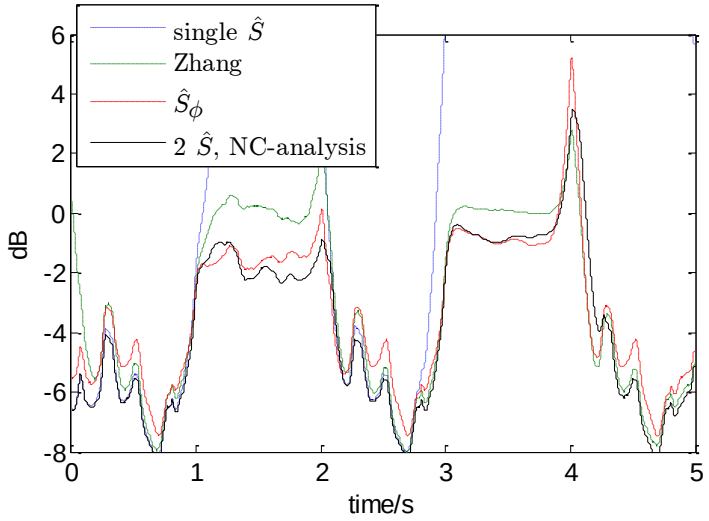

Figure 6.38 Relation between the residual-noise power P_e and the noise that entered the headphone in dB. The excitation signal is white noise. Negative values denote active noise cancellation whereas positive values mean that the noise inside the headphone is being amplified.

If the tight measurement is taken as secondary path model, the residual error is amplified by 6 dB if the secondary path changes to S_{2leaks} and the FxLMS diverges completely when the secondary-path changes to S_{open}. Zhang's method keeps the algorithm stable, but our secondary-path model S_Φ which is designed form the phase information

yields better results when the headphones are lifted. Even better results are obtained, if two secondary path filters are implemented and weighted according to the noise-cancelling analysis.

In the next simulation, the white excitation noise is filtered with a second-order high-pass. In this case, there is not enough low-frequency excitation to apply the noise-cancelling analysis. Therefore, the infrasonic test-tone is used instead. The results are shown in Figure 6.39. Again, without precautions about the secondary-path model, the FxLMS would drive unstable if the secondary-path changes to S_{open}. Zhangs's method keeps the FxLMS stable, but its residual-error power is 1-2 dB larger than with our proposed model S_{Φ}. Implementing two secondary-path models and weighting them according to the correlation gain of the injected infrasonic signal brings another improvement of ~2 dB, if the headphones sit regularly tight.

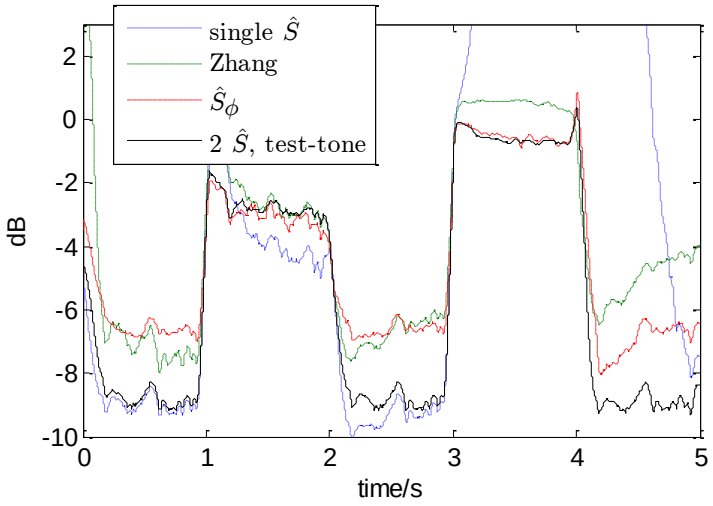

Figure 6.39 Relation between the residual-noise power P_e and the noise that entered the headphone in dB. The excitation signal is white noise that is high-pass filtered.

Finally, we test the algorithms with a narrowband excitation around 800 Hz. Figure 6.40 shows that Zhang's method does not diverge, but it hardly yields ANC compared to our approaches. Denote too, that for this narrow band excitation, the implementation of the two secondary-path models does not have so much benefit. It yields a better ANC if the secondary-path changes to S_{open}, but its performance is slight worse than the approach 6.3.3.1 if the secondary-path changes to S_{2leaks}.

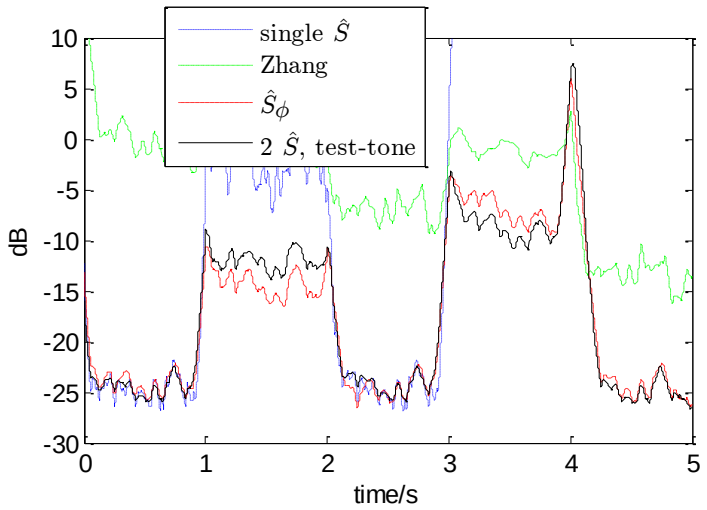

Figure 6.40 Relation between the residual-noise power P_e and the noise that entered the headphone in dB. The excitation signal is narrowband noise around 800 Hz.

The results show that the proposed methods keep the FxLMS stable, even for abrupt and violent changes in the secondary path. Compared to Zhang's method, we do not constrain the filter update and therefore we yield improved ANC results. Since the secondary-path models can be implemented as IIR filters, our approaches are also more cost-efficient and easier to implement.

7 Conclusion

In this report, several techniques of ANC for headphones are reviewed. An analogue feedback prototype is presented and new procedures are introduced for both, analogue feedforward filter-design and for the assessment of ANC. The dependency of digital feedforward ANC on the latency of the converters is examined and a further prototype for a hybrid digital/analogue solution is presented, and the performance of digital feedforward and digital feedback ANC are compared.

Adaptive feedback-ANC is a very powerful solution for headphone applications, but (as all feedback systems) it suffers from the risk of instabilities. We present an algorithm that avoids these instabilities and preserves all the benefits from adaptive feedback ANC at the same time.

In particular, we examine how the secondary path changes when the headphone is lifted and demonstrate that these changes affect the stability of the FxLMS adaption and the feedback loop. We propose to use the leaky FxLMS to overcome the first stability issue. We show that the leaky FxLMS keeps the adaption stable even during the biggest changes in the secondary path. To overcome the feedback stability issue, we study the pole locations that cause the instabilities under different wearing- and noise conditions. In this study, we identify three different frequency bands where the poles of the feedback loop exceed the unit circle. The poles at frequencies above 1200 Hz can easily be controlled by a first-order low pass filter that hardly affects the ANC bandwidth.

To control the poles in the two lower frequency bands, we develop an algorithm that detects changes in the secondary path. We use the fact that the adaptive filter increases its low-frequency gain if the headphone is lifted. We show that this low-frequency amplification is independent form the excitation-noise characteristic and that it is sufficient to check the filter's DC-gain to identify a lifted headphone. Once the lifting is identified, the adaptive filter is gradually changed to a stable default filter from which the leaky FxLMS adaption starts again.

We tested our algorithm for various use cases and show that it yields robust ANC when the headphone sits regularly tight and still preserves stability if the headphone is suddenly lifted. The algorithm is derived from measurement data on a prototype headphone, but it can also be generalized since the effects of leakages between the ear and the ear-cup are the same for all headphones.

8 Appendix – Preliminary Empirical Study on the Secondary-Path Influences

Headphones with ANC (Active Noise Cancellation) have at least one microphone for each side (left and right respectively), which deliver information about the ambient noise in order to create an adaptive filter for a noise cancelling system (basically an inversion of the phase). The reproduced noise-cancelling-signal by the loudspeakers in the headphones will cancel itself with the incoming noise from outside the headphones. The adaptive filter that changes and adapts itself accordingly to the angle of the arriving noise, will be controlled by a LMS algorithm. This algorithm requires, besides the reference signal (noise signal), also an error signal which will provide information about the remaining noise (residual noise) after the noise cancellation process. The reference and error signals must thereby have the same time displacement. The error signal will, during active noise cancellation, always be delayed. This is a consequence of the AD- and DA-conversions that will take place during the ANC process as well as the group delay of the transmission path from the loudspeaker to the error-microphone (the so-called secondary path). The reference signal must therefore be artificially delayed. Whereas the conversion time of the AD and DA converters does not change, the group delay of the secondary path may constantly vary, depending on the current case and will be different every time one puts on the headphones. The effects of a changing secondary path as well as the estimation accuracy of latter on the ANC are to be analyzed.

We will take a look at the importance of knowing the secondary path S and the accuracy needed in order to create a good anti-noise signal. This will be done by reducing the length of the transfer function of the secondary path and by using an estimation of $\hat{S}$, e.g. when the headphones are not correctly positioned. This last effect can be simulated by generating a leakage of air when measuring the secondary path. We will show the effects of not knowing the secondary path accurately for an ANC-system.

For the first considerations, we assume the transfer function of the secondary path to be TF_tight. This was made by measuring the secondary path when the headphones were put on in a leak-proof manner. The estimated secondary path $\hat{S}$ will be a shorter version of the original secondary path. For the windowing process a Hanning window was used and the length was chosen by default to be one quarter of the length of the original secondary path.

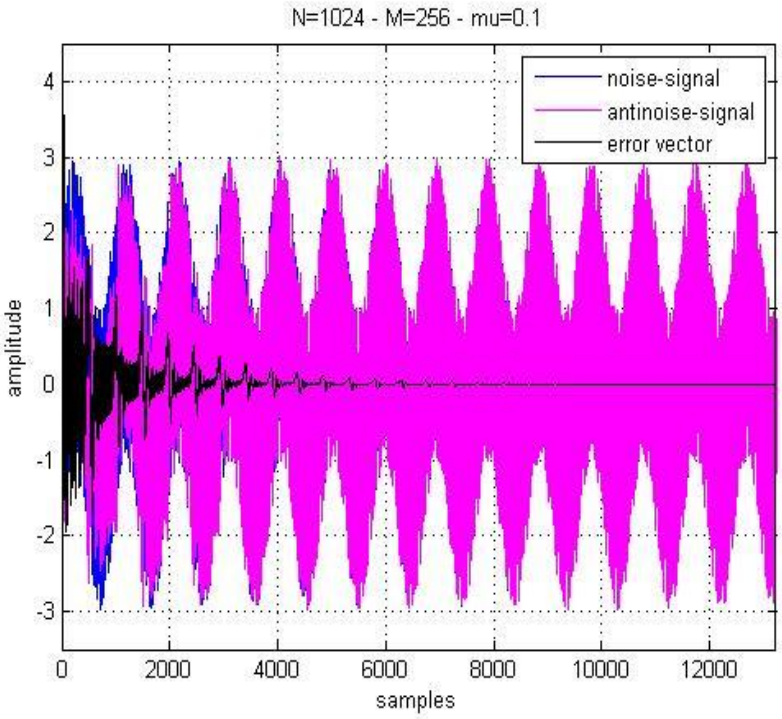

Figure 8.1. Noise, anti-noise and residual error in a feedforward LMS application with a headphone that was pulled tight to the artificial ear.

For the next case $\hat{S}$ = TF_onhead, meaning the estimated transfer function of the secondary path will be described when the headphones are put on an artificial head. For this simulation it is necessary to change the learning rate to 0.01 in order to get stable results. The impact of this factor will be analyzed later on.

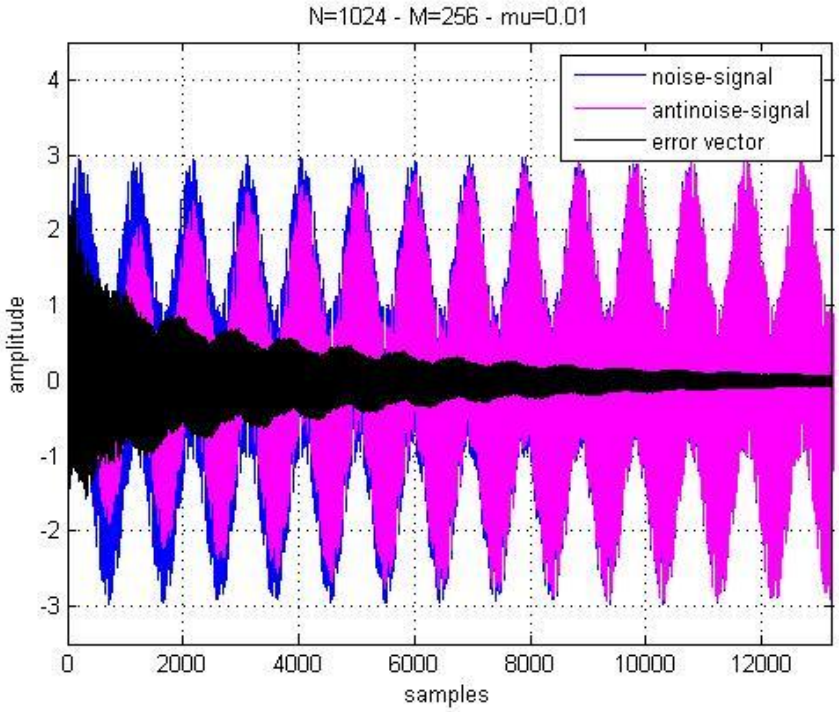

Figure 8.2. Noise, anti-noise and residual error in a feedforward LMS application with headphone that was regularly put on a dummy head.

For the next case we assume that $\hat{S}$ = TF_3mm, which means that the headphones were again not put on in a leak-proof manner. An opening of 3mm was made for simulating an air leakage by separating the headphones from the artificial head.

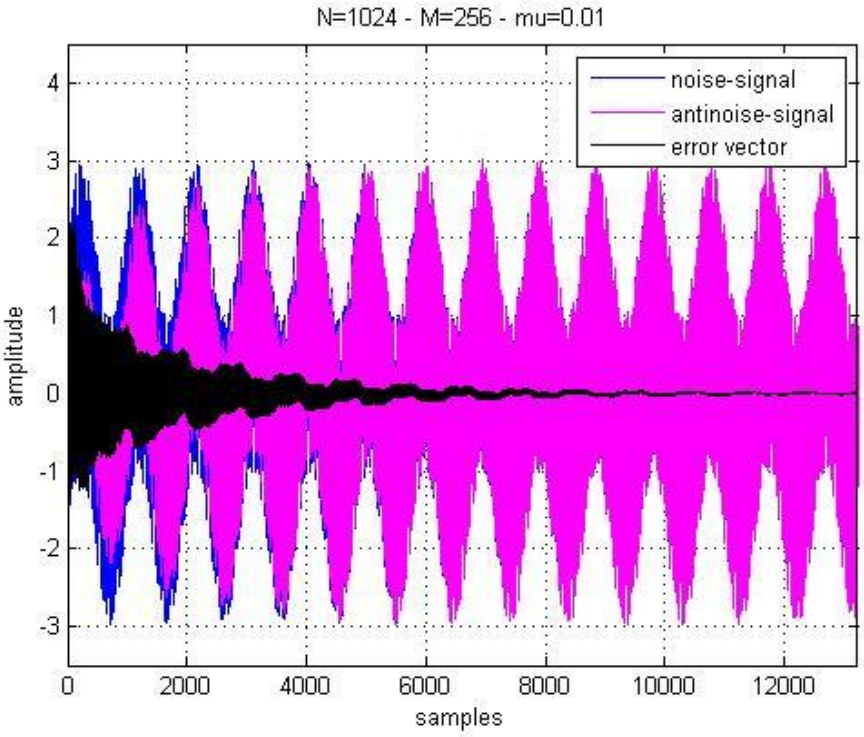

Figure 8.3. Noise, anti-noise and residual error in a feedforward LMS application with a leaky headphone.

When simulating the next case, 2 conic slots where inserted to the sides of the headphones pads for the measurement of the secondary path. Apparently a small leakage of air is worse than actually separating the headphones from the surface.

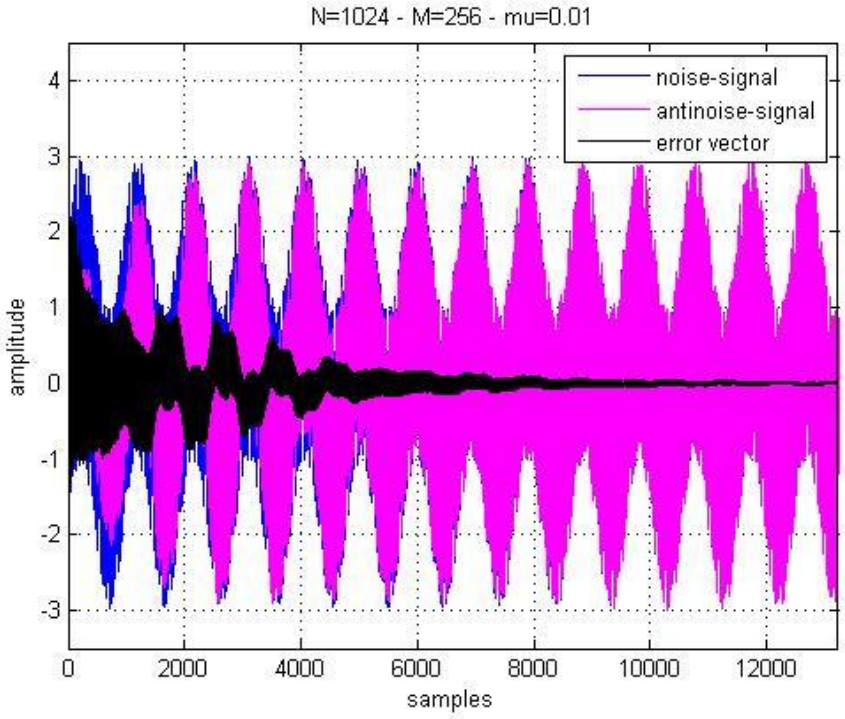

Figure 8.4. Noise, anti-noise and residual error in a feedforward LMS application with a very leaky headphone.

We now want to simulate the real case when using ANC headphones. For this purpose we will assume that tf_hat (meaning the estimated secondary path implemented in the algorithm) to be tf_tight (this represents the measurement of the secondary path on an artificial head when headphones are densely worn). Interesting for us is to know how exactly we need to know the secondary path. This will be simulated by decreasing the length of tf_hat.

For the actual secondary path, we take different transfer functions in order to simulate the different cases when using the headphones (concretely, when the headphones are not worn in a leak-proof manner). The length of this transfer function will not be changed (4096 taps).

This comparison is done for two different conversion times. At first, we'll take a look at it, for a conversion time of 0,7 ms and then for a more real conversion time of 21ms. These conversion times are valid for each conversion unit in the system.

At last we examine the error signal in the frequency domain for a better understanding of the achieved anti-noise signal.

• Case n°1 conversion time of 0,7 ms

TF_real = tf_1sl (1 conic slot simulates that the headphones are worn in a non leak-proof manner)

The plots show that the error signal stays similarly for most of the different lengths. There is nonetheless a kind of maximum in the error signal to be found in all cases but for a length of 512 taps. We can see that there is no big difference between 2048 and 256 taps in the error signal (see scaling of y-axis).

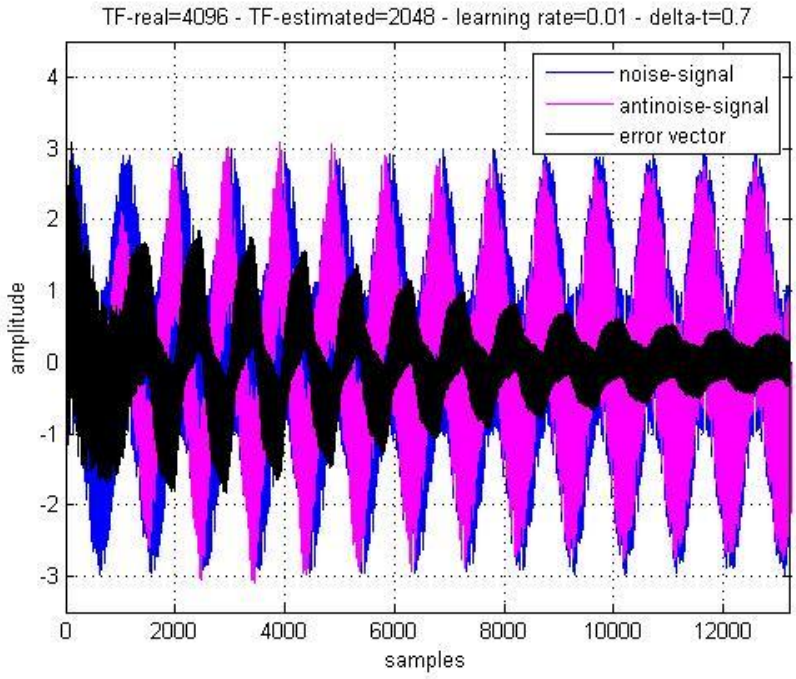

(a)

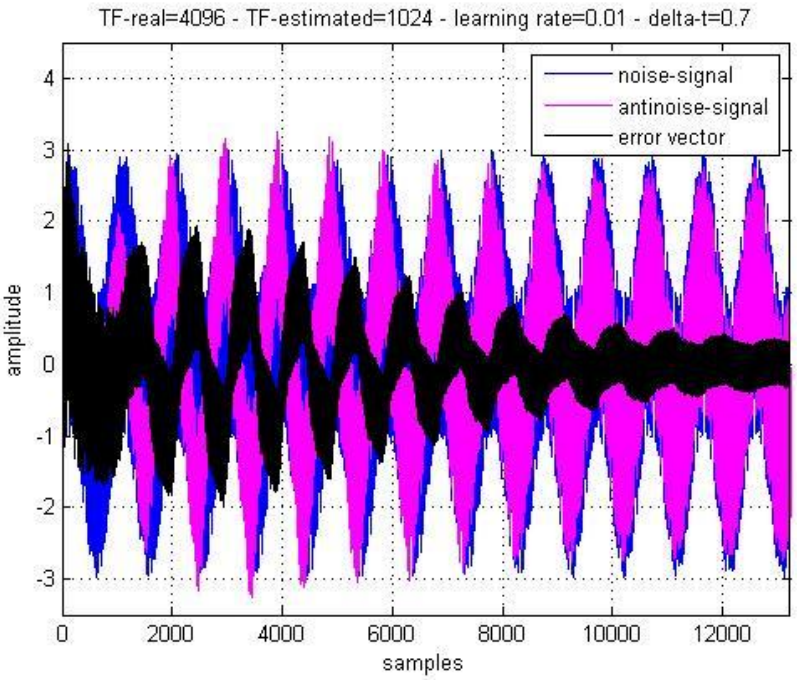
TF-real=4096 - TF-estimated=1024 - learning rate=0.01 - delta-t=0.7
noise-signal
antinoise-signal
error vector
amplitude
samples
4
3
2
1
0
-1
-2
-3
0
2000
4000
6000
8000
10000
12000

(b)

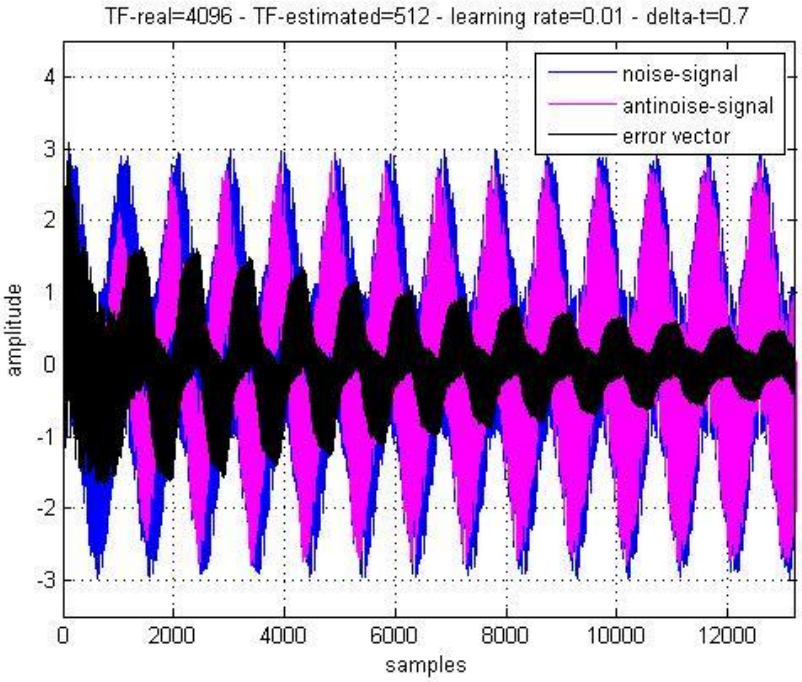
TF-real=4096 - TF-estimated=512 - learning rate=0.01 - delta-t=0.7
noise-signal
antinoise-signal
error vector
amplitude
samples
4
3
2
1
0
-1
-2
-3
0
2000
4000
6000
8000
10000
12000

(c)

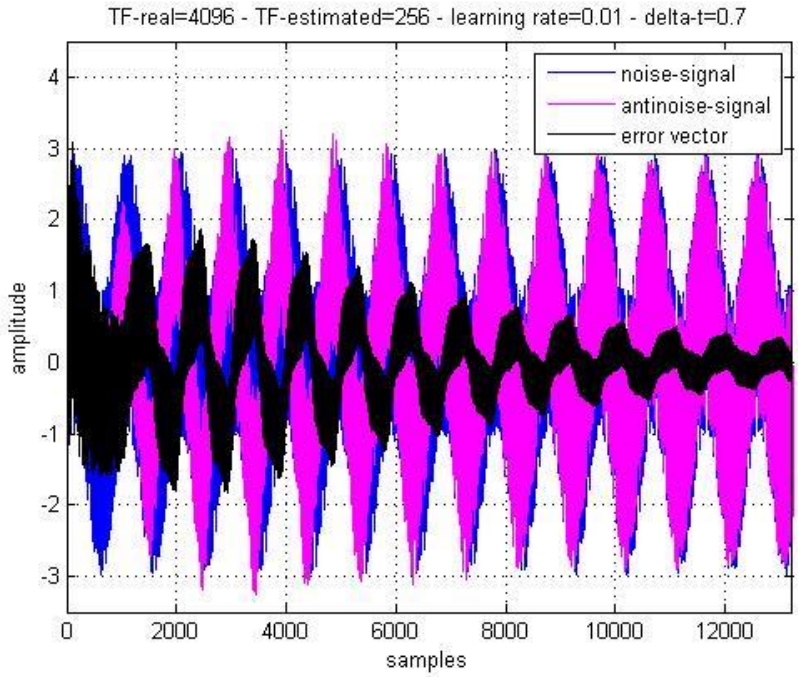

(d)

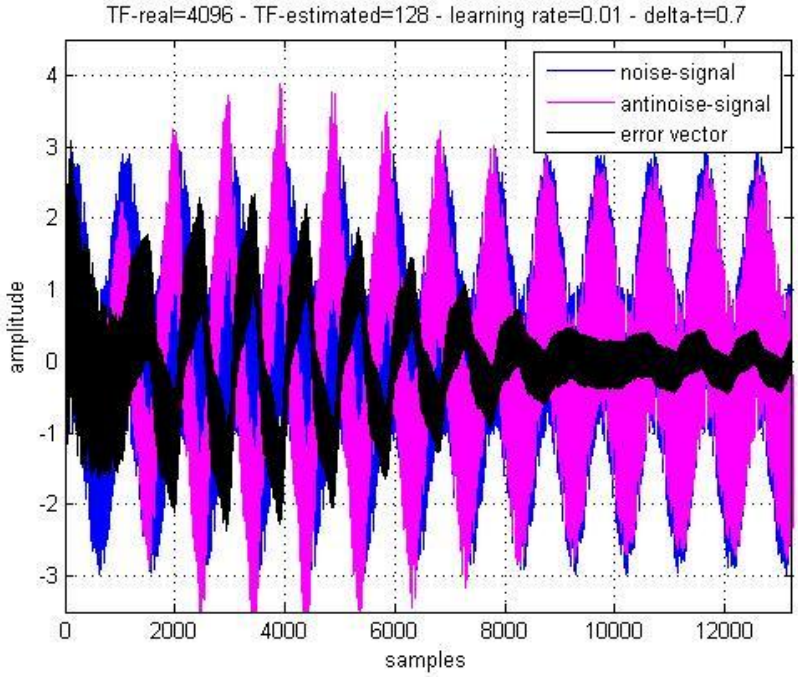

(e)

Figure 8.5. Comparison of the anti-noise and the residual error in a feedforward LMS application with an estimated secondary path of different length. The length is given in taps at 44.1 kHz: (a) 2048, (b) 1024, (c) 512, (d) 256, and (e) 128 taps. The actual secondary path is derived from the measurement with one conic leakage (whereas the estimate is taken form the tight measurement). The conversion time is 0.7 ms.

Now the actual secondary path is changed to TF_real = tf_2sl (2 conic slots simulate that the headphones are worn in a non leak-proof manner). For this particular case, the length of the estimated secondary path (tf_hat) does not have any influence at all. The 2 slots make a fast adaptation impossible.

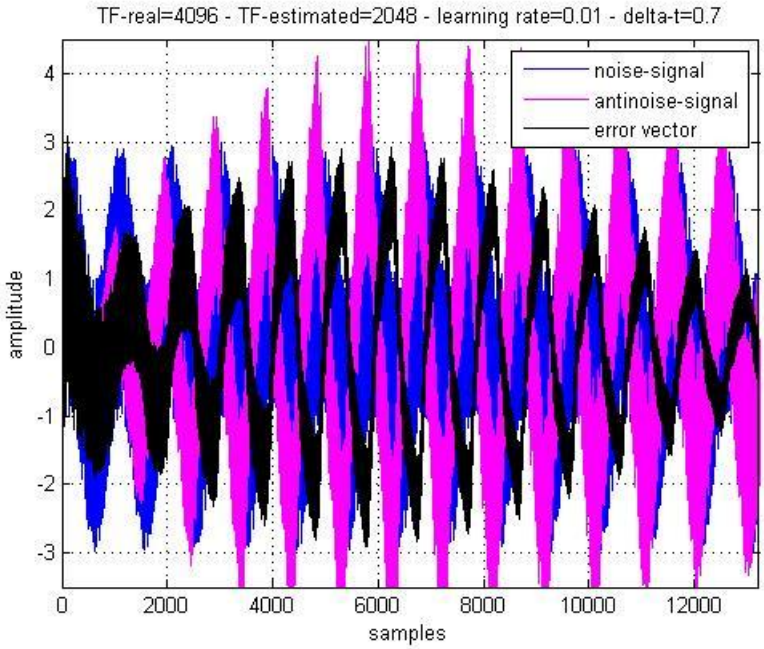

(a)

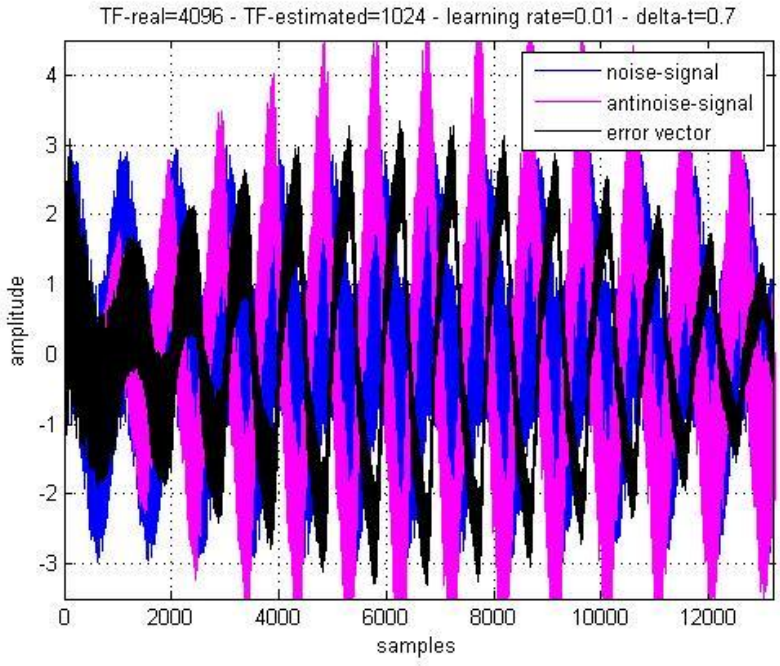

(b)

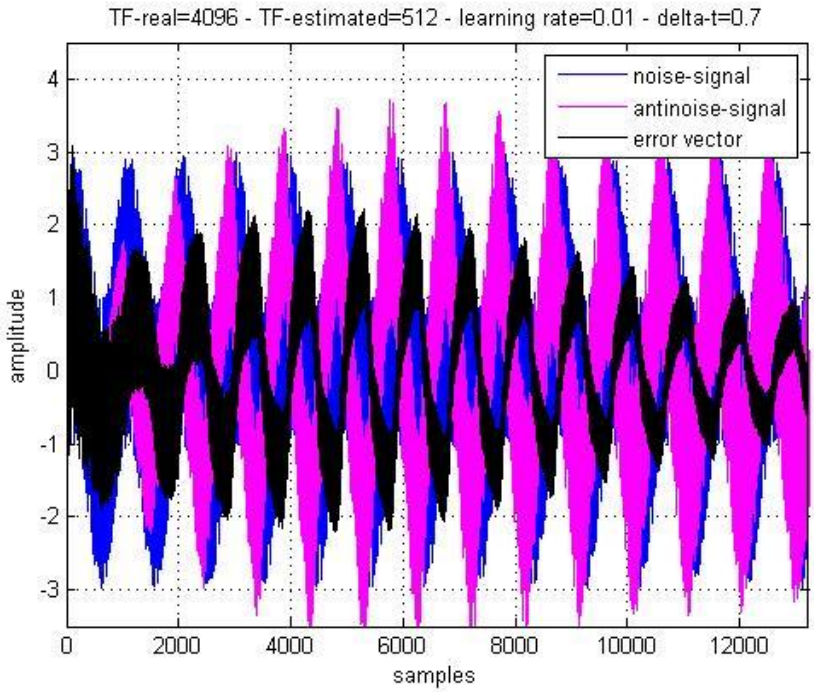
TF-real=4096 - TF-estimated=512 - learning rate=0.01 - delta-t=0.7
noise-signal
antinoise-signal
error vector
amplitude
samples
4
3
2
1
0
-1
-2
-3
0
2000
4000
6000
8000
10000
12000

(c)

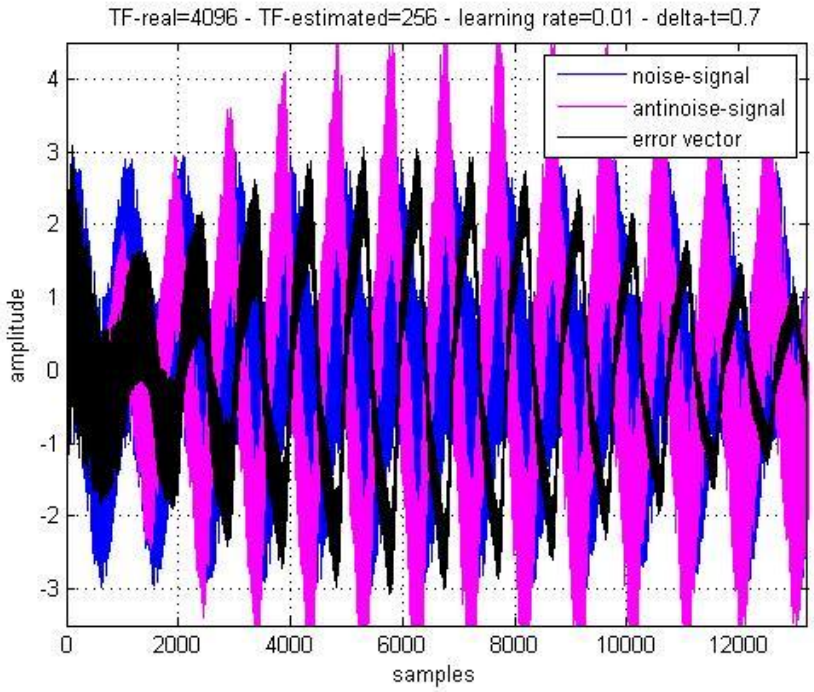
TF-real=4096 - TF-estimated=256 - learning rate=0.01 - delta-t=0.7
noise-signal
antinoise-signal
error vector
amplitude
samples
4
3
2
1
0
-1
-2
-3
0
2000
4000
6000
8000
10000
12000

(d)

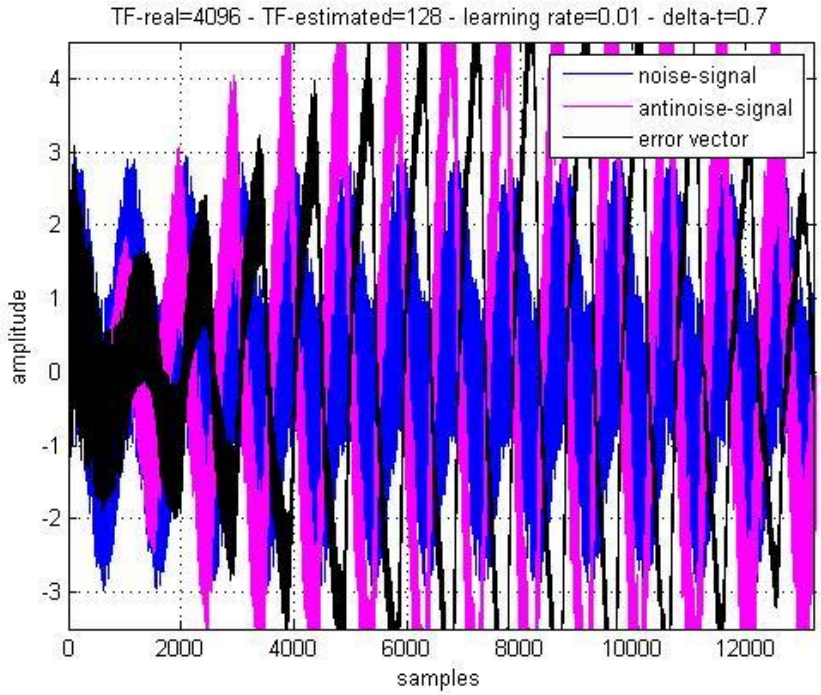

(e)

Figure 8.6. Comparison of the anti-noise and the residual error in a feedforward LMS application with an estimated secondary path of different length: (a) 2048, (b) 1024, (c) 512, (d) 256, and (e) 128 taps. The actual secondary path is derived from measurements with two conic leakages. The conversion time is 0.7 ms.

For the following simulation, TF_real = tf_2mm (a distance of 2 mm between headphones and artificial head is kept in order to simulate an air leakage). Again, no big influence is to be seen between all the different lengths chosen for the implemented secondary path.

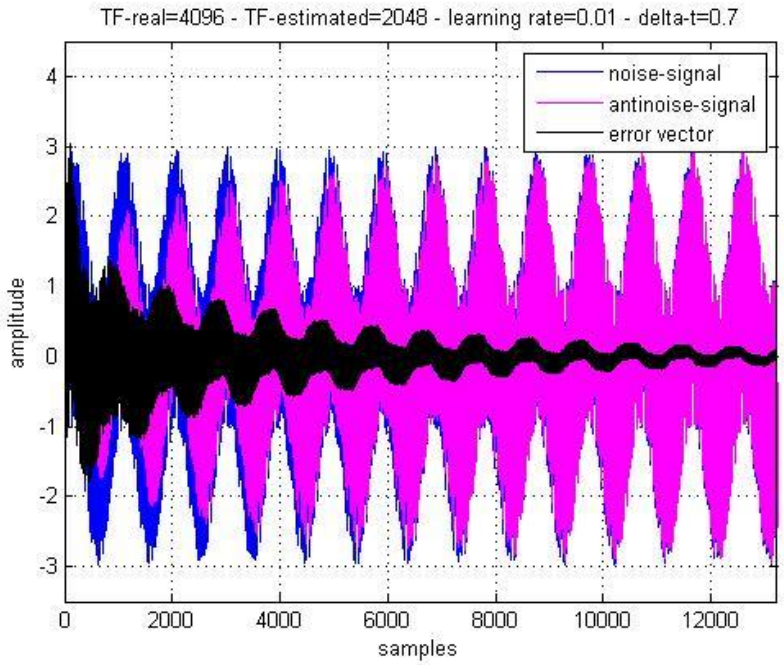

(a)

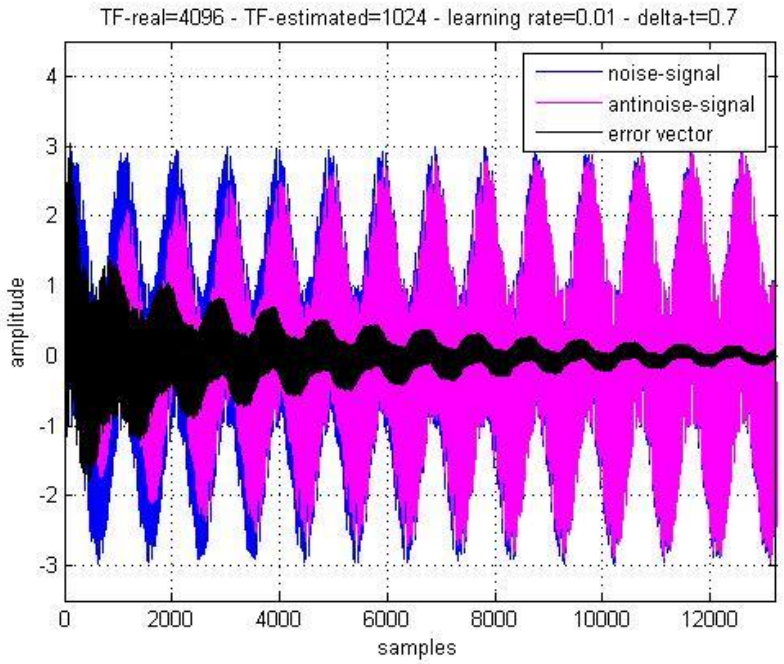

(b)

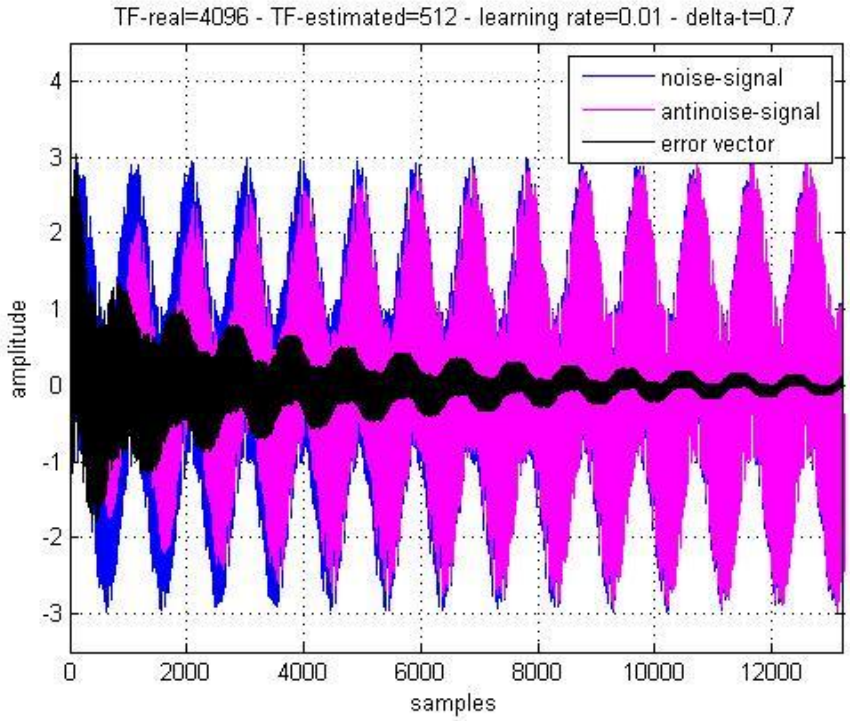
TF-real=4096 - TF-estimated=512 - learning rate=0.01 - delta-t=0.7
noise-signal
antinoise-signal
error vector
amplitude
samples
4
3
2
1
0
-1
-2
-3
0
2000
4000
6000
8000
10000
12000

(c)

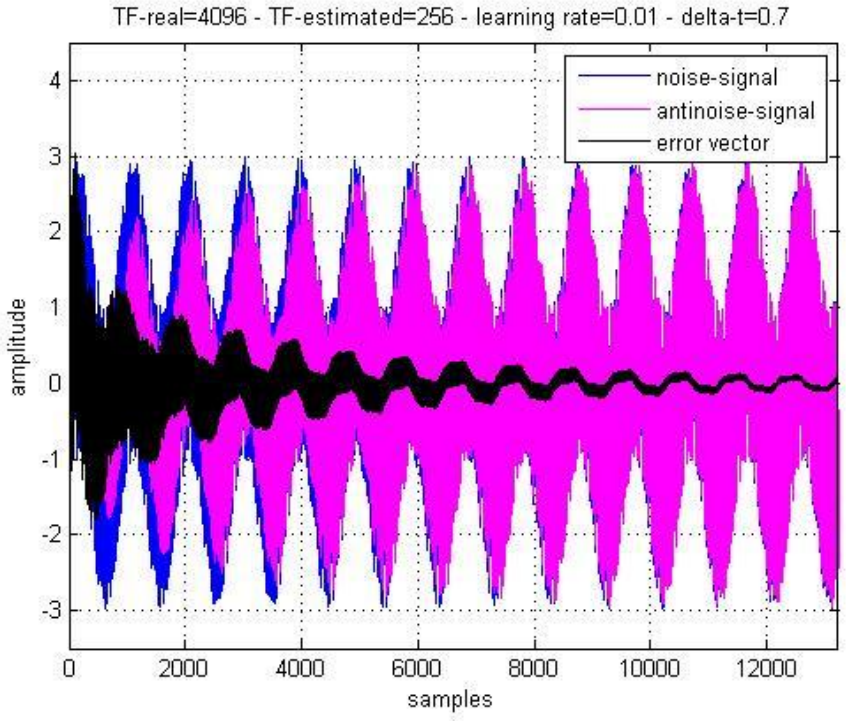
TF-real=4096 - TF-estimated=256 - learning rate=0.01 - delta-t=0.7
noise-signal
antinoise-signal
error vector
amplitude
samples
4
3
2
1
0
-1
-2
-3
0
2000
4000
6000
8000
10000
12000

(d)

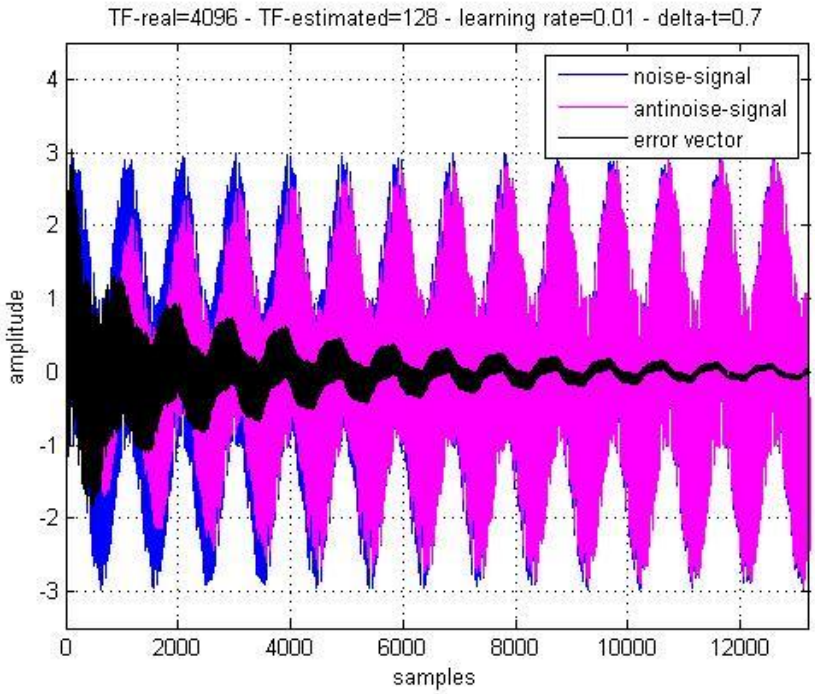

(e)

Figure 8.7 Comparison of the anti-noise and the residual error in a feedforward LMS application with an estimated secondary path of different length: (a) 2048, (b) 1024, (c) 512, (d) 256, and (e) 128 taps. The actual secondary path is derived from measurements with a 2 mm leakage between the headphone and the artificial ear. The conversion time is 0.7 ms.

TF_real = tf_4mm (a distance of 4 mm between headphones and artificial head is kept in order to simulate an air leakage. For a distance of 4mm we get a similar result as with the 2mm leakage.

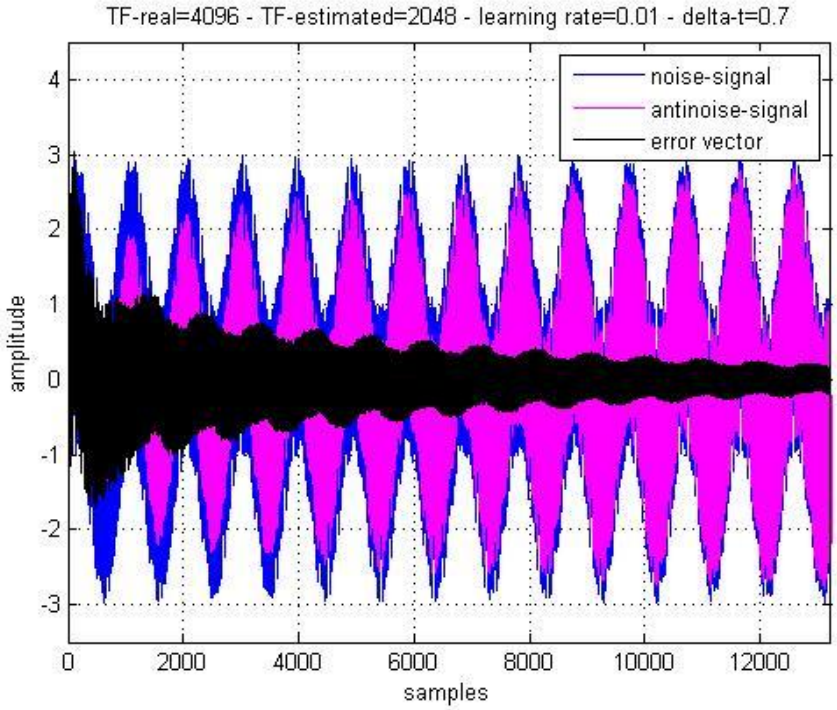

(a)

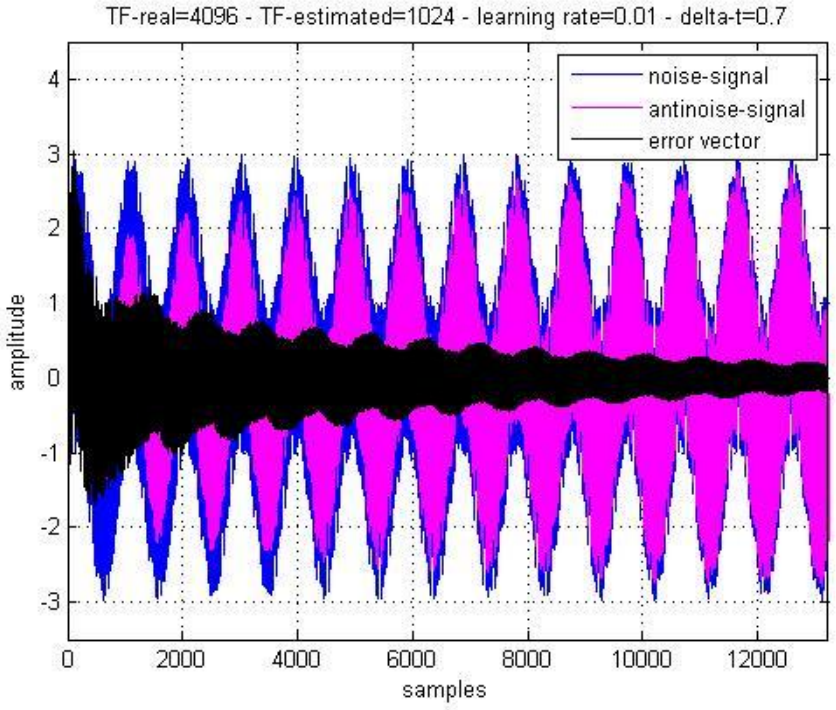

(b)

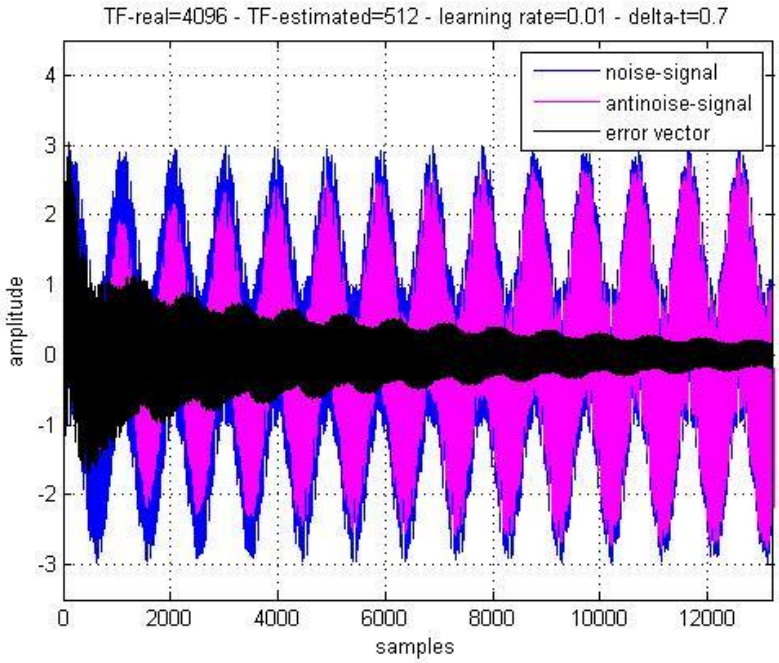
TF-real=4096 - TF-estimated=512 - learning rate=0.01 - delta-t=0.7
noise-signal
antinoise-signal
error vector
amplitude
samples
4
3
2
1
0
-1
-2
-3
0
2000
4000
6000
8000
10000
12000

(c)

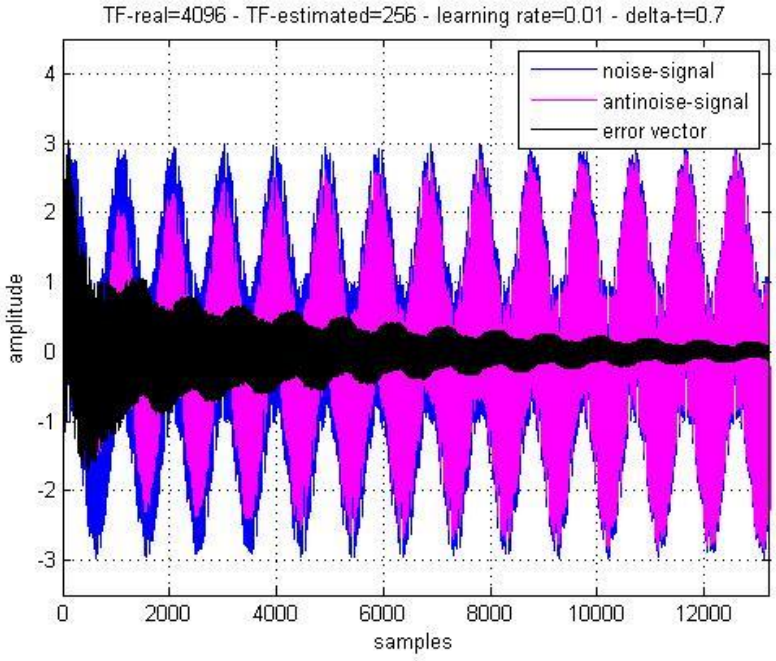
TF-real=4096 - TF-estimated=256 - learning rate=0.01 - delta-t=0.7
noise-signal
antinoise-signal
error vector
amplitude
samples
4
3
2
1
0
-1
-2
-3
0
2000
4000
6000
8000
10000
12000

(d)

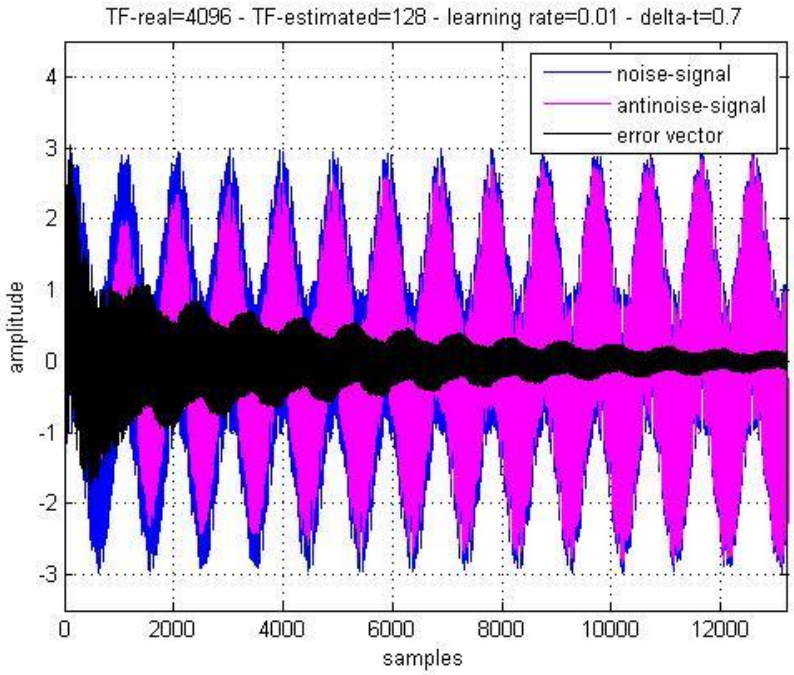

(e)

Figure 8.8 Comparison of the anti-noise and the residual error in a feedforward LMS application with an estimated secondary path of different length: (a) 2048, (b) 1024, (c) 512, (d) 256, and (e) 128 taps. The actual secondary path is derived from measurements with a 4 mm leakage between the headphone and the artificial ear. The conversion time is 0.7 ms.

In order to have a good reference, we present the results when the headphones are worn in a leak-proof manner. Thus, TF_real = tf_tight . This case only reassures the behavior we have seen before. The length of the estimated secondary path does not have a considerable influence on the ANC behavior.

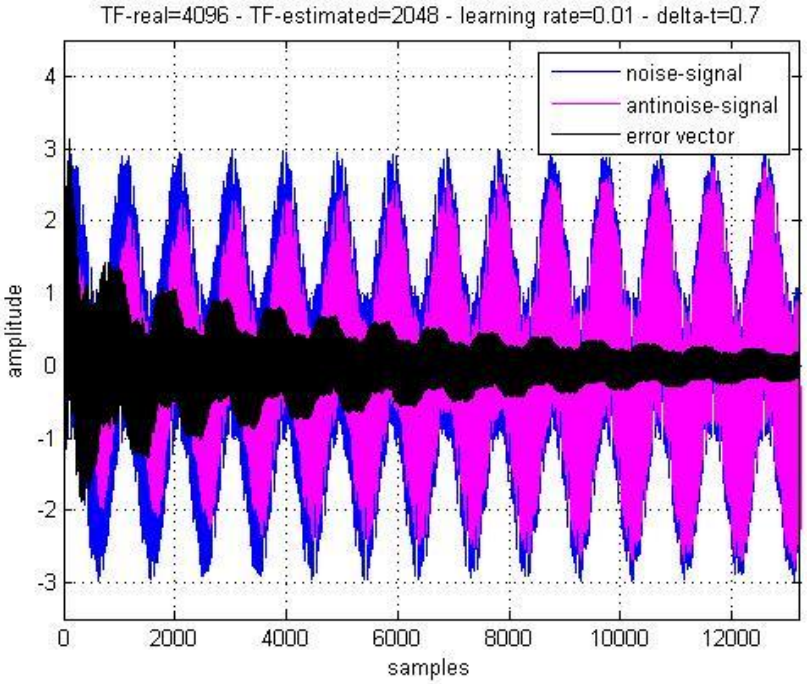

(a)

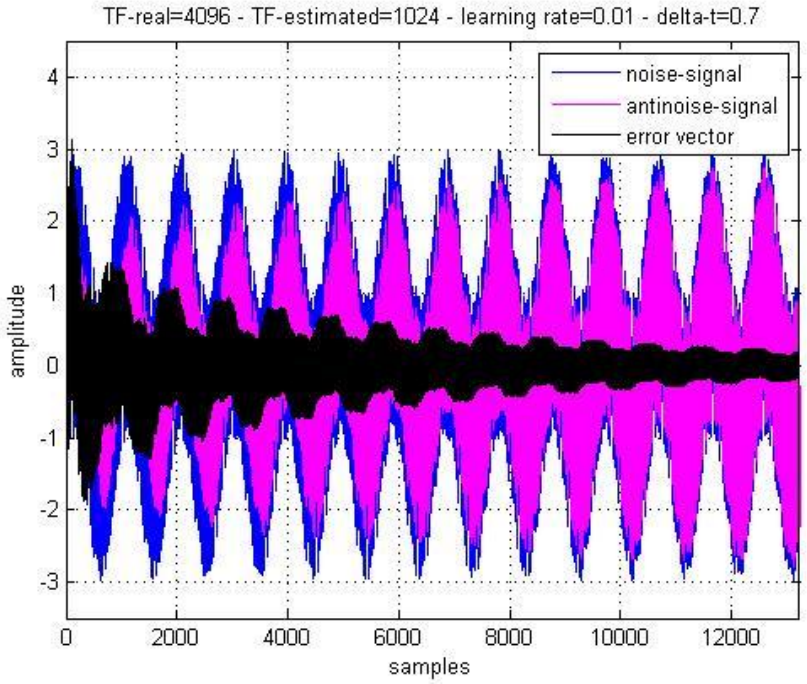

(b)

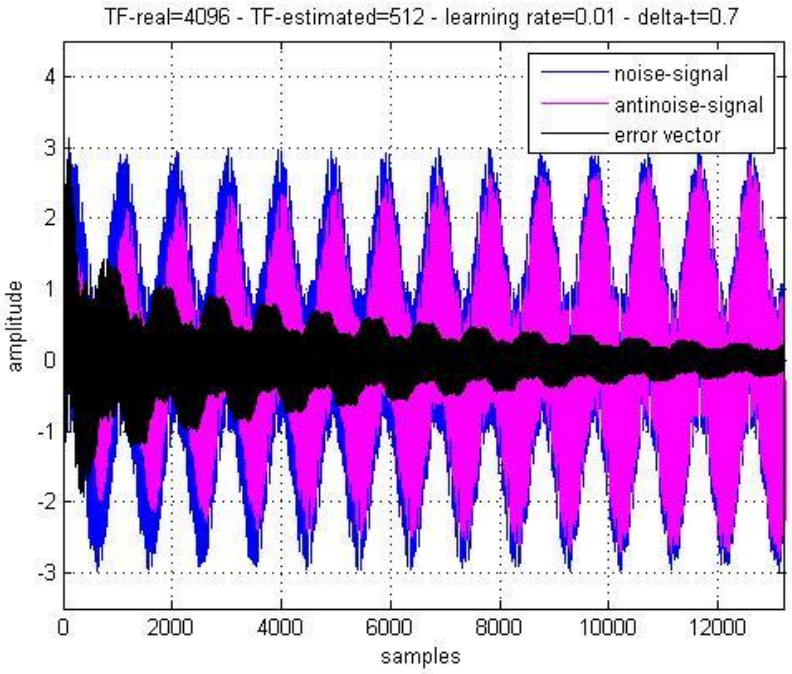
TF-real=4096 - TF-estimated=512 - learning rate=0.01 - delta-t=0.7
noise-signal
antinoise-signal
error vector
amplitude
samples
4
3
2
1
0
-1
-2
-3
0
2000
4000
6000
8000
10000
12000

(c)

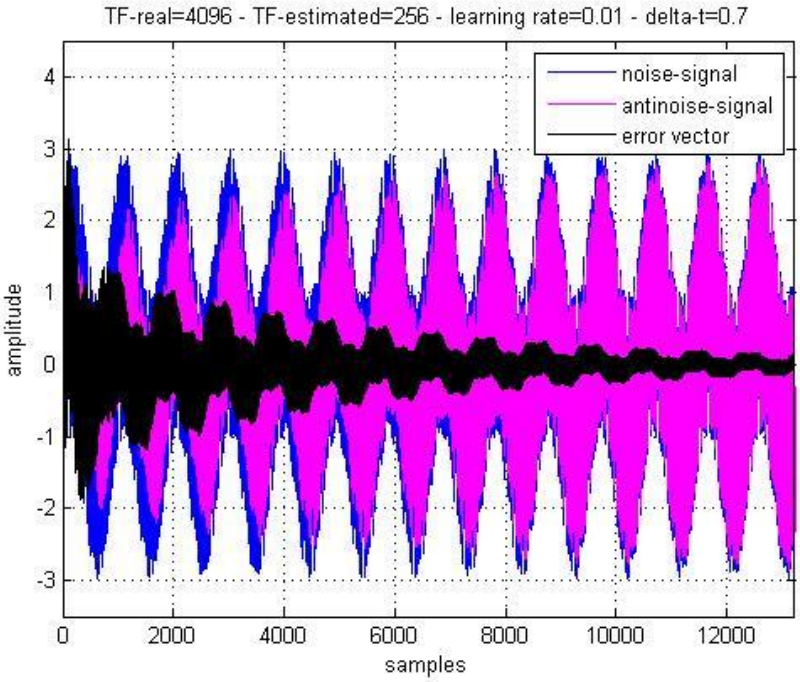
TF-real=4096 - TF-estimated=256 - learning rate=0.01 - delta-t=0.7
noise-signal
antinoise-signal
error vector
amplitude
samples
4
3
2
1
0
-1
-2
-3
0
2000
4000
6000
8000
10000
12000

(d)

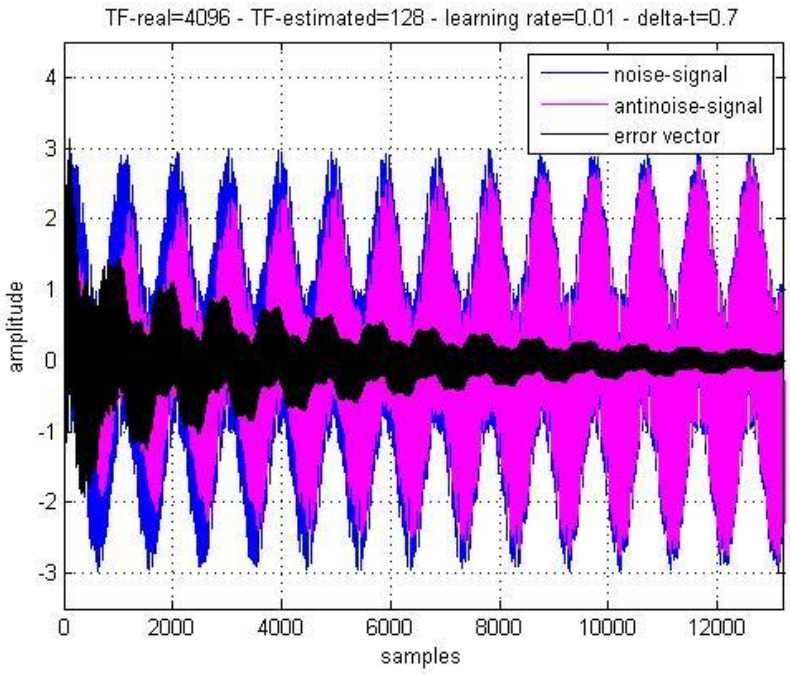

(e)

Figure 8.9. Comparison of the anti-noise and the residual error in a feedforward LMS application with an estimated secondary path of different length: (a) 2048, (b) 1024, (c) 512, (d) 256, and (e) 128 taps. The actual secondary path is derived from measurements under tight condition (and so is the estimated secondary path). The conversion time is 0.7 ms.

9 References

[1] Bech S. and Zacharov N. “Perceptual Audio Evaluation – Theory, Method and Application”, *Wiley*, Chichester, 2006

[2] Langberg et.al. “Active Noise Reduction System” United States Patent 4,985,925, Jan. 1991

[3] Bose “Feedback Control”, United States Patent 4,494,074, Jan. 1985

[4] Berge “Device for Reducing Noise”, United States Patent 6,122,383, Sep 2000

[5] Bartels, Volker “Headset with Active Noise-Reduction System for Mobile Applications”, *Journal Audio Engineering Society*, Vol. 40, April 1992

[6] Laroche, Jean “Optimal constraint-Based Loop-Shaping in the Cepstral Domain”, *IEEE Signal Processing Letters*, Vol. 14, Nr. 4, April 2007

[7] Turner, M.J. and Wilson, D.A. “The use of negative source impedance with moving coil loudspeaker drive units: an analysis and review”, *Audio Engineering Society Convention 122*, Vienna, May 2007.

[8] Haykin, S. “Adaptive Filter Theory”, *Prentice Hall*, New Jersey, 2002

[9] Kuo, S.M. and Morgan, D.R. “Active Noise Control: A Tutorial Review”, *Proceedings of the IEEE,* Vol. 87, No. 6, June 1999

[10] Bai, M. R. et.al. “Reduction of electronic delay in active noise control systems- A multirate signal processing approach”, *Journal of the Acoustical Society of America, 111 (2): 916-924*, February 2002

[11] Park, S.J. et al. “Delayless Subband Active Noise Control system for Wideband Noise Control”, *IEEE Transactions on Speech and Audio Processing,* Vol. 9, No. 8:892.899, Nov. 2001.

[12] Clemow, R. “Digital circuit arrangements for ambient noise-reduction”, UK Patent _Application 2465681, June 2010.

[13] Foudhaili, H. “Kombinierte Feedback- und adaptive Feedforward-Regelung für die active Lärmreduktion in einem Kommunikations-Headset”, PhD thesis, Leibniz Universität Hannover, 2008

[14] Gan, W.S. "Adaptive Feedback Active Noise Control Headset: Implementation, Evaluation and its Extensino", *IEEE Transactions on Consumer Electronics*, Vol. 51(3):957-982, Aug. 2005.

[15] Zwicker E. and Fastl H. "Psychoacoustics. Facts and Models" Springer 1990

[16] Oppenheim, A.V. "Single-Sensor Active Noise Cancellation", *IEEE Transactions on Speech and Audio Processing*, Vol. 2, Nr. 2: 285.290, Apr. 1994.

[17] K.C. Zangi, "A new two-sensor active noise cancelaltion algorithm" in *Acoustics, Speech and Signal Processing 1993, ICASSP-93, 1993 IEEE International Conference on*, April 1993, Vol.2,pp. 351-354 Vol.2.

[18] Rafaely, B. and Jones, Matthew "Combined feedback-feedforward active noise-reducing headset – The effect of the acoustics on broadband performance", *The Journal of the Acoustical Society of America*, 112(3):981-989, Sept. 2002.

[19] A. Jain and S. Ranganath, "Extrapolation algorithms for discrete signals with application in spectral estimation," *Acoustics, Speech and Signal Processing, IEEE Transactions on*, vol. 29, no. 4, pp. 830 – 845, aug 1981.

[20] Sen M. Kuo, Sohini Mitra, and Woon-Seng Gan, "Active noise control system for headphone applications*," IEEE Transactions on Control Systems Technology*, vol. 14, pp. 331–335, 2006.

[21] G. Kannan, A.A. Milani, I.M.S. Panahi, and R.W. Briggs, "An efficient feedback active noise control algorithm based on reduced-order linear predictive modelling of fmri acoustic noise," *Biomedical Engineering, IEEE Transactions on*, vol. 58, no. 12, pp. 3303 –3309, dec. 2011.

[22] P.P. Vaidyanathan, "The Theory of Linear Prediction, Synthesis lectures on signal processing." *Morgan & Claypool*, 2007.

[23] Schumacher, Th. et.al. "Active Noise Control in Headsets: A New Approach for Broadband Feedback ANC", *Proceedings of the International Conference on Acoustics, Speech and Signal Processing*, Prague, May 2011.

[24] Ying Song, Yu Gong, and S.M. Kuo, "A robust hybrid feedback active noise cancellation headset," *Speech and Audio Processing, IEEE Transactions on*, vol. 13, no. 4, pp. 607 – 617, July 2005.

[25] B. Widrow, J. R. Glover, J. M. Mccool, J. Kaunitz, C. S. Williams, R. H. Hearn, J. R. Zeidler, Eugene Dong, R. C. Goodlin, and R. C. Goodlin. Adaptive noise cancelling: Principles and applications. Proceedings of the IEEE, 63(12):1692–1716, 1975.

[26] M. Widrow, D. Shur, and S. Shaffer. On adaptive inverse control. In Proc. 15th Asilomar Conf., pages 185–189, 1981.

[27] John C Burgess. Active adaptive sound control in a duct: A computer simulation. The Journal of the Acoustical Society of America, 70:715, 1981.

[28] S.D. Snyder and C.H. Hansen. The influence of transducer transfer functions and acoustic time delays on the implementation of the lms algorithm in active noise control systems. Journal of Sound and Vibration, 141(3):409–424, 1990.

[29] S.D. Snyder and C.H. Hansen. The effect of transfer function estimation errors on the filtered-x lms algorithm. Signal Processing, IEEE Transactions on, 42(4):950–953, 1994.

[30] P.A.C. Lopes and M.S. Piedade. The behavior of the modified fx-lms algorithm with secondary path modeling errors. Signal Processing Letters, IEEE, 11(2):148 – 151, feb. 2004.

[31] Larry J Eriksson and Mark C Allie. Use of random noise for on-line transducer modeling in an adaptive active attenuation system. The Journal of the Acoustical Society of America, 85:797, 1989.

[32] Ming Zhang, Hui Lan, and Wee Ser. Cross-updated active noise control system with online secondary path modeling. Speech and Audio Processing, IEEE Transactions on, 9(5):598–602, 2001.

[33] S. Gholami-Boroujeny and M. Eshghi. Online secondary path modeling in active noise control system using pbs-lms algorithm. In Signal Processing (ICSP), 2010 IEEE 10th International Conference on, pages 2600 –2603, oct. 2010.

[34] G.Y. Jin and Hongtian Zhang. An adaptive active vibration and noise control system with online secondary path modeling. In Measuring Technology and Mechatronics Automation, 2009. ICMTMA '09. International Conference on, volume 1, pages 582–585, 2009.

[35] S.M. Kuo and D. Vijayan. Optimized secondary path modeling technique for active noise control systems. In Circuits and Systems, 1994. APCCAS '94., 1994 IEEE Asia-Pacific Conference on, pages 370–375, 1994.

[36] M.T. Akhtar, M. Abe, and M. Kawamata. A new variable step size lms algorithm-based method for improved online secondary path modeling in active noise control systems. Audio, Speech, and Language Processing, IEEE Transactions on, 14(2):720 – 726, march 2006.

[37] Jian Liu, Yegui Xiao, Jinwei Sun, and Li Xu. Analysis of online secondary-path modeling with auxiliary noise scaled by residual noise signal. Audio, Speech, and Language Processing, IEEE Transactions on, 18(8):1978 –1993, nov. 2010.

[38] Ming Zhang, Hui Lan, and Wee Ser. A robust online secondary path modeling method with auxiliary noise power scheduling strategy and norm constraint manipulation. Speech and Audio Processing, IEEE Transactions on, 11(1):45 – 53, jan 2003.

[39] CharlesE. Kinney and RaymondA. Callafon. Robust estimation for automatic controller tuning with application to active noise control. In Paul M.J. Hof, Carsten Scherer, and Peter S.C. Heuberger, editors, Model-Based Control:, pages 107–124. Springer US, 2009.

[40] S.M. Kuo, S. Kuo, and D.R. Morgan. Active noise control systems: algorithms and DSP implementations. Wiley series in telecommunications and signal processing. Wiley, 1996.

[41] David A. Cartes, Laura R. Ray, and Robert D. Collier. Experimental evaluation of leaky least-mean-square algorithms for active noise reduction in communication headsets. The Journal of the Acoustical Society of America, 111(4):1758–1771, 2002.

[42] M. Kamenetsky and B. Widrow. A variable leaky lms adaptive algorithm. In Signals, Systems and Computers, 2004. Conference Record of the Thirty-Eighth Asilomar Conference on, volume 1, pages 125–128 Vol.1, Nov.

[43] I.T. Ardekani and W.H. Abdulla. Effects of imperfect secondary path modeling on adaptive active noise control systems. Control Systems Technology, IEEE Transactions on, 20(5):1252–1262, 2012.

[44] Monson Hayes, Jae Lim, and Alan Oppenheim. Signal reconstruction from phase or magnitude. Acoustics, Speech and Signal Processing, IEEE Transactions on, 28(6):672–680, 1980.